Photochromism of Spiropyran in UHV-Prepared Thin Films

Im Fachbereich Physik der Freien Universität Berlin eingereichte Dissertation.

Michael Karcher

April 2011

Erstgutachter: Prof. Dr. Paul Fumagalli
Zweitgutachter: Prof. Dr. Robert Bittl
Termin der Disputation: 22. Juni 2011

Selbstständigkeitserklärung

Ich versichere, dass ich alle verwendeten Hilfmittel, Hilfen und Quellen angegeben zu habe, und die Arbeit selbstständig angefertigt zu habe.

Contents

1 Introduction

1.1 Motivation

Currently, the interest in physical and chemical research on switchable molecules is very active, as there are plenty of possible applications. In general, switchable molecules are used to be able to manipulate material properties. Depending on the nature of the molecular switch and its incorporation into the material, a wide variety of different applications is possible.

One important class of molecular switches are *photochromic* molecules, i.e. molecules that respond to light irradiation (*photo-*) with a change in their color (*-chromic*). Applications for these molecules include self-coloring sunglasses, optical modulators (using rapidly switching molecules [1]), optically controlled light switches [2, 3]), and optical memory (for bistable molecules, [4–6]). There are many photochromic molecules, for examples diarylethenes, diazenes, fulgides, fulgimides, spiropyrans and spirooxazines. While the former two compound classes show a photoinduced isomerization, the photochromism of the latter two molecules is caused by a reversible photochemical ring opening reaction.

This thesis focusses on one specific photochromic molecule, a spiropyran derivative. There exist many publications on the topic of spiropyrans since the discovery of their photochromism in 1952 [7, 8]. These publication cover spiropyran in solution [9–18], in polymer matrices [19–27], as self-assembled monolayers (SAM) [13, 28–32] and in microcrystalline structures [33], but very few publications about growth of spiropyran in high vacuum conditions and interactions with the surface layer exist. A notable exception is the recent report of ordered growth [34–36]. In the literature about spiropyrans in polymer matrices, the polymer was used as thinner and carrier material. The sparse 3D structures created that way are useful for applications like holographic memory, but interaction between the spiropyran and the polymer film or the substrate is treated as minor topic at most.

As the physical properties of the spiropyran molecules highly depend on the current conformation, switching spiropyran films at a substrate surface might cause effects in the substrate, and changes in substrate properties might in turn induce spiropyran switching. As the spiropyran and the merocyanine states have different large dipole moments, it is expected to interact with the electric field at the material surface, spiropyran coated ferroelectrics might cause ordering in the evaporated film, and even interaction between ferroelectric domains and their respective walls with the state of the spiropyran molecules in the film is conceivable. The goal of the work for this thesis was to first evaporate a spiropyran thin films in ultra high

vacuum to different substrates to investigate substrate dependent properties, getting a reliable recipe to grow such films of some monolayers down to one monolayer. Having accomplished evaporation, the films were characterized to tune parameters like the quantum yield for switching, the absorbance, the stability of the states and quantum yield of fluorescence in the merocyanine state.

1.2 Outline

In the remaining part of the introduction, the history and current state of the art in spiropyran research is outlined, starting at the basics of photochromism. In chapter 2, an introduction into the materials used in this thesis and the methods applied to them is given. This includes the basic physics of absorption spectroscopy at the level of detail needed to understand the principle of in the experiments, see standard literature for further details [37–39]. It also describess well as the specific setups used for data acquisition. In chapter 3, the results of spectroscopy on both of the spiropyran and the merocyanine state is presented and discussed, followed by chapter 4 investigating the kinetics of the switching on a timescale of seconds. A short conclusion is finally presented in chapter 5.

1.3 Molecular Switches

1.3.1 Introduction

A molecular switch is a molecule with at least two stable or metastable states, and possible transitions between these two states, as shown in fig 1.1(a). The molecule has the actual ground state *a*, and a second, usually metastable, state *b*. Transitions in both directions can usually be induced by either light irradiation or electron injection, but in some cases other stimuli are also applicable. In the case of light-induced switching, the wavelength to induce switching is typically different for the different switching direction, but overlapping spectra are common.

Fig. 1.1(b) shows the simplified potential energy diagram of a molecular switch with two configurations *a* and *b* of the electronic ground state *g*, manifesting as minima in the energy diagram, separated by a barrier. The state *a* is the ground state, while the state *b* is metastable. Depending on temperature and the height of the barrier between the two states, thermal relaxation from state *b* to state *a* can be possible.

Often, the controlled switching of that molecule involves a third state, the excited state *e*. Excitation of both switch configurations into the state *e* is possible, and relaxation of that state into either configuration of the electronic ground state is possible.

One classification of molecular switches is by the most prominent differences between the states. Typical properties that expose a notable difference between the

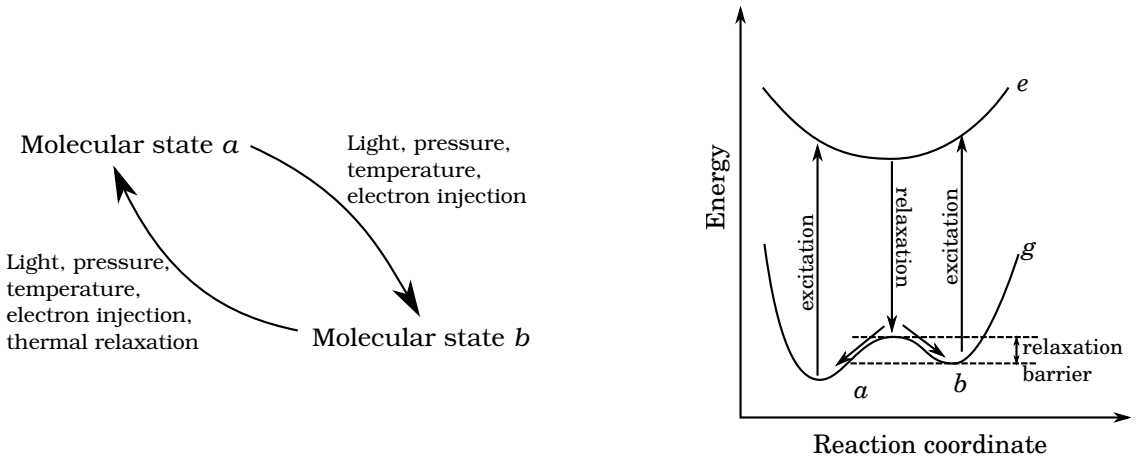

(a) operation principle (b) energy scheme

Figure 1.1: Molecular switch introduction.

two states are color (i.e. visible absorption spectrum), conductivity, electric dipole moment, electric polarizability and magnetic susceptibility, and many molecular switches have prominent changes in more than one of these properties. Of course, the state change is also accompanied by a lot of further property changes that can be used to characterize molecules, like IR vibration spectra, UV absorption, X-ray absorption (including fine structure at the absorption edges), NMR and EPR spectra, but while these properties give valuable information to the researcher, they are typically not the effect one is interested in for application.

Another classification is by the stimulus that induces switching. A very common one is photon absorption, and molecular switches that can respond to photon absorption by state switching are called *photoswitchable*. Furthermore, electron injection/extraction using a nanoscale contact like e.g. an STM tip or strong local electric or magnetic fields are also used in research. Finally, the metastable state can relax to the stable state by thermal activation.

1.3.2 Photochromic Molecules

As photoswitchable molecules have to interact with the light that induces the switching process, these molecules are colored if the absorbed light is in the range of visible light, whereas they may appear colorless if the photoswitching process happens completely outside the energy range of visible light, which usually means completely in the ultraviolet range, as organic molecules absorbing only near infrared light are rare.

As the absorption spectra of molecules change when they are switched from one into the other state, it is very common for photoswitchable molecules to have different colors in the different states. Such molecules are called *photochromic*. While

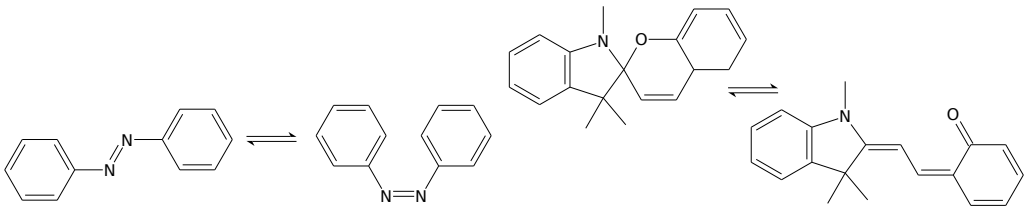

(a) azo-type cis/trans (b) spiro-type ring-open/close

Figure 1.2: Example for two very common classes of photochromic molecules.

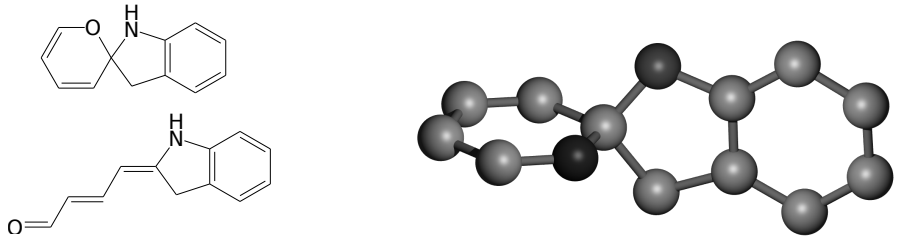

(a) spiropyran and merocyanine structure (b) spiropyran geometry

Figure 1.3: Generic indolinospiropyran structure and 3D geometry. Geometry shows a NO_2BIPS molecule reduced to the core shown here, atomic coordinates from [40]

the back-reaction from the meta-stable state b to the ground state doesn't have to be photo-induced as well to call a molecule photochromic, molecules with photo-induced back-reactions are most interesting for applications, as the molecule state can be controlled solely using optic effects, in this case, the phenomenon is called reversible photochromism.

Two main mechanisms of photochromism are observed in molecular switches, namely ring-open/ring-close reactions and cis-trans-isomerization. The first class includes fulgides, fulgimides and spiropyrans, while the latter class includes azobenzenes and stilbenes. Stilbenes are especially interesting as the cis state is also able to undergo a ring-close reaction to yield dihydrophenanthrene which is stable after being oxidized to phenanthrene. Typical examples for ring-open/ring-close isomerization (also called electrocyclization) and cis/trans-isomerization (also called E-to-Z-isomerization) are given in figure 1.2.

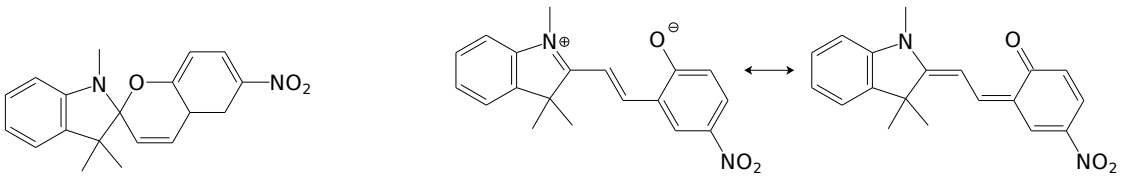

(a) Spiropyran state (b) Merocyanine state

Figure 1.4: The structure of NO_2BIPS – the spiropyran used in this thesis

1.3.3 Spiropyrans

Description of the System

Derivatives of the 2H-pyran in which the saturated carbon atom is part of a spiro bond, i.e. it is part of two cycles at the same time, are called spiropyrans. (see figure 1.3(a), showing an indolinospiropyran). The carbon-oxygen bond in these systems is fragile, and after breaking that bond, a merocyanine structure is formed instead (see figure 1.3(a)). This reaction is reversible in some merocyanine molecules.

As spiro bonds cause the two rings to be orthogonal to each other (see 1.3(b), the electronic coupling between the two moieties in the spiropyran molecules is low in the spiropyran state. The merocyanine ground state on the other hand has an in-plane structure, so the state transition is accompanied by considerable geometric changes in the molecule, which significantly influence the chemical properties of the molecule: Most important, the size of the aromatic system next to the oxygen is increased from four carbon atoms to reach up to the nitrogen atom in the other molecule part. Second, the merocyanine has two resonant forms in its aromatic part, giving rise to a zwitterionic alternate form (with a positive charge at the nitrogen and a negative charge at the oxygen) which creates a dipole moment of the merocyanine state, see figure 1.4(b).

This thesis focusses on one specific spiropyran, the 1',3'-Dihydro- 1',3',3'-trimethyl-6-nitro-spiro[2H-1-benzopyran-2,2'-[2H]indole], called NO_2BIPS for short. Its structure is shown in figure 1.4(a). The nitro group added to the benzopyran (also called chromene) moiety of the molecule gives rise to a dipole moment of $(14.3 \pm 0.1) \cdot 10^{-30}\,\mathrm{C\,m} \approx 4.3\,\mathrm{D}$ even in the spiropyran state [9], and shifts the equilibrium towards the merocyanine state and eases inter-system-crossing to the triplet state [12]. The dipole moment in the merocyanine state is $(58.9 \pm 0.5) \cdot 10^{-30}\,\mathrm{C\,m} \approx 18\,\mathrm{D}$.

There is plenty of literature available concerning this spiropyran and close derivatives, starting at solvatochromism and thermochromism [41–44], over the discovery of photochromism [7, 8, 45], the properties of the different states, and detailed analysis of the details of the photoinduced state transition [12, 46, 47] to application in molecular logic [17] or memory devices [5].

The spiropyran state of NO_2BIPS shows optical absorption in the near UV range, but is transparent in the visible and near IR. The absorption spectrum of NO_2BIPS

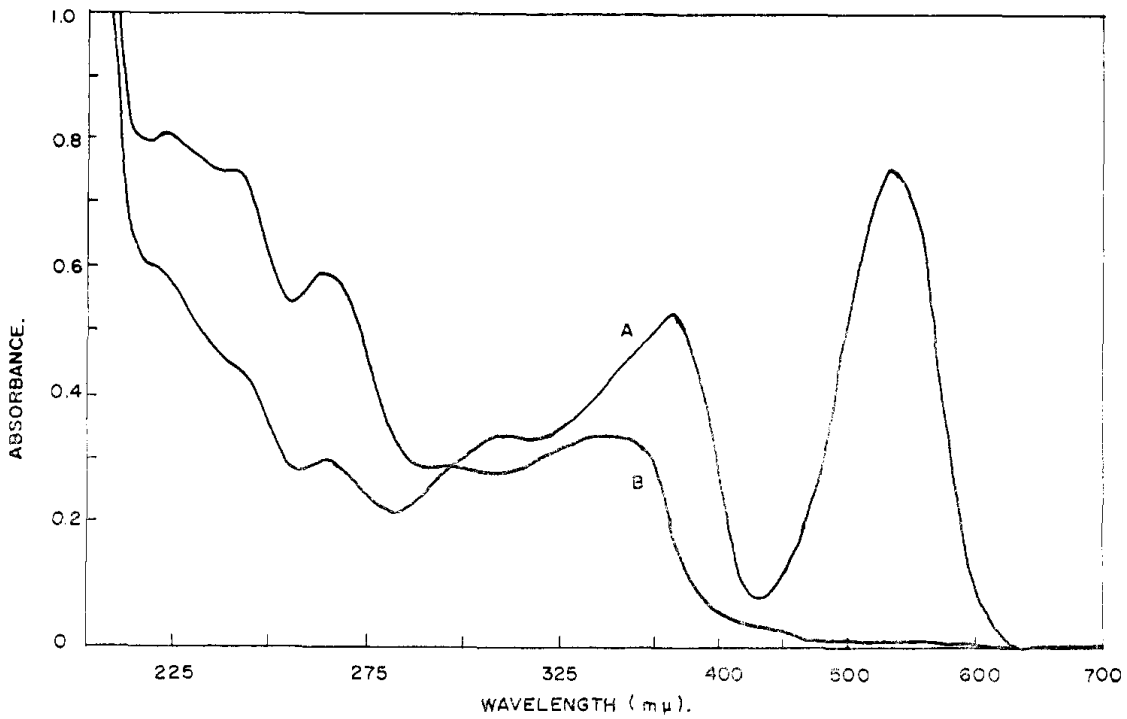

Figure 1.5: Absorption of NO_2BIPS in ethanol at 6 °C. Curve B shows the absorption pure spiropyran state, while curve A shows a mixed state after UV irradiation. Quoted from [48].

as observed by [48] in ethanol is shown in figure 1.5. The solution was cooled to 6 °C to enhance the lifetime of the merocyanine state. The absorption spectrum of NO_2BIPS in the spiropyran form can be decomposed into the absorption spectra of the two constituents chromene and indole [49], as the electronic coupling between the halves is weak. The merocyanine form on the other hand contains only one conjugated system that extends into both halves. This system is bigger than the original systems resulting in lower transition energy, according to the Woodward-Fieser rules, see for example [50].[1] The primary electronic transition of the merocyanine state is around 580 nm, depending on the environment of the molecule.

The dipole moment change is directly shown in the wettability experiment by Rosario et al, shown in figure 1.6 [32]. The left picture shows the surface in the spiropyran state obtained after irradiating green to blue visible light. The lower dipole moment causes a lower adhesion of water, so the surface area of the drop shrinks, increasing the contact angle. The right-hand picture shows a drop of the

[1] These empirically determined rules predict the wavelength of the first absorption band of an aromatic system. The quantum physical background is that all atoms of the conjugated system provides a kind of "box" for all the electrons taking part in it. The bigger the box, the smaller the energy difference between adjacent states, so in larger systems, the lowest-energy transition is at lower energy than in small systems.

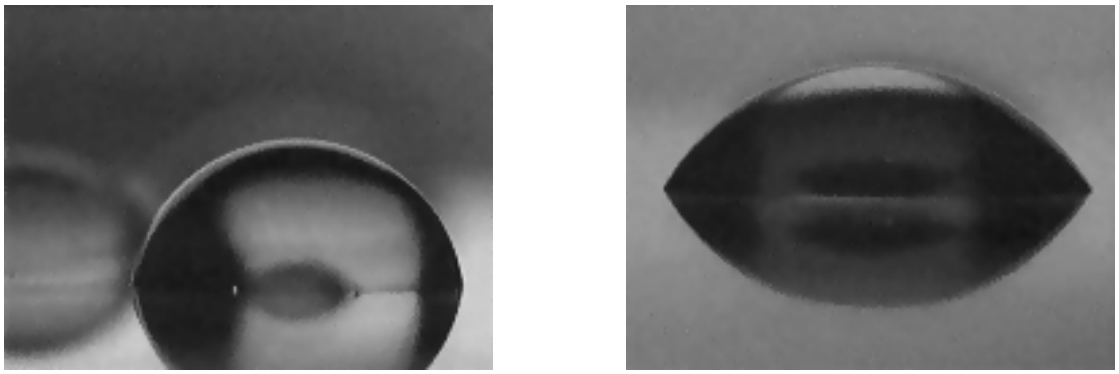

Figure 1.6: Wettability changes of a spiropyran containing chemically bond layer on a glass surface. Left image: low-polarity (hydrophobic) spiro state, right image: high-polarity (hydrophilic) merocyanine state. From [32]

same size on the same surface after UV light (366 nm) irradiation. The merocyanine state present in that case has a higher dipole moment, i.e. is more hydrophilic. This causes the adhesion to rise and thus increase the surface contact area of the drop, thus decreasing the contact angle.

At room temperature NO_2BIPS solution is in an equilibrium between the two states, with no noticeable amount of merocyanine in non-polar solvents, and a considerable amount of merocyanine in polar solvents like methanol. Increasing the temperature shifts the equilibrium towards the merocyanine state.

Switching Dynamics

Figure 1.7 shows the states involved in switching NO_2BIPS, as presented by Helmut Görner in [51], which applies to most nitro-derivatives of benzoindolinospiropyrans. The spiropyran ground state (a singlet state) is excited optically into an excited singlet state (2). The excited singlet state then relaxes into a less excited triplet state (3), still in the original molecular structure. The carbon-oxygen bond to the spiro atom breaks in this triplet configuration, yielding the *perp* configuration of merocyanine (4), in this configuration, the indoline and chromene moiety are still perpendicular to each other, as in the spiropyran configuration. This excited configuration either converts into the excited triplet *trans* configuration (5) or relaxes into the ground state singlet *perp* configuration (6). The *perp* configuration has an energetically unfavorable geometry. The molecule relaxes by rotating one half by 90° to obtain either the *cis* or the *trans* configuration. As indicated by that diagram, the *cis* configuration has a higher energy than the *trans* configuration. The time constant for that relaxation is in the order of milliseconds [51], so finally the trans-merocyanine is formed (7). The trans-merocyanine is optically excitable into a state that has an reaction pathway back into the singlet spiropyran ground state (8).

Both of the optical excitation processes do not necessarily lead to molecular

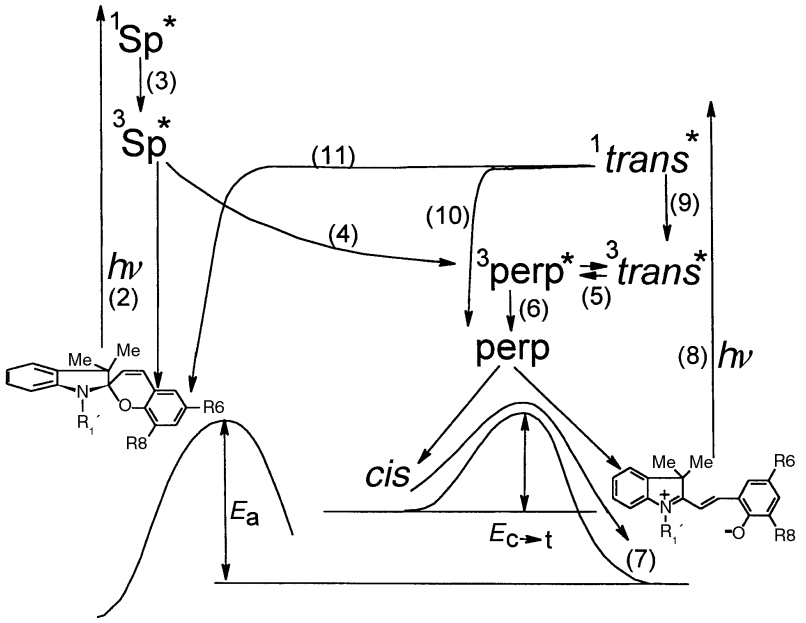

Figure 1.7: switching process of NO_2BIPS (R6=NO_2; R8=H), from [51]

switching, as the relaxation back into the original state is possible as well as the ring-opening and ring-closure reactions, but continuing light irradiation that excites one of these transition can be used to continually shift the ratio away from the state that can be excited by that light. This works best for irradiating with green light to get rid of the merocyanine state, because the spiropyran state does not absorb in the visible range, but does not work as good for the reverse direction, as in the ultraviolet range, not only spiropyran can be excited, but also higher excited states of merocyanine are reachable. So the switching process proceeds only up to a photostationary state and not up to having 100% of merocyanine.

Current Film Preparation Methods

Preparation of monolayers of spiropyrans is possible in different ways. An established method is the creation of Langmuir-Blodgett films [52], which is used for spiropyran films since 1979 [53]. The preparation of Langmuir-Blodgett requires amphiphilic molecules, that are molecules with a hydrophobic and a hydrophilic part. In aqueous solution, these molecules arrange in a single layer on top of the solvent with the hydrophilic end pointing towards the solvent and the hydrophobic end towards the air. These single-layer films are called Langmuir films. A very basic property of these Langmuir films is the surface-to-pressure relation, which is the pressure inside the 2D-film (thus measured in N/m instead of N/m^2 as for pressure applied to bulk) plotted over the surface area for the individual molecules. Typically on compressing the film, the pressure is low until the molecules are closely packed and shows a steep rise at that point. [54]

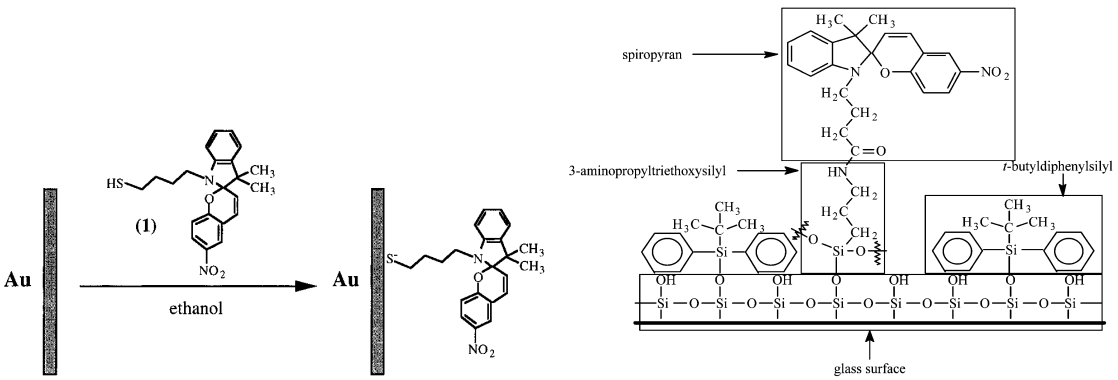

(a) chemisorption to gold [28] (b) chemisorption to glass [32]

Figure 1.8: Attachment functionalized spiropyrans to a surface by chemical.

The preparation of Langmuir-Blodgett films on a substrate starts with the preparation of a closely packed Langmuir film. A substrate (usually a hydrophilic glass substrate) is inserted into the solution. As the glass surface repels the hydrophobic air-side surface of the molecule layer, resulting in a convex meniscus and only the hydrophobic side of the Langmuir film touching the substrate. nothing will be adsorbed at that point. When pulling the substrate back out of the solution, the wetted substrate lifts the solution with it and this time the hydrophilic end of the molecules is near to the substrate. While the water flows downwards at the substrate surface, the closely packed Langmuir film can't flow down and will touch the substrate. As this time the hydrophilic end touches the substrate, so the layer will stick to the substrate, resulting in a monolayer.

For spiropyran molecules, the amphiphilic functionalization is realized by substituting one or two long aliphatic chains as hydrophobic parts. The structure and orientation of the molecules at the water-air-interface is shown graphically in [53], indicating that the aliphatic chain really points away from the water. This technique is still used, for example in [55] investigating optical response of aggregates.

For certain kind of experiments, the physisorption of the molecules to the surface is not stable enough for some experiments, like [28] performing electrochemistry on spiropyran coated electrodes or [32] performing wettability experiments. In these cases, chemisorption (i.e. chemical binding to the surface) has been used to obtain films of higher stability. While the electrochemistry experiment used thiol-substituted spiropyrans on a gold surface, the wettability experiment was performed with carboxy group binding to silicon oxide.

Recently, monolayers of non-functionalized spiropyran films prepared by deposition in ultra high vacuum have been prepared. In [34], Tian Huang et alprepared a close-packed monolayer of NO_2BIPS on gold (see figure 1.9(a)) and investigated the film structure using low-temperature scanning tunneling microscopy (LT-STM) at nitrogen temperature. The structure of the layer was found to not be defined by the

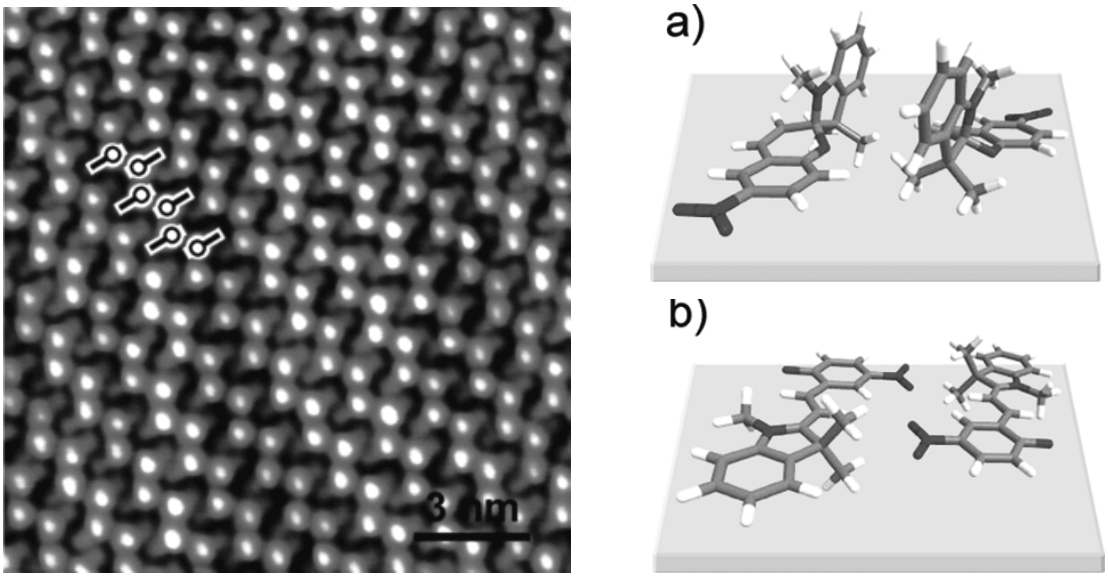

(a) STM picture from [34]

(b) DFT simulations from [35]

Figure 1.9: Adsorption geometry of NO_2BIPS on gold surface, STM picture and DFT simulation. In the simulation, a) is the spiropyran and b) is the merocyanine state.

substrate geometry, but dominated by interaction of the adsorbed film. The film consists of closely packed lines of two different types, which are attributed to different adsorption geometries. Each line consists solely of one adsorption geometry, although the chirality of the molecules in one line is alternating from one molecule to the next.

Investigation of Non-Functionalized Films

Further LT-STM investigations (at 5 K) have been performed, observing a thermally driven phase transition on the adsorbed monolayer. The STM investigations have been complemented by X-ray photoelectron spectroscopy (XPS), near-edge X-ray absorption fine structure spectroscopy (NEXAFS) and high-resolution electron energy loss spectroscopy (HREELS) to identify the states and geometries of the adsorbed molecules [35]. It turns out that on gold surfaces, the merocyanine configuration is the more stable one, as once the merocyanine configuration was obtained, it is impossible to switch the molecules back to the open spiropyran configuration. The reversal of stability is attributed to molecule-substrate interaction. As the merocyanine state of the molecule is planar, that state can be adsorbed flat on the surface maximizing the molecule-substrate interaction, whereas the spiropyran state can adsorb with only one moiety flat on the surface, which has been observed to be the nitrobenzopyran, as shown in figure 1.9(b).

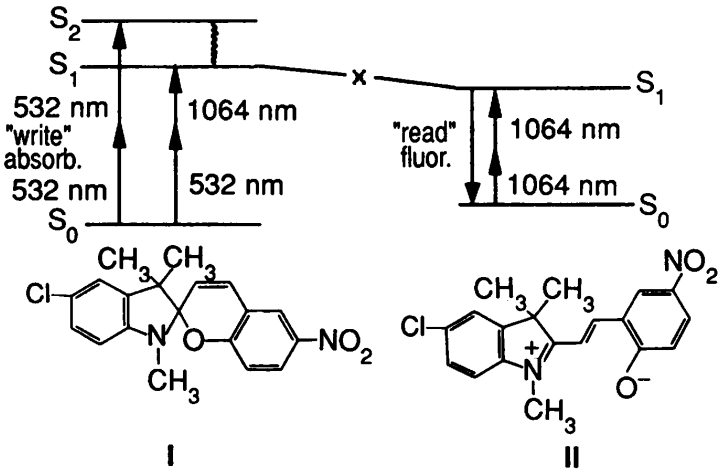

Figure 1.10: Two-photon processes for writing and reading processes in spiropyran based memory, from [56]

The behavior of NO_2BIPS on gold (Au(111)) and Bismuth (Bi(110)) surfaces has been investigated more in detail by Gunnar Schulze [36]. On the gold surface, thermal and STM induced switching to the merocyanine state was observed, whereas the quantum yield of photoswitching was found to be below 10^{-9}, as no photo-induced switching could be observed at all. On the other hand, on the bismuth surface, photo-switching was observed in addition to STM-induced and thermal switching. Illumination of the NO_2BIPS-on-bismuth system created different phases interpreted as different mixing ratio of the merocyanine and the spiropyran state. The observed photostationary phase is supposed to be a dynamic equilibrium between merocyanine and spiropyran which would indicate reversible photo-induced switching.

Applications

Reversibly switchable molecules are inherently memory molecules, as they store one bit of information in their state. Reading the memory translates into checking the molecule's state, whereas writing the memory is accomplished by switching the molecule into the desired state. A promising approach of creating high-storage-density memory is three-dimensional data storage, which means storing data in volume elements stacked in all three dimensions instead of writing data into 2-dimensionally arranged surface elements like on a CD. In a very basic way, three-dimensional storage is already implemented in multi-layer discs as DVD and blue-ray discs, and with a grain of salt, even multi-surface magnetic media could count as kind-of three-dimensional storage, but the number of layers is very low (up to two), whereas advanced optical three-dimensional data storage could work down to a layer spacing of $2\,\mu$m if the light to be used for accessing is around 1000 nm. A three-dimensional storage medium using spiropyrans has been proposed in 1989 by Dimitri Parthenopoulos et al [56]. For that work, the spiropyran molecules have

been embedded into a polymer matrix. The key to three-dimensional data storage is using two-photon processes that only occur at the intersection of two light beams (typically laser beams) to select a volume element. The processes for switching the spiropyran (I) state into the merocyanine (II) state and probing the states are shown in figure 1.10. The specific spiropyran derivative chosen for that memory exhibits low fluorescence during the write process to avoid writing to neighboring memory cells.

A photonic half-adder (i.e. an integrated XOR and AND gate) has been implemented using two different kind of photochromic switches, namely spiropyran and quinoline-derived dihydroindolizine [17]. The addition is performed by a molecule containing one spiropyran and two dihydroindolizine moieties, in which the spiropyran is used as UV absorber and fluorescent probe at the same time, while the dihydroindolizine moieties act as UV absorber and fluorescence quenching agents.

2 Material and Methods

2.1 Materials

Quartz substrates used were Suprasil, typically bought from Heraeus, MgO(100) substrates were bough from MaTecK. The solvents used for spectroscopy, cyclohexane, isopropanol, acetone and methanol were generally of spectroscopic quality, from either Sigma-Aldrich or Merck. NO_2BIPS (CAS number 1498-88-0) was bought from TCI Europe and used without further purification. Details about NO_2BIPS are described in the next section.

Quartz and MgO substrates were cleaned by sonicating in isopropanol and acetone before insertion into vacuum. Substrates were degassed if possible in the evaporation chamber. Three different chambers were used during the thesis, the first one without degassing capability, the second one using a halogen filled tungsten-filament bulb as heat source without any temperature monitoring, while the finally used MBE system contains multiple heatable manipulators with temperature control of the radiation temperature in closed volume behind the substrate carrier.

Silicon substrates are obtained from Wacker as 4 inch wafers, and cut to pieces of approximately 12 by 4 millimeters. These pieces were cleaned using organic solvents the same way quartz and MgO substrates were treated, then degassed at 650 °C and finally flashed by direct current heating. The flashing process is used to clean the surface from any residues and to remove the native oxide layer. In case of Si(111) substrates, the 7x7 reconstruction is formed by flashing. More details of flashing is described in section 2.2.2.

2.2 Methods

2.2.1 High-Vacuum Evaporation

The NO_2BIPS thin films have been prepared by physical vapor deposition (PVD). The NO_2BIPS powder is put into a metallic crucible, which is heated by a filament up to around 150° to sublimate the spiropyran molecules. The high-vacuum setups used at the beginning of the thesis before the UHV chamber expansion was ready consisted of a ceramic crucible evaporator by Pfeiffer Vacuum, that contained a second inner stainless steal crucible with a thermocouple spot-welded to it. While the dual-crucible setup increases thermal inertia of the system, it allowed the use of the available equipment and worked well enough. In the basic HV system (base

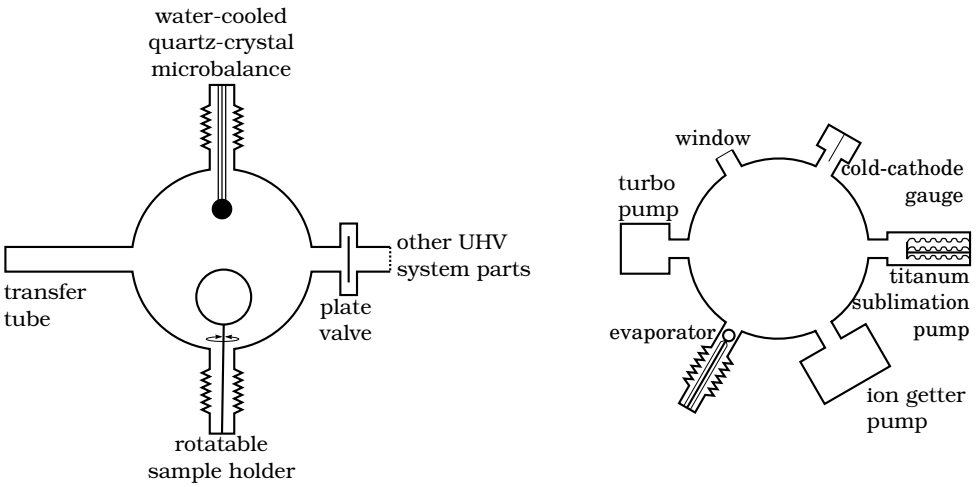

Figure 2.1: spiropyran evaporation subchamber for the UHV system. Left side shows the upper level and the right side the lower level of the chamber.

pressure around $3 \cdot 10^{-7}$ mbar) a primitive shutter was used that covers both the material and the quartz crystal microbalance, so there was no way to stabilize the evaporation rate before opening the shutter to the sample.

The non-bakeable glass chamber was abandoned for a bakeable UHV evaporation chamber with a base pressure of $2 \cdot 10^{-8}$ mbar. This chamber includes a source shutter as the previous chamber, but also includes a rotatable sample holder that can be used to turn the sample out of the evaporator's beam, acting like a sample shutter.

Finally, during a diploma thesis [57], the UHV system in our work group was extended to contain a chamber designed for spiropyran evaporation and the possibility to create monolayers by Langmuir-Blodgett methods from solution under inert gas atmosphere. The spiropyran evaporation part was finished during that thesis and is presented in figure 2.1.

The chamber consists of two layers, the upper layer contains the sample holder to pick up the sample from the transfer tube and put it into the molecular beam of the evaporator, and the quartz crystal microbalance (see section 2.2.8) to monitor evaporation progress. In the lower layer the pumps (a turbo pump, an ion getter pump and a titanium sublimation pump), the evaporator, a cold-cathode (Penning) vacuum gauge and a window are mounted.

The sample holder can be moved to the center of the chamber for evaporation and pulled back to allow the transfer tube to pass. Also it can be turned around the mounting axis. This is needed to turn the sample from the vertical orientation it has on the transfer tube to the horizontal orientation needed for evaporation from below. At the same time, it can be used to turn the sample to the top, so the sample holder is below the sample and blocks the molecular beam from the evaporator, which is used like a sample shutter.

The evaporator is also mounted on a linear motion stage, so it can be pulled back into the flange it is mounted to, or put to the center of the chamber for optimum evaporation geometry. Pulling it back to the flange works like a source shutter and is used to shut the crucible after evaporation. The evaporator consists of a molybdenum crucible containing the spiropyran material. This crucible is supported by a MACOR stand mounted on a copper base block. The copper base block also contains insulated conductors to supply the tungsten filament mounted below the crucible. A thermocouple (type K, chromel/alumel) is mounted to the crucible to monitor crucible temperature during evaporation.

The three different pumps (a Varian Turbo-V 200 turbo pump, a Varian StarCell ion getter pump and a titanium sublimation pump) complement each other to obtain a base pressure around 10^{-9} mbar. The pressure is monitored using the cold cathode ionization gauge (penning-type, Pfeiffer IKR-270). A rough indication of the pressure can also be obtained from the pump current in the ion getter pump, as displayed by the Terranova Model 741 ion getter pump power supply.

2.2.2 Flashing Silicon

Silicon crystals are formed by covalent bonds and have diamond structure. At the surface, an ideal crystal has a lot of dangling bonds, which are very reactive. Typical wafers have a native oxide layer saturating these bonds, while some preparation methods create so-called H-terminated silicon, in which each dangling bond is saturated by a hydrogen atom.

In ultra-high vacuum, a silicon surface without saturating the dangling bonds can be prepared. In this case, the dangling bonds interact with each other to form a *reconstructed surface*. The silicon atoms at the surface are displaced a bit so the bonds get into an energetically more favorable configuration. On Si(100) surfaces, the typical reconstruction is a 2x1 reconstruction, indicating that the size of the primitive cell of the lattice at the surface is 2 silicon atoms along one of the two base vectors and 1 silicon atom along the other base vector, i.e. a setup of periodically arranged dimers. For the Si(111) surface, the most favorable reconstruction of a clean surface is the 7x7 reconstruction, with a primitive cell of 49 atoms. [58, 59]

The idea of preparing clean silicon surfaces in vacuum is to heat the silicon substrate above the desorption temperature of typical surface contaminations like carbon dioxide or oxygen and finally anneal the substrate to get the well-ordered reconstructed surface. The procedure with specific details for the parameters to use in our setup has been taken from the PhD thesis by Kai Schwinge [60]. The temperature needed for this process is around 1200 °C, and the maximum allowed pressure is $2 \cdot 10^{-9}$ mbar. To improve the efficiency of the substrate cleaning, it is advantageous to heat as little as possible of the environment of the silicon substrate to get a low background pressure. To achieve that, a *direct current* heating method is used. Direct current heating means that the silicon substrate is not heated by either radiation or heat transport (which both requires some other component to be

at least as hot as the target temperature of the silicon), but by an electrical current through the substrate, with the ohmic losses heating it.

The temperature of 1200 °C is needed for the reconstruction to develop. At that temperature, the crystal lattice isn't very tightly bond anymore, and the silicon is sensitive to contaminations, as they can diffuse into the silicon. So the surface has to be cleaned before approaching this temperature. The pressure inside the vacuum chamber is used as indication for surface cleanliness. In our chamber, the pressure at the ionization gauge should stay below $2 \cdot 10^{-9}$ mbar to avoid volume contamination. The first part of annealing process takes 2 minutes, after which the temperature is rapidly decreased to around 650 °C which decreases the mobility inside the bulk to make it insensitive to contaminations (which could happen at local spots, as the temperature is below the oxygen desorption temperature), while still providing enough surface mobility that the surface reconstruction is formed during a second 10 minute annealing phase followed by a ten-minute slow cool-down phase.

The substrate temperature was not monitored directly as a thermocouple of the silicon substrate would result in metal contamination of the surface and pyrometric measurement is not available inside the chamber, but results of an early thermocouple-based calibration of the relation between applied current through the silicon and temperature of the substrate has been used, after normalization to the substrate cross-section. This results in around 11A for 4.5 mm samples in the first annealing step and 4A in the second step.

2.2.3 Wide-Range Absorption Spectroscopy Setup

The spectrometer used for wide-range UV-VIS absorption spectroscopy (shown in figure 2.2) consists of a monochromatic light source (in this case, high-pressure xenon arc lamp (Perkin-Elmer Cermax, 300W) or an incandescent tungsten filament bulb (Osram, 150W) followed by a double grating monochromator (Oriel 77225)) that is imaged to a translation stage containing multiple samples under investigation and a reference sample. The transmitted or reflected light is imaged to the detector. The available detectors are a photomultiplier, a silicon photodiode and a indium-gallium-arsenide diode (with thermo-electric cooling). To increase the signal-to-noise ratio and get rid of electronic offsets, the setup also includes a chopper that periodically interrupts the light beam (around 213 Hz) and the detector are connected to a lock-in amplifier (Perkin-Elmer, Model 7265).

While the description of the spectrometer clearly shows its one-beam nature, the spectrometer is usually used in a pseudo two-beam mode. In that mode, for each wavelength the sample stage is moved to put a reference sample and afterwards the sample to investigate (or multiple samples in order) into the beam path. This yields two intensity values that can be interpreted like the intensities measured at the same time in a real two-beam setup. The main shortcoming of the one-beam setup is the increased time for moving the sample stage at each wavelength, which can be circumvented by first measuring the reference spectrum followed by the sample

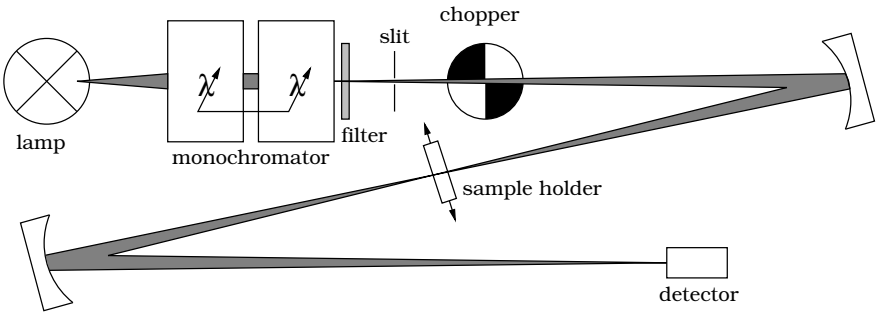

Figure 2.2: Setup of the one-beam spectrometer. Typically a reference is mounted at the sample holder, too, enabling a pseudo two-beam mode.

spectrum at the cost of decreased accuracy, as light source intensity fluctuations on a significantly longer timescale influence the measurement result.

Wavelength Resolution and Accuracy

The wavelength resolution is determined by the double monochromator system. The specified dispersion of the system is around 3 nm/mm per monochromator, resulting in 1.5 nm/mm for the double monochromator system. The resolution is thus determined by the width of the output slit. As reducing the width of the output slit increases the spectral pureness by blocking the unwanted components of light, increased spectral resolution inevitably reduces the amount of light entering the spectrometer and thus decreases the signal level and results in a worse signal/noise ratio.

As the output slit of the monochromator is imaged to the sample, if a small spot is needed (for example on photochromic samples where only a small area has been treated by UV light), the width of the output slit is around 0.5 mm for most samples. Widths of up to 2 mm have been used for more homogeneous samples however, especially strongly scattering samples measured in reflection. This results in wavelength resolution between 0.7 nm and 3 nm. Furthermore the accuracy of the calibration of the monochromator needs to be taken into account. The calibration was not monitored during the thesis, but just checked at the end (and a correction function was determined). The expected calibration error for the corrected is about 2 nm.

Error of the Absorption Values

Due to the lock-in detection of this setup, noise can be traded with time. The noise level of a lock-in detection scales with the square root of the time constant. So reducing the noise level by a factor of two incurs the quadruple time for spectrum acquisition. The digital lock-in used in this setup employs a finite impulse response (FIR) low-pass filter, so the output signal does not take infinite time to exactly

approach the input signal, as would be the case with a classical analog lock-in amplifier incorporating infinite impulse response output filters. In the configuration used (a filter steepness of 24 db/oct), the impulse response duration is below 8 time the time constant. Typical time constants for absorption spectroscopy in this setup are 50 ms to 200 ms.

Lock-in detection is not able to reduce errors in the measured signal which are not caused by statistical noise, for example like lamp intensity drifts that occur between measurement of the reference spot and the sample spot (although this specific influence is quite low as the time between measuring sample and reference is in the order of 1 second).

The physical quantity observed by the detectors and demodulated by the lock-in amplifier is the photocurrent in the detectors which is proportional to the power of the light approaching the detector. The error is a result of different components, some of them scaling linearly with the intensity of incident light (the fluctuations of lamp intensity), the shot noise which scales with the square root of the intensity, and sources like electro-magnetic interference that does not scale at all.

2.2.4 CCD Absorption Spectroscopy Setup with in-situ Light Exposure

The absorption spectrometer presented in the last section has two major drawbacks for the spectral investigation of photoswitches. First, it is a scanning spectrometer, so not all wavelengths are observed at the same time. In the presence of decaying non-equilibrium state of photoswitches, this is a major problem. Second, as the presented spectrometer is in fact a slightly modified Kerr spectrometer setup, illumination of the sample with light to change the molecular state would be very difficult to add, as the sample is mounted inside a bulky magnet with a small hole for the probe beam, so there is no space for a second beam.

Both of these issues have been addressed in the CCD setup with an illumination beam which is shown in figure 2.3. The white light of standard 12V halogen bulb (5W, 10W or 20W) is imaged to an aperture directly before the sample. The transmitted light is finally imaged on the entry slit of an imaging spectrograph (Triax 320) and the spectrum is acquired by an EMCCD camera (Andor Newton BU970 BV). A second beam images filtered light from a short-arc high-pressure Xenon bulb (Perkin-Elmer Cermax, 300W) to the sample. This beam path contains a computer-controlled filter wheel with one position blocking the beam completely to automate irradiation of light to switch the molecule state.

While the advantage of this setup is that there are no moving parts in it (except for the filter wheel) which will enhance the stability of the setup, the disadvantage is that this setup is not able to be run in a virtual two-beam mode as the wide-range spectrometer described above, so it is a nice tool to observe the spectral changes induced by state transition, but it is not suited for precision absolute absorbance measurements.

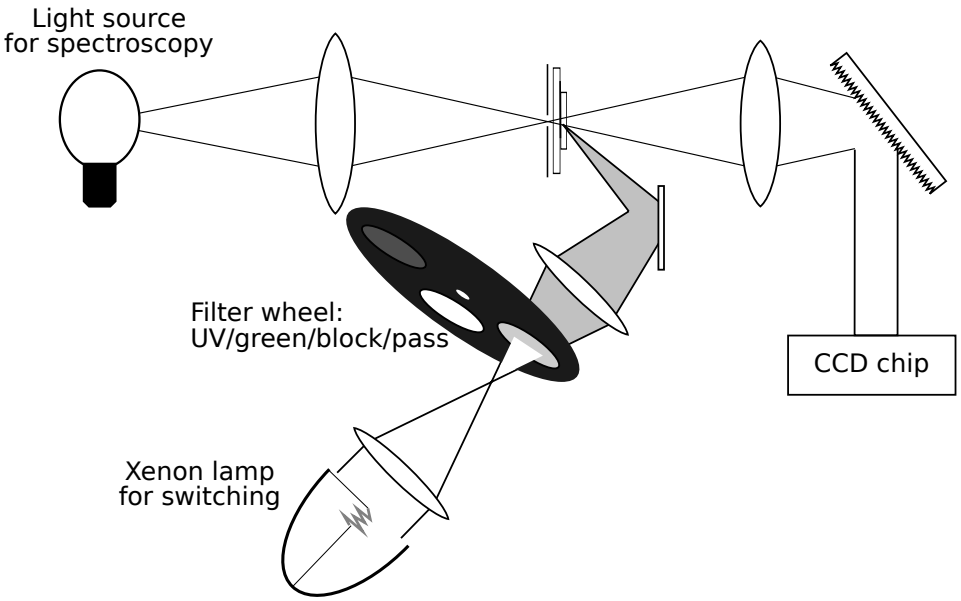

Figure 2.3: setup of the no-moving-parts spectrometer

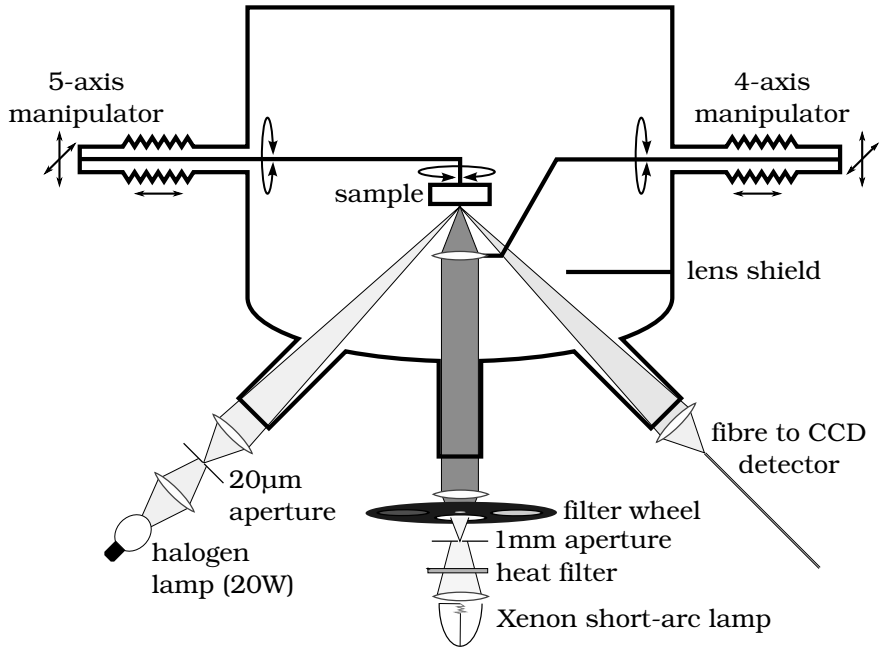

Figure 2.4: setup of the in-vacuum absorption spectrometer

2.2.5 Absorption Spectrometer for In-Vacuum Spectroscopy

The CCD spectrometer setup has been further adapted to be mounted to the UHV system the spiropyran films are grown in. The spectroscopy illumination is placed on an optical bench setup outside the vacuum that is mounted on a flange with window at the chamber, the transmitted light is collected into an optical fiber mounted in the same way. The light beam for switching the molecules is prepared the same way on a third optical bench mounted to a window, but the final focussing is performed inside the chamber to increase the numerical aperture of the illumination and thus the energy density.

The setup is show in detail in figure 2.4. The type of sample holders used does not allow transmission measurements, so the setup is a reflection spectrometer. The angle of incidence is 45° for reflectometry and normal incidence for switching. The lens focussing the light for switching is mounted on a three-axis manipulator to allow exact focussing of the light to the spot illuminated by the probe light.

2.2.6 Absorption Spectrometer for In-Vacuum Fluorescence Measurements

The advantage of detecting fluorescence is that in this case it is a method without a background signal. In the case of probing the spiropyran state, exciting with a green laser is only able to excite only molecules in the merocyanine state, and thus the fluorescence signal is proportional to the amount of merocyanine in the sample (it is also proportional to the incident laser intensity I_0, of course):

$$I_{fl} \propto I_0 n_{\mathrm{MC}}$$

Contrary to this, absorption spectroscopy depends on very small relative changes of the transmitted light while the total signal is proportional to the incident light intensity:

$$I_{tr} = I_0(1 - \alpha n_{\mathrm{MC}})$$

with a very small value for α. For films of a couple of nanometers, αn_{MC} turns out to be around 10^{-2} for the merocyanine saturated state. Solving both formulas for n_{MC} yields:

$$n_{\mathrm{MC}} \propto I_{fl}/I_0$$

$$n_{\mathrm{MC}} \propto 1 - I_{tr}/I_0$$

As all in-vacuum spectrometer setups used for this theses were one-beam setups, it is impossible to measure I_0 at the same time as either I_{fl} or I_{tr}, so the value of I_0 at the time I_{fl} or I_{tr} is acquired is not known exactly, but just within the stability of the setup. Especially for the vacuum setup, the stability is indeed problematic,

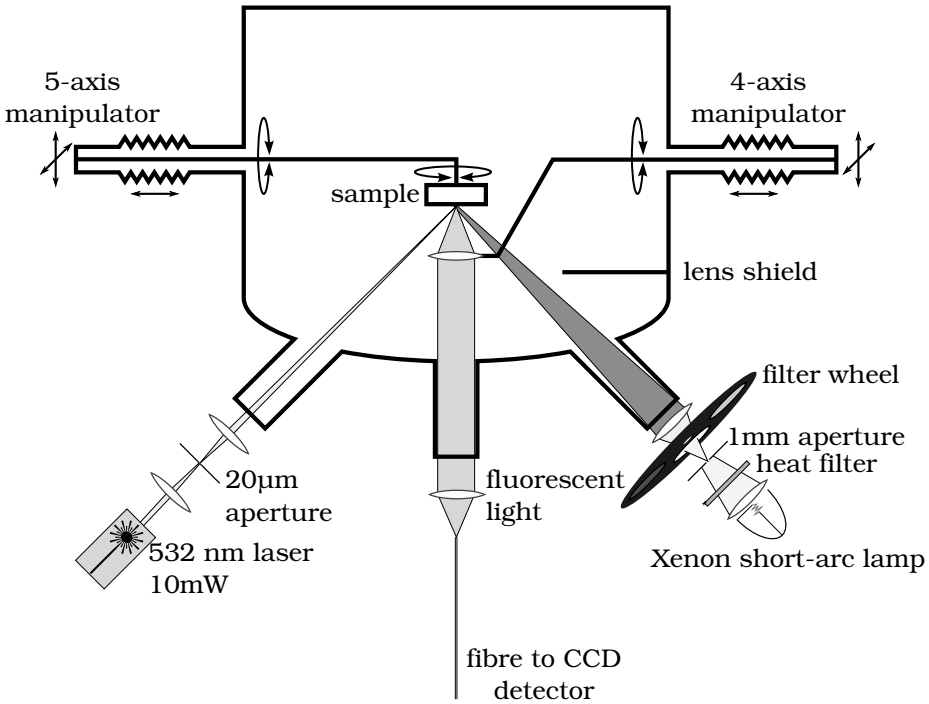

Figure 2.5: setup of the in-vacuum fluorescence spectrometer

as the sample and the optical components are mounted at different points on the chamber, most of them on long levers with only one supported point at the end. This is prone to vibration and to long-term drift. Especially drift of the adjustment causes the value I_0 to change.

Now consider a relative error δ in the term I_{fl}/I_0 or I_{tr}/I_0 respectively. In both the fluorescence and the absorption case, the relative error of this term causes an absolute error of $\delta I/I_0$ on the right side of the proportionality. In the case of fluorescence, the relative error of the result is obviously δ again, while in the absorption case

$$\delta_n = \frac{\delta I_{tr}/I_0}{1 - I_{tr}/I_0} \approx \frac{\delta}{1 - I_{tr}/I_0}.$$

The approximation holds because $I_{tr} \approx I_0$. As $1 - I_{tr}/I_0 \leq 10^{-2}$ in the absorption case, the relative error gets amplified by a factor of at least 100.

For fluorescence measurements, the spectrometer has been modified outside of the vacuum with the in-vacuum components still the same. A problem with fluorescence spectroscopy is that the photons are emitted isotropically, i.e. into all possible directions. To get a significant signal, one has to collect photons from a solid angle as large as possible. This makes only the beam setup that was used for switching light (with the in-vacuum lens) a suitable candidate for light collection. The excitation setup is placed on the bench that was previously used for the probe beam for absorption spectroscopy, with the light source being a 10 mW laser at 532 nm instead

of an incandescent bulb. The collection setup uses a dielectric long-pass filter with the edge at 550 nm to remove scattered light from the laser. A colored glass filter won't work at that point because it shows fluorescence of its own which is superimposed to the fluorescence that is intended to be observed. A clear indication of filter fluorescence is that the spot on the filter illuminated by the laser emits yellow light. This has been observed with a Schott OG550 filter.

2.2.7 Absorption Spectroscopy in Presence of Rough Films

In transmission absorption spectroscopy, the monochromatic light from a source is detected after transmission through the sample. In the case of a solution, the sample is a homogeneous volume with flat interface layers, and within certain limits, the relationship between the optical properties of the material and the detected absorption is according to Lambert-Beer-Law describing exponential decay in the medium. Especially if a reference beam exposed to the same setup, this time containing pure solvent instead of the sample solution, is used, the effects that are not to absorption in the sample (like for example reflection at the interface layers) cancel nearly perfectly.

On the other hand, on thin film spectroscopy there are two interface layers (film-to-air and substrate-to-film) on the sample, while an uncoated reference substrate has one interface layer between substrate and air (or vacuum). The properties of the substrate-to-air interface of the reference might be considerably different from the properties of the combined substrate-to-film and film-to-air interface. The morphology of the film-to-air interface furthermore strongly depends on the growth mode. If the film does not have an optically flat surface, scattering starts to influence the results, as the experimental method of absorption spectroscopy in transmission can not discriminate between scattered and absorbed light. As long as the morphology is not known, it is impossible to create a reference with the same scattering behavior than the surface to compensate the effect of scattering. So the discussion of a rough-film absorption spectrum needs to include scattering as well as absorption.

If the correlation length of the surface roughness is big compared to the wave length of the light, simple geometrical models are appropriate, whereas for correlations lengths of the roughness smaller than the wavelength, the rough surface can be described by as an effective medium, as also known from ellipsometry. The properties of this effective medium can be calculated from the constituents and the fractions they are composed in, as explained in appendix B of [61]. Opposed to ellipsometry, transmission spectroscopy is sensitive to the light scattered away from the film, so also the scattering spectrum needs to be taken into account.

For the films prepared in this thesis, it turns out that the Rayleigh model for particle sizes much smaller than the wavelength is not sufficient to describe the scattering losses. According to the Raleigh model, the total scattering cross-section (and thus the scattering loss) scales with the fourth power of the photon energy. This law obviously has to break down for higher photon energies (i.e. shorter wave

lengths), as the scattered power would get bigger than the incident power. A more general theory that works for spheric scattering particles of any size is the Mie theory. The Rayleigh scattering can also be obtained from Mie theory in the limit of long wave lengths.

2.2.8 Quartz Crystal Microbalance

The quartz crystal microbalance is a device to measure the mass of material deposited on an oscillating quartz plate [62]. It is commonly used to measure the thickness of films during evaporation. The quartz crystal is mounted inside the evaporator beam near the sample, so when evaporating material to the substrate, also the quartz crystal is coated. The weight of material deposited to the quartz crystal is detected by measuring the decrease of the resonance frequency caused by the increased mass.

The mass of the material deposited usually is displayed as thickness on commercial quartz crystal microbalance units. The thickness is calculated from the measured mass, the known size of the coated area and the density of the film. This implies that in case of uneven growth, the thickness measured by a quartz crystal microbalance is not the real thickness of the film, but the thickness of an equivalent homogeneous film with the same number of atoms or molecules per area, this is why the thickness indicated by the quartz crystal microbalance is referred to as *nominal thickness* at some points to emphasize the interpretation of the thickness as measured by a quartz crystal microbalance.

3 Results: Optical Spectra

3.1 Overview of Samples

Spiropyran solutions were investigated using four different solvents: Cyclohexane, acetone, isopropanol and methanol. These solvents have strongly different polarities and thus different equilibrium concentrations between spiropyran and merocyanine. An overview of the solvent polarities is given in table 3.2 in the discussion of the merocyanine peak of the solutions.

Also a couple of evaporated films on different substrates have been prepared, and their behavior constitutes the main part of the results chapter. An overview over all the films and their identifiers is given in table 3.1. One important difference between MgO and quartz on the one side and the slightly doped silicon on the other side is the conductivity. Conductive surfaces interact with local charges in adsorbed molecules by *image charges*. If a charge is approached to the substrate, a charge of the opposite sign develops inside a conductive surface by electrostatic induction, which stabilizes the adsorbate.

Silicon prepared in UHV has unsaturated bonds at the substrate surface. These

Film name	Substrate	Thickness/nm	Preparation conditions
film *a*	quartz	360	high vacuum
film *b*	quartz	40	high vacuum
film *c*	quartz	60	high vacuum
film *d*	quartz	40	high vacuum
film *e*	quartz	40	high vacuum
film *f*	Si(111)	40	high vacuum
film *g*	Si(100)	40	high vacuum
film *h*	MgO	40	high vacuum
film *j*	MgO	40	high vacuum
film *k*	Si(111)	20	high vacuum
film *l*	MgO	40	high vacuum
film *m*	MgO	10	high vacuum
film *n*	MgO	5	high vacuum
film *o*	Si(111)	10	UHV
film *p*	MgO	20	UHV

Table 3.1: List of evaporated NO_2BIPS films discussed in this thesis.

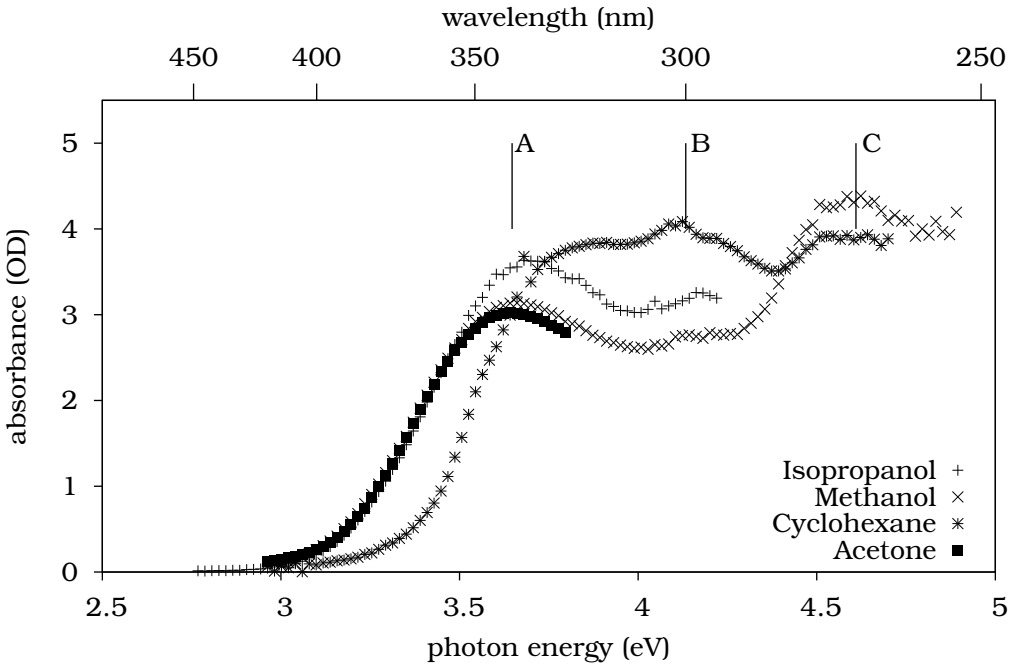

Figure 3.1: Absorption of NO_2BIPS in different solvents. The spectra for all solvents except cyclohexane have the same shape. The indicated transitions are A: chromene n $\rightarrow \pi^*$; B: indole $\pi \rightarrow \pi^*$; C: chromene $\pi \rightarrow \pi^*$

unsaturated bonds can adsorb molecules chemically. If silicon is not prepared in UHV, the unsaturated bonds quickly bind molecules from the environment, so that a saturated surface not consisting of silicon atoms evolves on top of it. The molecules bound to the surface can be chemically exchanged during sample preparation, for example to make a hydrogen-terminated silicon surface.

The main difference between quartz glass substrates and MgO substrates is the single-crystalline surface of MgO opposed to the amorphous structure of quartz glass. Single-crystalline surfaces are able to induce ordered growth of films, while quartz glass will not induce any order.

3.2 Absorption Spectra of Spiropyran

3.2.1 Spectra in Solution

Absorption spectra of NO_2BIPS in different solutions have been acquired using the absorption spectroscopy setup. The concentration of these solutions is 0.32 mM. The optical path length through the cuvettes is 10 mm. The absorption spectrum of spiropyran in different solvents is shown in figure 3.1.

While the absorption spectrum in acetone, methanol and isopropanol is approximately the same, the absorption spectrum in cyclohexane looks completely different,

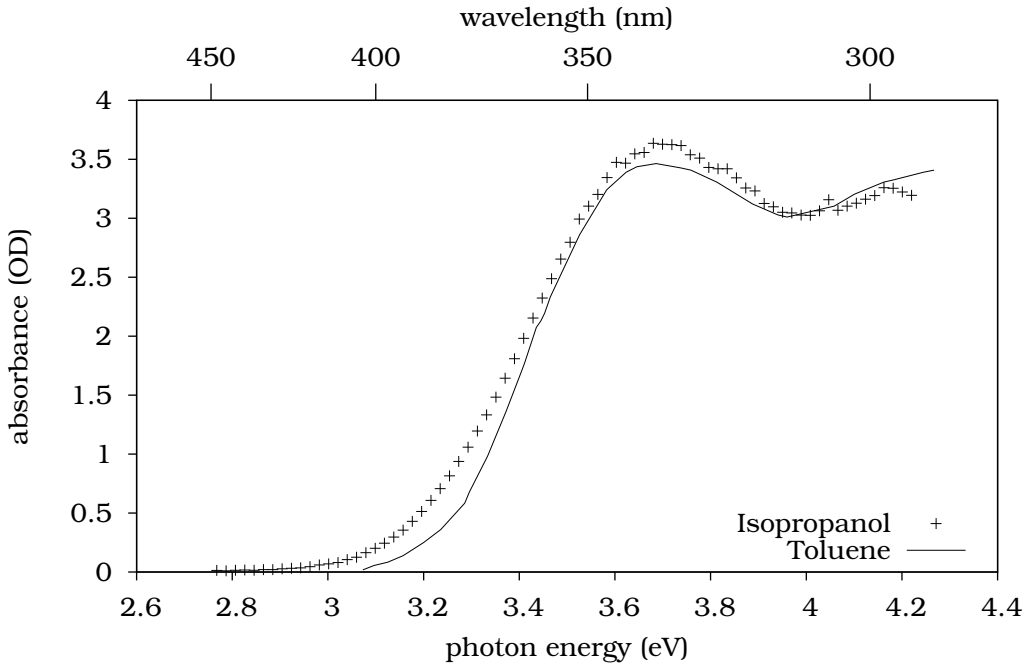

Figure 3.2: Solution absorption spectrum (isopropanol used as representative solvent) and a spectrum from literature in toluene [33]

	Cyclohexane	Toluene	Acetone	Isopropanol	Methanol
μ_D/D	0	0.375	2.88	1.58	1.70
E_T	0.006	0.099	0.355	0.55	0.762
P'	0	2.3	5.4	4.3	6.6

Table 3.2: Solvent polarity properties, showing the molecular dipole moment μ_D according to [63], the normalized Reichardt-Dimroth parameter E_T are according to [12, 64] and Snyder's polarity index P' according to [65].

which is probably caused by the non-polarity of the solvent.

As the NO_2BIPS molecule consists of two ring systems perpendicular to each other, there are two nearly independent π-systems, and the absorption peaks can be attributed to the different parts, the indoline and the nitrochromene part [49]. The lowest energy absorption band at around 3.65 eV (340 nm) is attributed to the nitrochromene half. A second band reported at 4.13 eV (300 nm) at liquid nitrogen temperature [49] is only barely visible in the room temperature measurements performed here. This peak is attributed to the indoline part of the molecule. A third peak at 4.61 eV (269 nm) is again attributed to the nitrochromene part.

Figure 3.2 compares the absorption spectrum to a literature spectrum that has been rescaled to match the concentration and optical path length from our setup. For comparison to the spectra obtained in this thesis, the isopropanol spectrum

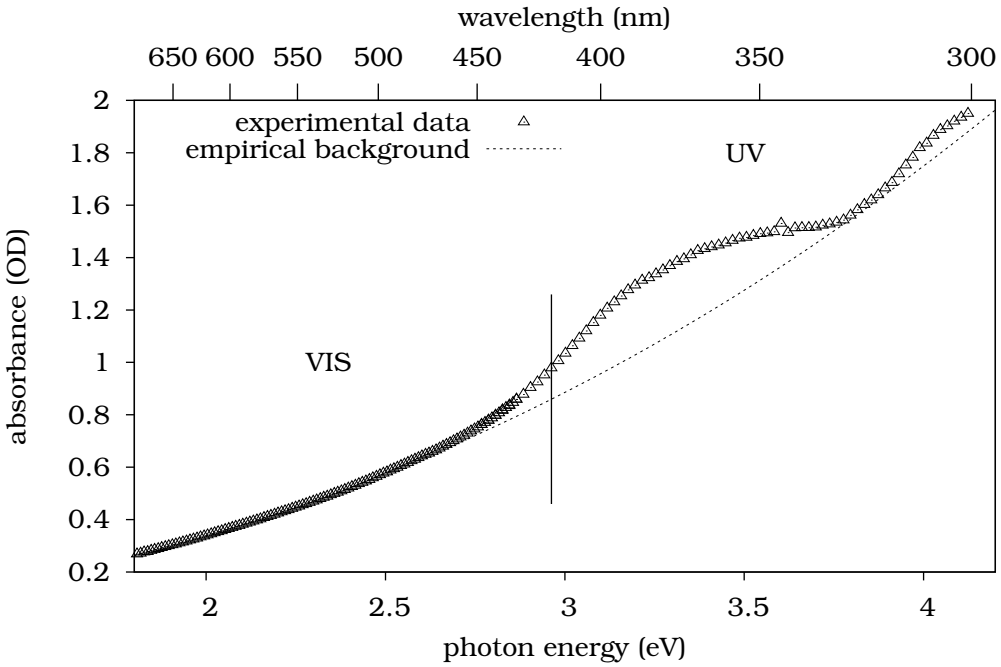

Figure 3.3: Absorption spectrum of film *a* (360 nm/quartz), also showing an empirical model for the background spectrum of this film

is shown as representative spectrum. While the toluene molecule is known to be essentially non-polar with a dipole moment below 0.5 D (see table 3.2), toluene as a solvent in general does not behave like cyclohexane. The empirical polarity parameters, e.g. the Reichardt-Dimroth parameter E_T and Snyder's polarity index P' show a considerable difference between cyclohexane and toluene. In this thesis, the parameter E_T will be used to describe the polarity of a solvent, as it is empirically shown that it describes the interaction between merocyanine and the solvent quite well. The polarity index P' has been added to the table to show that the increased polarity of toluene over cyclohexane is not a peculiarity of the Reichardt-Dimroth parameter, but also observable in different scales. The absorption of NO_2BIPS in toluene shows that the absorption band measured in this thesis is a little bit broader, and the intensity of the first absorption peak is a bit lower. The lower intensity of the first peak might be due to the considerably lower polarity of toluene, but the position and shape of the peak is quite independent of solvent polarity in the range between Toluene with an Reichardt-Dimroth parameter of $E_T = 0.1$ and Methanol with $E_T = 0.76$. The understanding of spiropyran and merocyanine absorption in different solvents (which is well explained in literature) is a prerequisite of interpreting film absorption spectra, which are investigated in the next section.

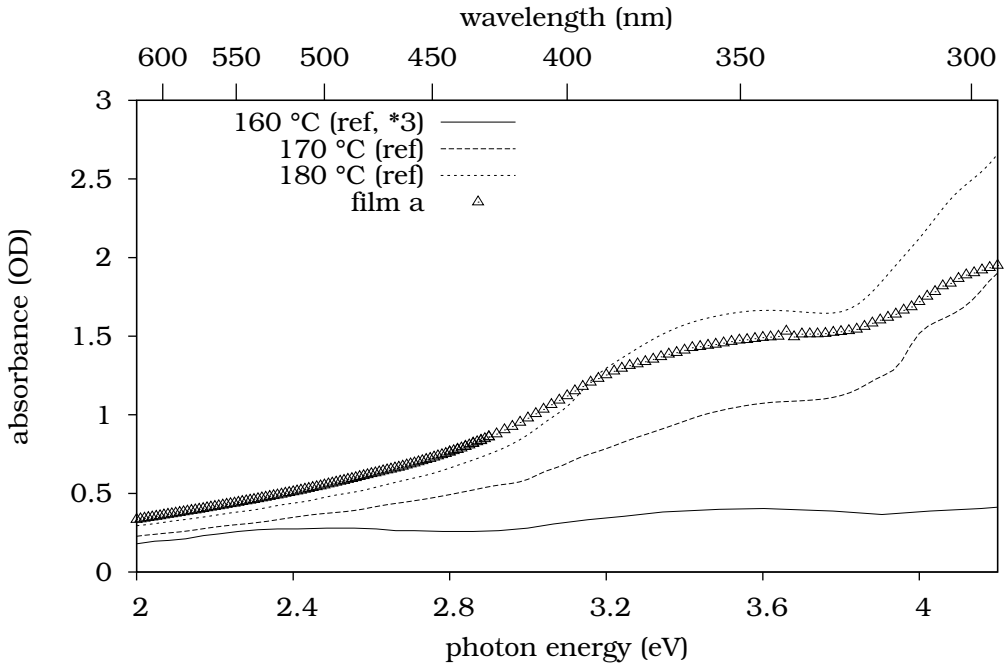

Figure 3.4: Absorbance of film *a* compared to literature for NO_2BIPS films prepared by HV evaporation at different source temperatures. The values are from [66] and scaled by 1.8 to compensate for the different film thickness.

3.2.2 NO_2BIPS Films on Quartz Surface

To investigate spiropyran molecules on surfaces, spiropyran has been evaporated in high vacuum onto chemically cleaned quartz substrates. After evaporation, the exposed area of the substrate surface is opaque. This is interpreted as sign that films were grown. The opaqueness was clearly visible for films of 40 nm or more, and even for 10 nm and 20 nm films on partly coated substrates with a sharp delimiting line. The thickness of these films has been determined during growth using a quartz microbalance. Figure 3.3 shows the absorption spectrum of a 360 nm film grown on quartz (film a). The spectrum contains a primary peak at around 3.25 eV and a second one at around 4.1 eV. these two peaks are on top of a big monotonically increasing background. Comparison to the spectrum in solution suggests that the second absorption peak is caused by the indoline moiety of the molecule, while the first one is at a significantly different position compared to the nitrochromene peak observed in solution. The background is attributed to scattering at the film surface. As the absorption spectrum is measured in a standard transmission setup with a small opening angle of the detector, scattering losses are detected as absorption just like actual absorption of light in the sample.

The interpretation of the observed spectrum as microcrystalline film is supported by literature: In figure 3.4, the absorption spectrum of film *a* is compared to liter-

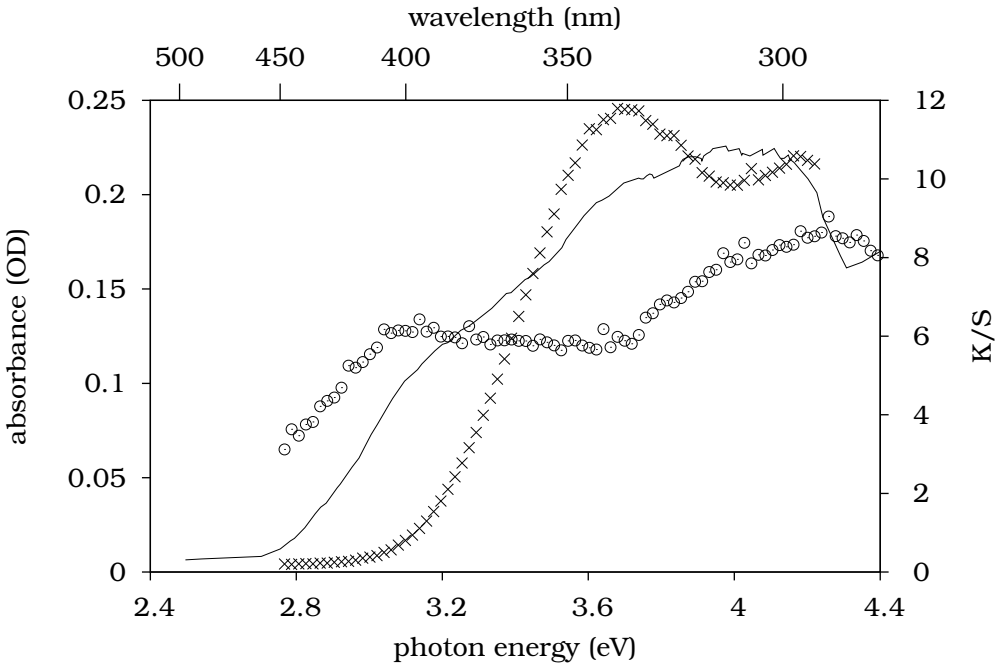

Figure 3.5: Absorbance in OD of film *d* (◯, shifted by −0.1 mOD for clarity), NO_2BIPS solution in isopropanol (×, scaled by 1/15), and the Kubelka-Munk function K/S of NO_2BIPS microcrystals (—) from [33]

ature spectra reported by Yoshida et al in [66]. The literature spectra obtained on a 200 nm film have been rescaled to be comparable with the 360 nm film, assuming linear scaling of the absorbance (i.e. the Beer-Lamber-law). A big increase in absorbance with increasing temperature is observed, which the authors attribute to spiropyran microcrystals. They claim that with increasing temperature one starts to evaporate clusters of spiropyran that assemble to microcrystals on the sample which give rise to big scattering losses. Interestingly, at 160 °C (note the additional scale factor of 3), an absorption peak in the VIS range is observed that might indicate the presence of merocyanine.

The absorption spectrum of film *a* resembles the overall shape of the 170 °C and 180 °C spectrum. The temperature-dependent evaporation rates in their chamber with a pressure during evaporation of $1.5..3 \cdot 10^{-5}$ mbar reported by Yoshida are very low at 150 °C and 160 °C, but start to rise quickly for 170 °C and finally 180 °. In the system preparing film *a* a similar onset of a quickly rising rate was observed at around 155 °C, at a pressure during evaporation around $5 \cdot 10^{-7}$ mbar. The lower threshold temperature is likely connected to the higher vacuum in the system used for this thesis. Film *a* was prepared at a temperature (around 160 °C) which provided "fast" evaporation in our system, and is thus most likely morphologically comparable with the cited spectrum for 170 °C.

In the range of visible light, film *a* has no peak-like features, which is interpreted

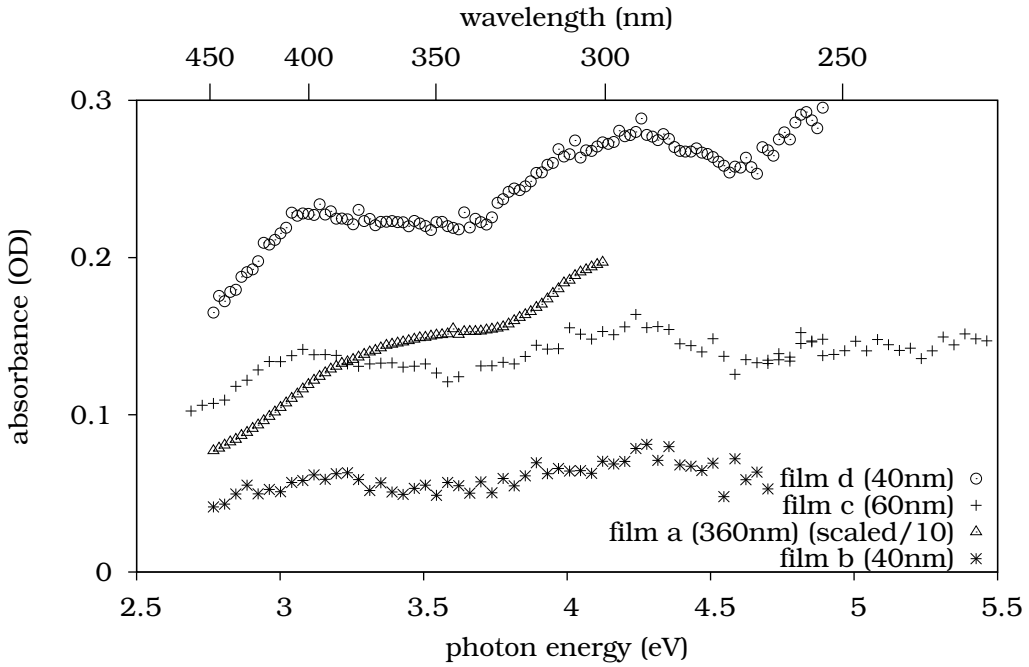

Figure 3.6: Comparison of the absorption of different NO_2BIPS-on-quartz films. No background correction has been applied, but the absorbance of film *a* has been divided by 10 to fit into the same scale. On film *b*, no switching could be observed in later switching experiments.

as indication that after evaporation all molecules are in the spiropyran state. In figure 3.5, the absorption spectrum of film *d* is shown together with the absorption spectrum of NO_2BIPS solution and the Kubelka-Munk parameter K/S of microcrystalline NO_2BIPS quoted from [33] for reference. Clearly the film absorption spectrum matches neither the absorption spectrum of the solution nor the absorption of the microcrystals. The quoted powder spectrum has three main peaks, at 3.1, 3.6 and 4.0 eV, with the latter two coarsely matching the two peaks observed in solution. The first peak of the film spectrum might be a double peak, with maxima around 3.2 and 3.4 eV. In that case, the first peak of the double peak and the second peak at 4.1 eV have corresponding peaks in the powder spectrum, while the second peak of the double peak appears at a different energy.

To compare the absorption intensity of the film with the spectra of solution, an "effective film thickness" of the solution can be calculated from the density of molecules in the solution and comparing that to the density of molecules in a film: A solution with a concentration of 0.32 mM solution has a molecule density of $1927\,\mathrm{nm^{-2}cm^{-1}}$, so the area density is $1927\,\mathrm{nm^{-2}}$ for an optical path length of one centimeter. On the other hand, in a film the volume per crystal unit cell is 3365 Å^3 and there are 8 molecules per unit cell [40], the density of molecules is $2377\,\mathrm{nm^{-2}}\mu\mathrm{m^{-1}}$, i.e. a one micrometer film has 2377 molecules per square nanometer. Thus the area density

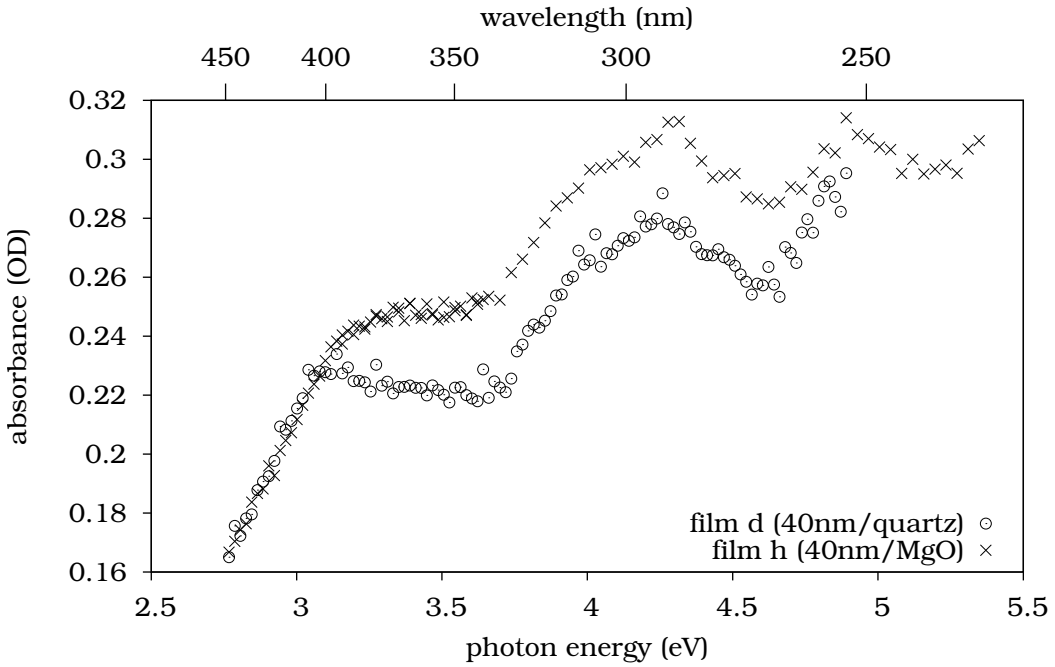

Figure 3.7: Absorption of NO_2BIPS on MgO(100), the absorption spectrum of film *d* (on quartz) is also included for reference (it has already been shown in figure 3.6).

of the solution is equivalent to a film thickness of 810 nm. Yet the 360 nm film exhibits (assuming the background model is valid) a peak absorbance of around 0.3 compared to a peak absorbance of 3.5 for the solution.

The empirically determined background function for the 360 nm film is a power function proportional to $\lambda^{-2.36}$. This indicates that pure Rayleigh scattering is insufficient to describe the background. In that case, the scattering losses are proportional to the fourth power of the wavelength. Rayleigh scattering would occur if the roughness is on a much larger scale than the wavelength of the light.

Figure 3.6 shows a comparison between the absorption spectra of several NO_2BIPS films of different thickness on quartz substrates as prepared. The comparison shows that there is no simple relationship between the nominal film thickness (indicated by the quartz microbalance). The data in these spectra were mostly left as-is, so no kind of scattering background or baseline correction has been applied. The qualitative shape of the three absorption spectra of films below 100 nm looks the same, but the height of the peaks is clearly different. As the curve with the most pronounced peaks as well as the curve with the smallest peaks both are measured at a film of the same nominal thickness, there is obviously no simple relation between the nominal thickness and the peak height, which mean either that the real and nominal thickness are not as closely related as desired or that the structure has a big influence.

As indicated in the caption of figure 3.6, film *b* did not show the spiropyran-to-merocyanine transition on UV irradiation (described more in detail in the following section). The low peak intensity of that film and the missing switching could be a sign that the preparation of that film failed, however film *c*, which also has a quite weak absorption structure in the UV range could successfully be switched.

3.2.3 NO_2BIPS Films on MgO

In contrast to quartz glass, single-crystalline magnesium oxide has a well-defined highly ordered surface, but it also is an insulator crystal and UV transparent like quartz. For this reason, magnesium oxide has been used substrates have been used additionally to quartz substrates, as they might cause the growth of more ordered films.

The absorption spectra of film *h*, 40nm NO_2BIPS on MgO(100), is shown in figure 3.7 as a representative spectrum for spiropyran on magnesium oxide. The film has been grown in the detached small evaporation chamber, on a chemically cleaned MgO substrate. It is compared with the absorption spectrum of film *d*, which is grown on a quartz substrate. The absorption spectrum of film *h* closely resembles the absorption spectrum of the quartz film *d*, so the influence of the different kind of insulating substrates is quite low if present at all.

3.2.4 NO_2BIPS On Non-Insulating Surfaces

As NO_2BIPS molecules have an intrinsic dipole moment, interaction with non-insulating surfaces via induced charges in the substrate could show interesting coupling effects. To investigate them, NO_2BIPS films have also been prepared on silicon and gold on silicon (figure 3.8). The absorption of these films has been measured in reflection, as the substrate is not transparent. The reflection geometry is near-normal. The first thing to note is that the spectral shape is completely different: There is a broad peak at around 2.6 eV to 2.9 eV. This peak is again attributed to scattering, just like the background in the quartz and MgO case, and the different shape may be caused by smaller structure size, shifting the scattering from a region with Rayleigh-like behavior into a Mie-like region. As we will see later, scattering is the dominant effect in these spectra, so the Y axis has been labeled as *extinction* instead of absorbance, as extinction is a more general term including both absorption and scattering.

Comparison between the actual extinction (combining absorption and scattering losses) to simulation of Mie scattering is shown in figure 3.9. The simulated extinction was calculated using MiePlot by Philip Laven [67] for particles with a log-normal size distribution centered at 248 nm and a standard deviation of 24.6%. The dielectric constant n was assumed to be the fixed value 1.6, a typical value for organic molecules. The size distribution data for the simulation is shown in figure 3.10. It shows the expected number of particles of the given sizes contributing to a solid

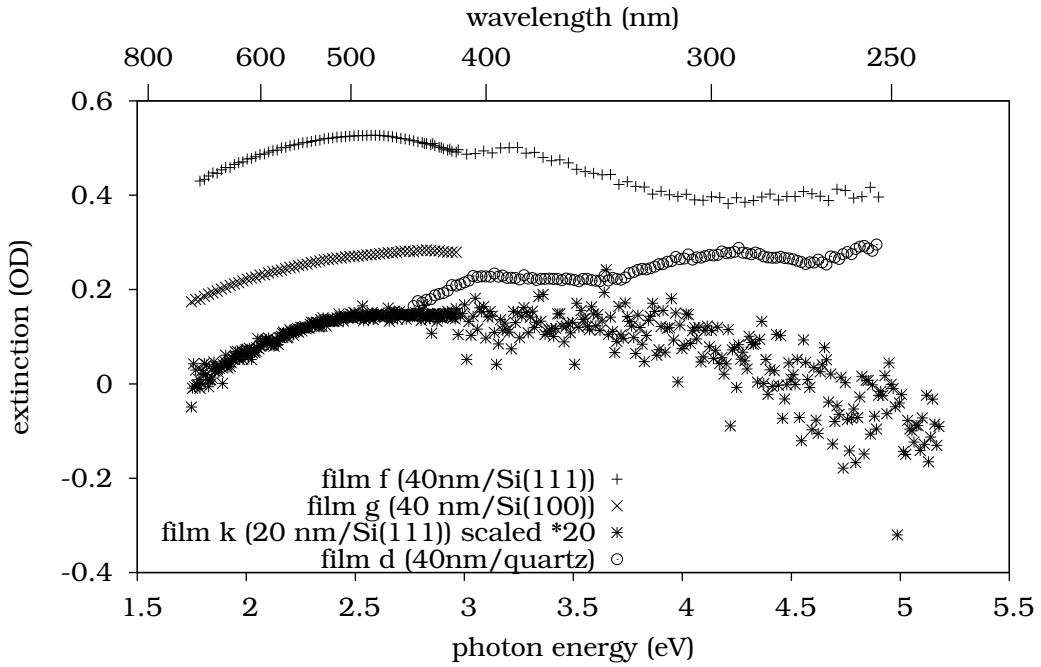

Figure 3.8: Absorption spectra of NO_2BIPS on silicon; the circled symbols for quartz show the same spectrum as in figure 3.7. Please note that the absorbances of film *k* have been multiplied by 20.

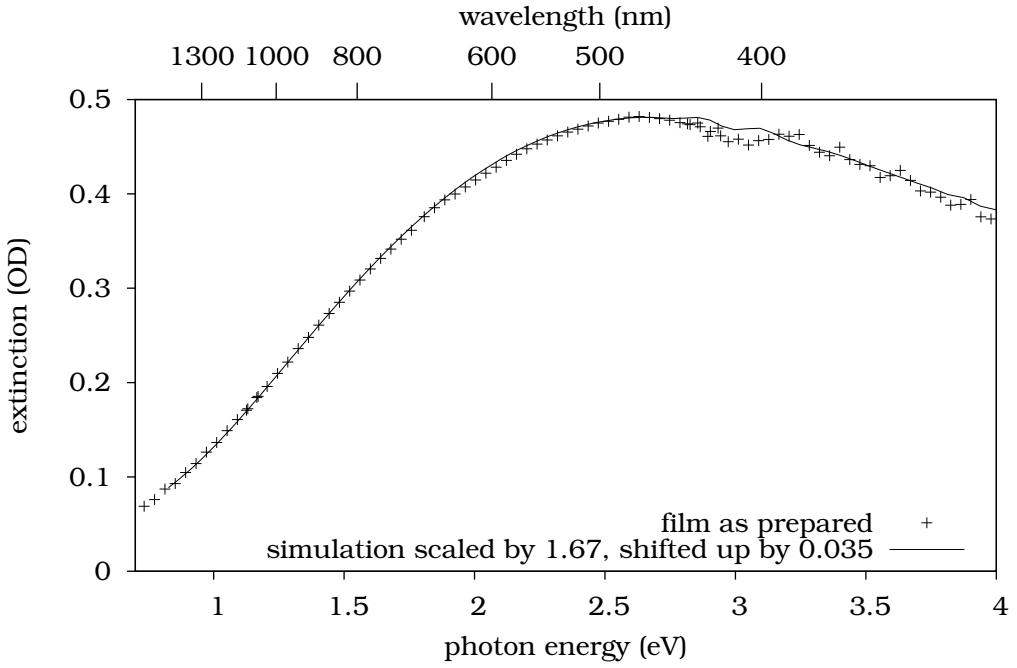

Figure 3.9: Comparison of experimental extinction at film *f*.

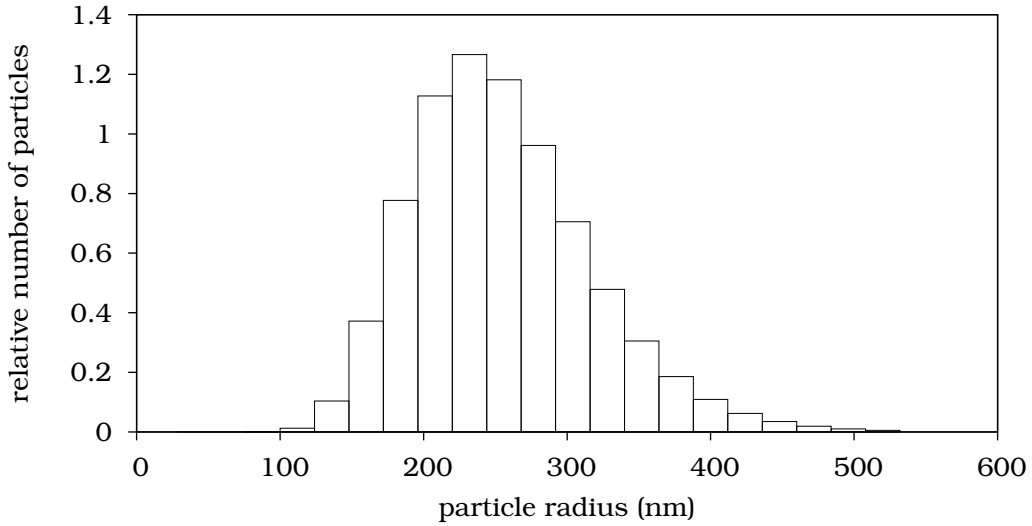

Figure 3.10: Size distribution of NO_2BIPS particles used in the scattering simulations. The y axis shows the number of particles in a 40 nm by 40 nm area in units of 10^{-5} particles for a given size.

volume of $(40\,\mathrm{nm})^3$. As the film thickness measured by the quartz microbalance is 40 nm, the simulated scattering cross-section σ for that volume can be converted to the extinction using $\epsilon = \sigma/A^2 \log_{10}(\mathrm{e})$ with A being the base area of the scattering volume, which is $(40\,\mathrm{nm})^2$. The factor $\log_{10}(\mathrm{e})$ is due to the extinction being presented as *decadic* logarithm. The simulation curve in figure 3.9 shows the calculated extinction multiplied by two because the beam passes the film before and after the reflection at the silicon substrate. It has been scaled by another factor of 1.67 to make the magnitudes of the simulated values and the experimental values match.

Finally, the modelled data curve has been shifted upwards by 35 mOD to correct for a general wavelength-independent baseline (e.g. caused by different overall transmission for the probe and reference beam). This value has been determined by fitting a rayleigh model to the low-energy extinction values.

The quite good match in shape over a wide wavelength range of 1400 nm to 480 nm supports the theory of microcrystalline growth causing scattering-dominated instead of absorption-dominated spectra for NO_2BIPS on silicon for unflashed silicon substrates.

3.3 Absorption of the Merocyanine State

3.3.1 Absorption in Solution

NO_2BIPS was dissolved in acetone, cyclohexane, isopropanol and methanol. All solutions except the solution in cyclohexane show absorption in the range of visible

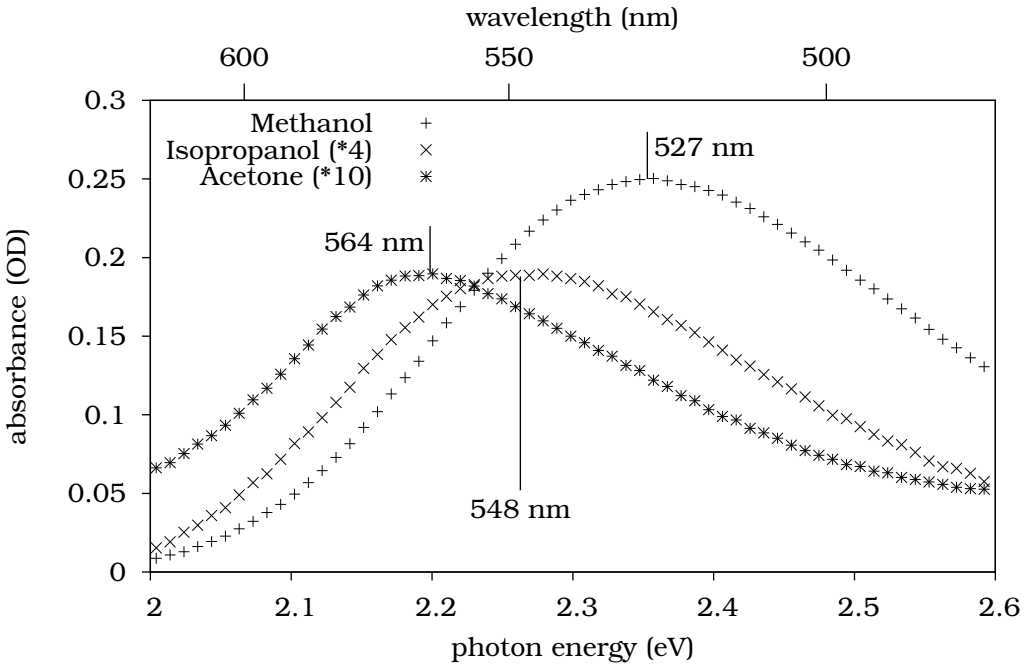

Figure 3.11: absorption spectrum of NO_2BIPS in different solvent - only the range of the merocyanine peak is shown. The curves are ordered by descending polarity of the solvent.

light. This absorption causes a purple color of the solution. This extra peak is attributed to the merocyanine state. The intensity of the absorption peak increases with increasing polarity of the solvent, because the NO_2BIPS molecules in solution are in an equilibrium between the spiropyran and the merocyanine form which is shifted towards the merocyanine state for more polar solvents, which is known [68]. This shift is due to the stabilizing effect of polar molecules on the merocyanine conformation with its high dipole moment. The merocyanine peak is missing in cyclohexane, as the equilibrium is shifted that much to the spiropyran at room temperature that the merocyanine state could not be observed.

Figure 3.11 shows the absorption spectra of NO_2BIPS in different solvents in equilibrium state. UV irradiation increases the intensity of the merocyanine peak, while green irradiation reduces the intensity of the merocyanine peak. Non-equilibrium spectra of solutions are not discussed in this thesis. The merocyanine absorption peak moves toward higher energies for more polar solvents, indicating a higher energy gap between the merocyanine ground state and its first excited state; the first UV transition of the spiropyran on the other hand is nearly independent of the solvent polarity [12].

All spectra of the visible range show just one transition: The merocyanine $\pi \rightarrow \pi^*$ transition, which is the lowest optically excitable one. The maximum position of the acetone peak at (564 ± 2) nm matches the position of 565 nm given in [12], or 562 nm

given in [13]. The observed maxima for for isopropanol and methanol, (548 ± 2) nm and (527 ± 2) nm also agree with 550 nm and 525 nm reported in [13]. The intensity of the peaks drop very steep with decreasing solvent polarity, so they are scaled differently to be comparable in the same graph. The strong intensity difference it not caused by different absorption efficiencies of the molecules depending on the environment but just by different concentration of the merocyanine state. While the total concentration of the solution is (as mentioned above in the discussion of the spiropyran peak) around 0.32 mM in all three of the solvents, the fraction of molecules in the merocyanine state is highly dependent on the polarity of the environment and the solution temperature.

3.3.2 Absorption of NO_2BIPS Films on Insulating Substrates

As the spiropyran molecule prefers the spiropyran form in non-polar environment and also in crystalline form, one can expect that the grown structure of the films will also be spiropyran, as none of the surfaces used has permanent dipole moments. The experimental data of this thesis support this assumption. The only film prepared during this work in which merocyanine could be detected in the state as grown is film *a*, the thick 360 nm film evaporated onto quartz shown in figure 3.12. The merocyanine peak (after subtraction of an empirical background line) has a height of 6 mOD. On thinner films, no significant absorption in the merocyanine range could be identified. The presence of a significant amount of merocyanine only in that thick film can be interpreted as a volume effect, as for a surface effect, the same amount of merocyanine would be expected in thinner films. However, this interpretation is only valid if the structure of the evaporated material is film-like. If the different measured film thicknesses were in fact caused by a different number of spiropyran clusters adsorbed to the surface, the total surface area of the clusters would be proportional to the number of clusters and thus scale linearly with the volume of the film, so volume and surface effects could not be distinguished.

The findings that the film after evaporation is in the spiropyran state seems to contradict the observation that at room temperature the preferred growth state is merocyanine [35]. The authors of that paper investigated the growth of sub-monolayer films of spiropyran on gold single crystals, characterized using STM. The conclusion is that at low temperatures the film grows as spiropyran, but at room temperature it grows as merocyanine. However, the growth conditions were considerably different to the ones used here. While quartz and MgO are insulating substrates, a gold single crystal is conducting and thus it thus stabilizes the more polar merocyanine conformation via image charges. Furthermore the preparation of sub-monolayer films puts an emphasis on the substrate-molecule interaction, while thick layers, especially if clusters or nanocrystals are formed, prefer the spiropyran state which is able to crystallize easily.

Still, this difference in crystallization structure motivated a cooperation experiment between the structural low-temperature STM measurements performed in the

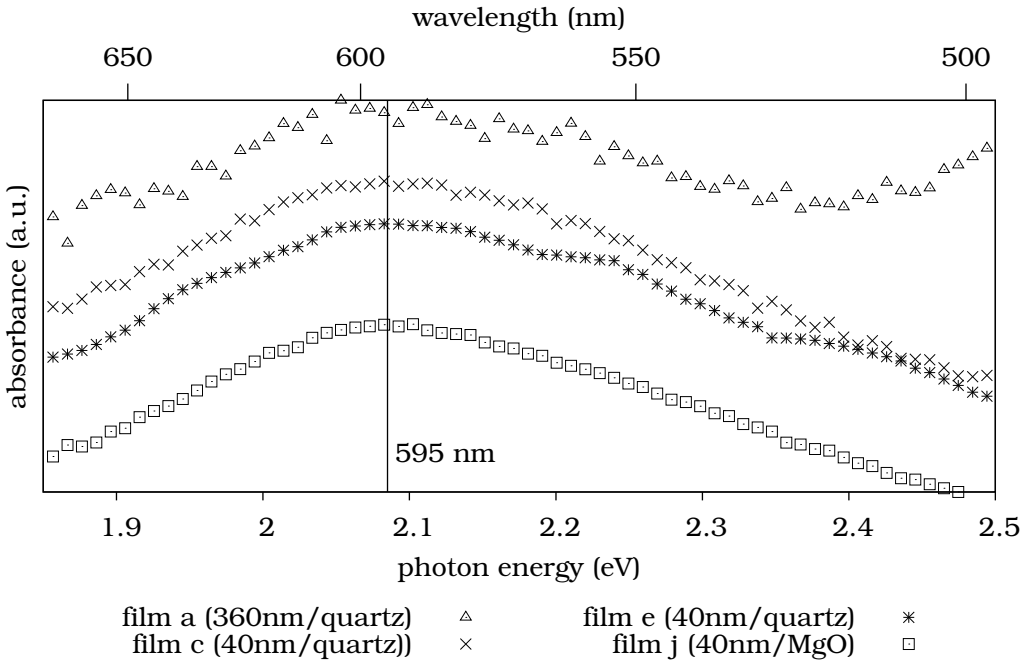

Figure 3.12: Comparison of merocyanine absorption spectra of three different NO_2BIPS films on quartz substrates and one NO_2BIPS on MgO(100) substrate. Spectra after UV irradiation (except for the quartz 360 nm film), arbitrary scale.

working group of Pascual and our optical investigation as complementary methods: An reflection spectroscopy setup had been installed to the LT-STM chamber to observe the reflectivity change of gold on coating with a monolayer spiropyran film. However, as the evaporator in that chamber is mounted in a place where no spectroscopic access is possible, the sample had to be moved from the spectrometer position after acquiring the reflectivity baseline to the evaporation position and back to the first position to measure the reflectivity of the film. It turned out that the spectral changes induced by geometry changes caused by insufficient precision in moving the sample back to exactly the position it had before caused much greater spectral changes (mostly near the plasma edge of gold) than the NO_2BIPS film did.

The discussion thus focusses on the films with a thickness of tens of nanometers listed at the beginning of this chapter. The merocyanine state was prepared by UV light irradiation of the films. The absorption spectra of UV-treated films on quartz is shown in figure 3.12 and compared to the as-prepared merocyanine absorption of film *a*, the only film merocyanine could be detected without UV irradiation. The spectrum of film *a* in figure 3.12 includes correction for the scattering background but no elimination of the spiropyran peak, which is present as well. The spectra of the other films *c*, *e* and *j* are differences between the state before and after illumination to obtain just the merocyanine state. As the intensity depends on

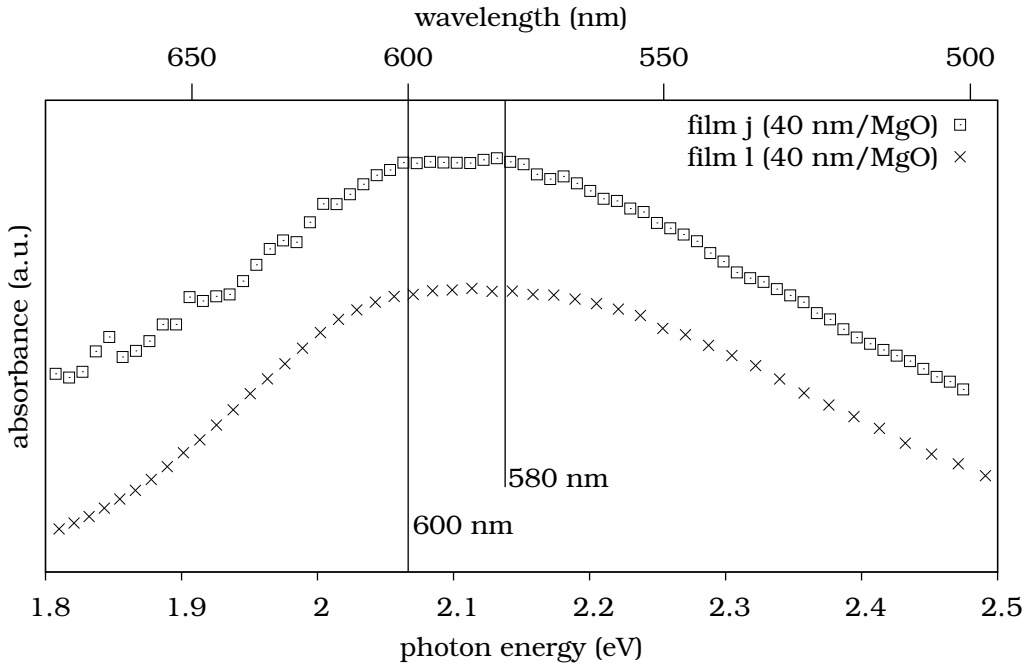

Figure 3.13: Spectra of two NO_2BIPS films on MgO(100). The lines at 600 and 580 nm indicate the maxima of a double peak in the spectrum of film j (upper trace).

merocyanine concentration which in turn depends on exact illumination conditions, the height of the peaks will not be considered, as illumination conditions were vastly different for the films and the merocyanine state was not generally saturated. In that figure, the peaks have been scaled to the same height.

The absorption spectrum of the merocyanine has a single peak at 595 nm. That number is comparable to the peak position of merocyanine in toluene at 600 nm [12]. As the peak position of merocyanine shifts considerably with the chemical environment, which is partly due to the polarity of the environment interacting with the dipole moment of the merocyanine molecules, this indicates a similar chemical environment for the merocyanine in the film, which is indeed the case as toluene is an aromatic solvent, which also applies to the spiropyran and merocyanine molecules.

The spectrum of film j (figure 3.13) has a double peak with maxima at 600 nm and 580 nm, see figure 3.13. The 580 nm peak matches the peak position of the merocyanine absorption maximum in microcrystalline powder reported in [33]. The 600 nm maximum matches the absorption maximum in toluene cited above. The most probable interpretation of this double peak is a mixture of two species of merocyanine which differ either in conformation or aggregation. As mentioned in [69], in non-polar solvents, even at very low concentration, J-aggregates are formed, which indeed have a red-shifted spectrum compared to non-aggregated merocyanine. So this double peak structure can be interpreted as a mixture of non-aggregated an

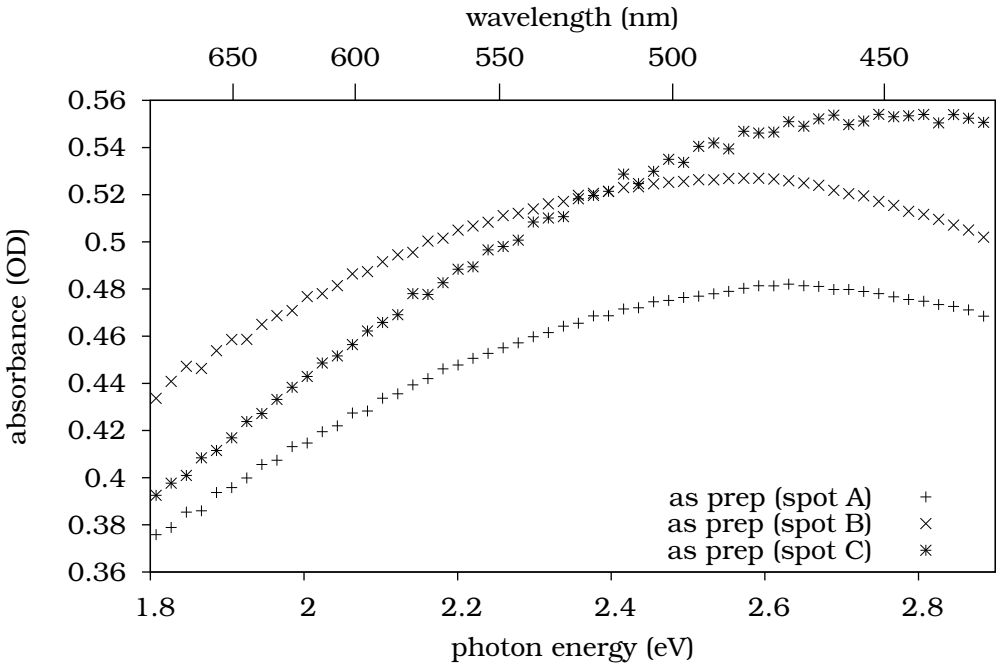

Figure 3.14: Reflection spectrum (near normal) of several unirradiated spots on film *f* (40nm NO_2BIPS/Si(111)) measured *ex-situ*.

J-aggregated merocyanine molecules.

3.3.3 Absorption of NO_2BIPS Films on Silicon

In contrast to the magnesium oxide and quartz samples, the silicon samples have been measured in reflection using near-normal incidence as silicon is not transparent. The structure of the spectrum as grown, even before UV irradiation, is dominated by a peak-like shape in the range around 2.5 eV (figure 3.8) This peak is, as discussed attributed to scattering. The spiropyran growth is microcrystalline on silicon cleaned with organic solvents, as discussed in the spiropyran film absorption spectrum. The scattering properties of the microcrystalline film which is determined by the microcrystal size distribution is found to have high local variations, resulting in significantly different spectra depending on the exact spot on the sample where the absorption spectrum is measured. Figure 3.14 shows the absorbance of three spots on film *f*, a 40 nm NO_2BIPS on Si(111) sample. The distance between the spots is several millimeters, which is larger than the spot diameter of 0.3 mm.

The illumination of these samples was performed outside the spectrometer, so it turns out that the data before/after light exposure are not directly comparable, but relaxation measurements, in which the sample stayed inside the dark spectrometer for 18 hours without being irradiated show the relaxation of merocyanine back to the spiropyran state on a constant background. Figure 3.15 shows the initial absorption

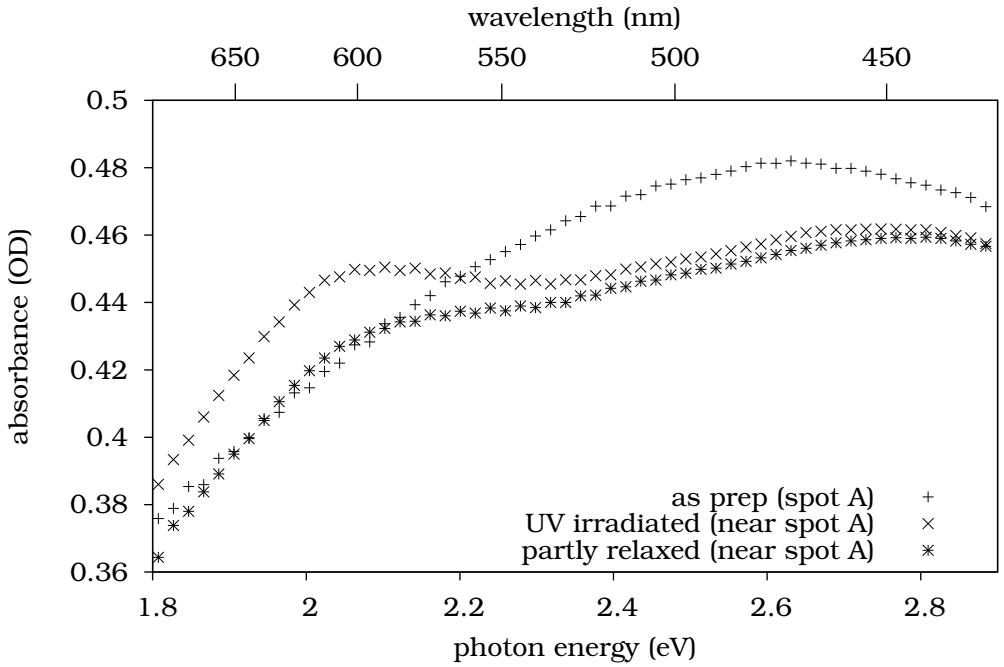

Figure 3.15: reflection spectrum (near normal) of film f (40nm NO_2BIPS/Si(111)) measured *ex-situ* before/after UV irradiation. Spectra have been smoothed by a five-point moving average filter.

at some spot of the sample (+), the absorption measured at approximately the same spot after irradiating UV light having the sample removed from the spectrometer ($\times$), and finally after 18 hours in the dark with the sample inside the spectrometer ($*$). The spectrum of spot A before and after irradiation of UV looks considerably different. This observation has two possible explanations: Either, as discussed above, it indicates that the sample position is not reproduced good enough, or it indicates structural changes caused by the light irradiation. The latter explanation is also plausible through heating the sample during irradiation, but the net effect of either reason is that the spectral change induced by UV irradiation is not just due to the formation of merocyanine.

Figure 3.16 shows the absorbance change from relaxation of film f after UV irradiation. Two curves for two relaxation processes are shown. The solid curve is the difference between the two spectra $*$ and $\times$ in figure 3.15. The dashed curve is a second relaxation observed after another UV irradiation on the same film at nearly the same position. Both difference spectra show the same overall structure: A single peak with an maximum around 640 nm. This peak is red-shifted compared to peak observed on MgO and quartz substrates.

The longest wavelength of merocyanine absorption reported in solution is 605 nm for apolar solvents [12]. On the other hand, an absorption peak at 626 nm is reported for merocyanine platelets consisting of J-aggregates [14]. The polarity of the me-

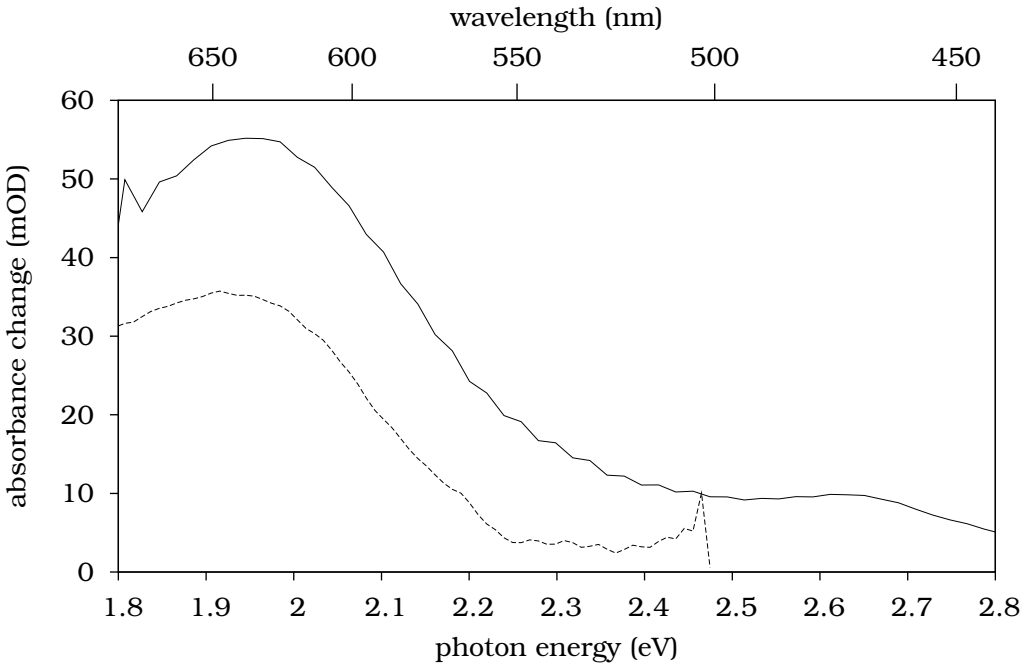

Figure 3.16: Absorbance change by relaxation of film *f* (40 nm NO_2BIPS on Si(111)), measured *ex-situ*. The difference of the absorbance after illumination relative to the absorbance after 18 hours in the dark is shown for two relaxation processes. The spectra have been smoothed by a five-point moving average filter, applied twice.

rocyanine molecules causes a shift of the electron density in neighboring molecules, influencing the energy of the electronic states. In the case of J aggregates, the molecules are oriented parallel to each other. As the absorption wavelength of 640 nm observed here is considerably longer than all wavelengths observed in solutions, the red-shift can not be explained by the environment of single molecules, the red-shift is considered to be caused by inter-molecular interactions. There are still two possibilities for the cause of the extreme red-shift: Interaction between NO_2BIPS molecules and interaction between NO_2BIPS and the silicon substrate.

The big, inhomogeneous scattering background in the NO_2BIPS-on-silicon samples indicates an inhomogeneous, microcrystalline growth. The substrates used in that experiment were only cleaned chemically with organic solvents and thus still contain the native oxide layer. This layer is not necessarily atomically flat. Also the growth at around 10^{-7} mbar is expected to result in films contaminated with residual gas molecules. Finally the spectroscopy outside of the UHV chamber is not able to prevent moisture from air interacting with the spiropyran film. Therefore, the experiment has been repeated inside an UHV system where sample preparation, growth and spectroscopy is possible.

The UHV system enables to prepare the Si(111) surface by flashing, and thus

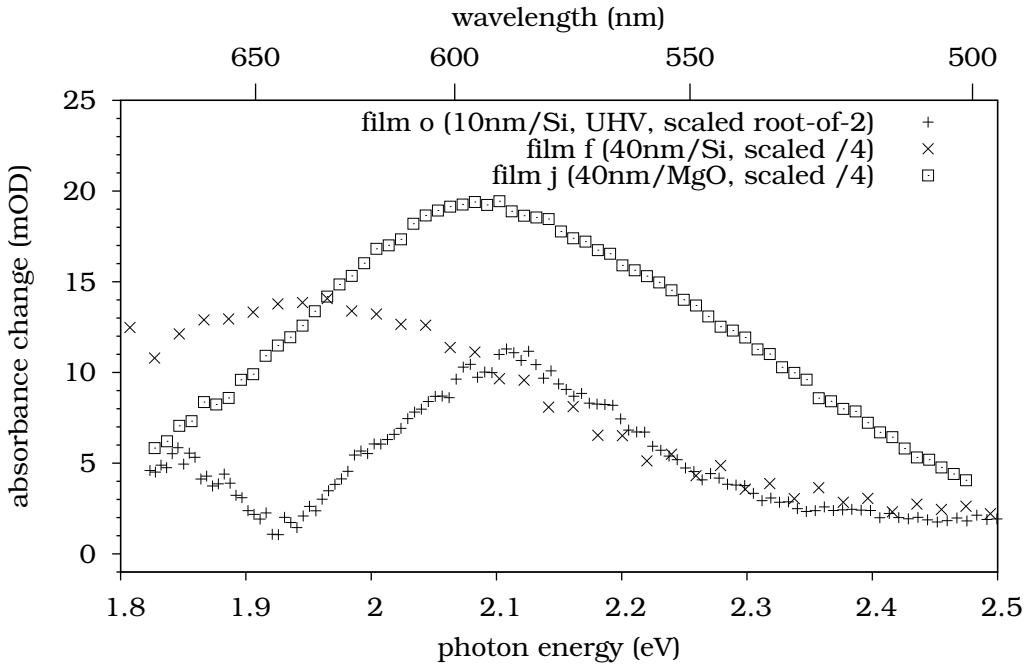

Figure 3.17: reflection spectrum 45° incidence of film *o* (10 nm NO_2BIPS/Si(111)) measured *in-situ* on a flashed substrate. For comparison with an *ex-situ* investigated film, a near-normal-incidence spectrum of film *f* (40 nm NO_2BIPS/Si(111) is shown. The absorbance on a 40 nm NO_2BIPS/MgO film also shown for comparison with a more film without structured scattering background in the VIS range.

completely removing any adsorbed molecules and oxygen layers.The Si(111) surface has one dangling bond per atom in the top layer, which is energetically not favorable. This causes the atoms in the top layers to rearrange to get an overlap of the electronic wave functions, yielding the 7x7 reconstruction. The successful preparation of Si(111) was verified by LEED and STM imaging. The prepared atomically flat surface was then coated with NO_2BIPS in an evaporation chamber at around 10^{-8} mbar and investigated at 10^{-10} mbar.

Figure 3.17 shows the absorbance change on UV irradiation of a 10 nm NO_2BIPS film on Si(111) film prepared and investigated in the UHV system (+) compared to merocyanine-induced absorbance change of the 40 nm NO_2BIPS/Si(111) film discussed above (∗). The spectra look completely different. While the HV-grown, on-air characterized spectrum shows one broad peak around 640 nm, the UHV-grown sample measured in-situ has two peaks in the spectrum: One at 588 nm (= 2.11 eV) and a second one at 670 nm (= 1.85 eV). The picture also includes film *j* which has been grown on MgO. On MgO, the spectral difference between UHV-prepared samples and HV-prepared samples is minimal, see figure 3.13.

As the in-situ measurement used for the UHV grown film has no reference beam,

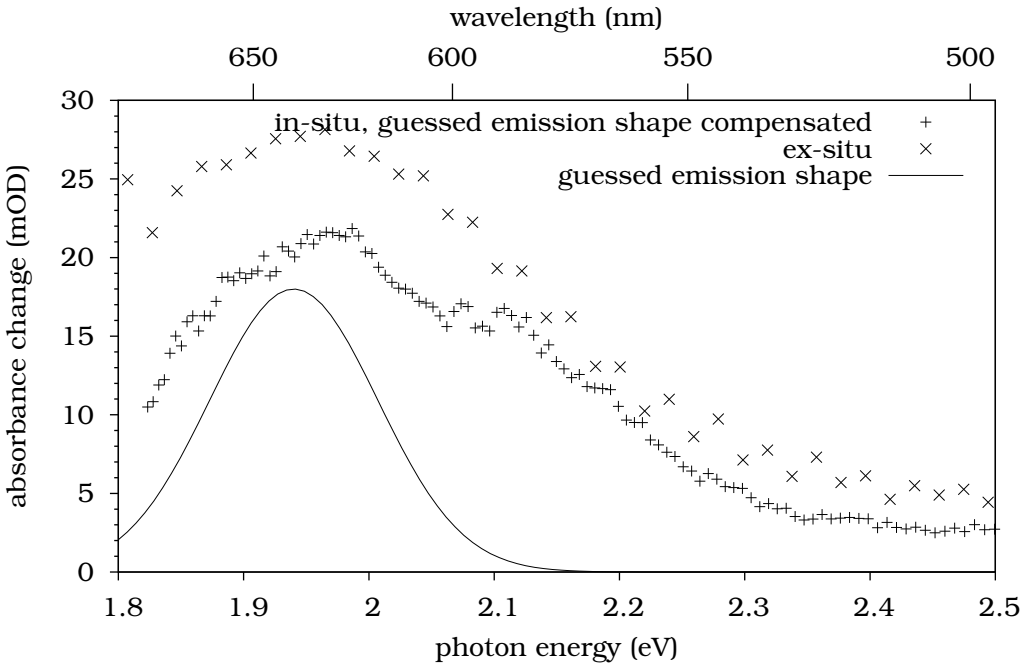

Figure 3.18: Comparison of the absorption spectrum of film *o*, grown and investigated in UHV with the spectrum of film *g*, investigated *ex-situ*, after compensating for the suspected emission dip in the spectrum.

no absolute absorptions could be determined, but just absorbance changes, e.g. induced by light irradiation. The curves shown for comparison are also absorbance differences between the initial state (assumed as spiropyran) and illuminated state (contains merocyanine). The spectrum of the *ex-situ* investigated film on silicon as well as the spectrum of the NO_2BIPS film on MgO, show only one broad absorption peak, while the *in-situ* grown and measured film shows two absorption peaks, which appear to have sharper edges than the single broad peaks of the other two films.

The sharper peaks could be interpreted as a sign of more ordered growth, as the position of the absorption maximum of an individual molecule depends on the properties of the environment of this molecules. In an unordered ensemble of these molecules, each molecule has a different environment and absorbs at a different wavelength, causing absorption peaks to broaden. With this assumption, the double-peak structure would be explained as merocyanine molecules in two different, well-defined environment, for example in thin film and in microcrystals.

But that assumption must be rejected, because after further illuminations of film *o*, it becomes obvious that both peaks of the supposed double peak structure have the same kinetic behavior, which is not expected for a double peak caused by spiropyran molecules in different environments, as the quantum efficiency of switching is highly environment dependent. Instead, the spectrum is assumed to be from a single species of merocyanine in a single environment, but in that case the peak

shape needs further explanation.

The *in-situ* spectroscopy setup uses white light illumination and wavelength-resolved detection. This has the direct consequence that fluorescent light getting to the detector is considered as increased transmission on the emission wavelength. As standard fluorescence is undirected and the acceptance angle of the spectroscopy setup used is quite small, the amount of collected light from fluorescence is expected to be very small compared the the reflected light from the source. But this reasoning only takes spontaneous emission into account. By stimulated emission, on the other hand, the emitted photons go into the same direction as the stimulating photon, so both of these photons reach the detector. There is a report of notable amplification of spontaneously emitted light by stimulated emission in an NO_2BIPS doped PEMMA[1] matrix in [70]. While that paper focusses on the amplification of originally spontaneously emitted fluorescence photons, there is no reason for spontaneous emission not to work with stimulating photons from the white-light source used for spectroscopy.

The interpretation of the peak shape as broad peak with a dip in it caused by stimulated emission rises the question why that peak shape could be observed only in *in-situ* UHV spectroscopy, although white-light spectroscopy has also been used outside of UHV for some samples. The explanation seems to be that the fluorescence of the excited merocyanine state is quenched by the presence of oxygen. In [51], the life-time of the excited merocyanine (of a different spiropyran derivative, though) is claimed to have the 100-fold lifetime in argon-saturated solution (around 4 μs) compared to oxygen-saturated solution (around 40 ns). As in the ex-situ spectroscopy the sample was always in contact with air (and thus oxygen), the excited state is not long-lived enough in that case to observe stimulated emission.

Figure 3.18 shows a possible emission peak and the resultant absorption curve after correcting for it (+) as well as the *ex-situ* investigated absorption peak. While the guessed corrected spectrum still does not look the same as the *ex-situ* acquired spectrum, the overall peak shape now resembles the *ex-situ* acquired spectrum both in the peak position (which of course is very sensitive to the exact guessed emission shape and thus not really considered relevant) and the peak width.

3.4 Fluorescence Properties of Merocyanine

Using fluorescence instead of absorption is advantageous for detecting the merocyanine state because the relative change of the signal is much higher than in absorption spectroscopy: As an example, at an optical density of 0.004, the light intensity is reduced to 99 % of the original level. This means the detected signal shows a relative change of 1 % comparing transmission through spiropyran to transmission through merocyanine. Considering the relative change is sensible, since some noise sources increase with increasing signal intensity. For example, illumination light intensity

[1] poly(ethyl methacrylate-co-methyl acrylate), a copolymer

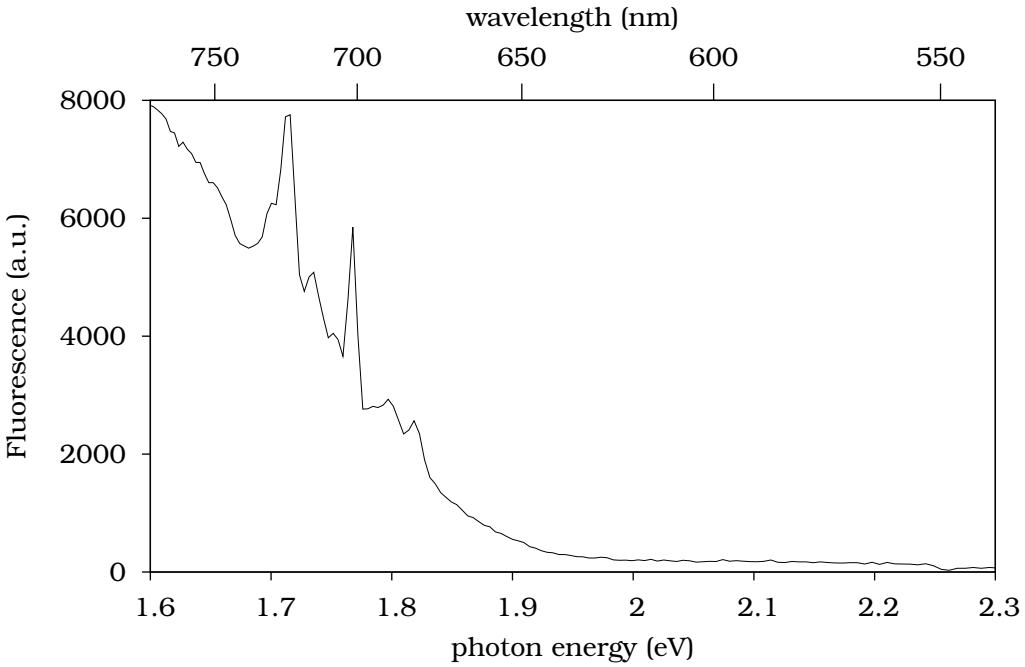

Figure 3.19: fluorescence of an uncoated MgO substrate

variations directly affect the measured signal, and shot noise in the detector is proportional to the square root of the incident light intensity.

On the other hand, in a fluorescence setup exciting at 532 nm, spiropyran does not exhibit any fluorescence, while merocyanine does. That means that if there is no merocyanine present, the detected optical signal just consists of stray light. This stray light can be kept below the intrinsic noise of the detector in good optical setups. If merocyanine is present, a sufficiently sensitive setup can detect the fluorescence at a level way above the background noise, so the relative change of the signal in the fluorescence case is 100 % which is considerably larger than the 1 % in absorption spectroscopy.

For monomolecular films, the absorbance signal is expected to be even lower than the 4 mOD used in the example above, thus gaining an even higher advantage of fluorescence compared to absorption in respect to relative signal change.

All fluorescence spectra in this chapter have been acquired using a standard frequency doubled Nd:YAG laser at an emission wavelength of 532 nm. The fluorescencent light is collected into the entrance port of an imaging spectrograph and acquired using a CCD camera. Figure 3.19 shows the fluorescence spectrum of an MgO substrate as delivered from MaTecK. It shows a background in the the red and near IR range, starting at 660 nm, and some quite sharp characteristic peaks. This fluorescence is caused by crystal impurities. The peak around 700 nm is the Cr^{3+} R-line [71]. The crystal field of the magnesium oxides induces an (unresolved) crystal field splitting of this line into two lines called N-lines at 699.2 nm an 703.8 nm,

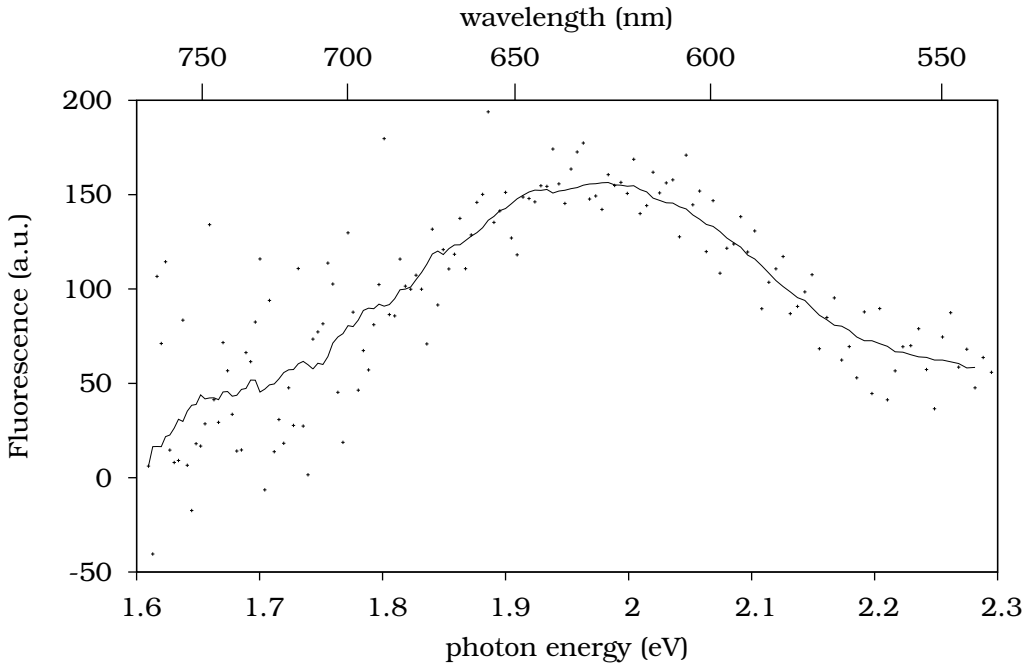

Figure 3.20: Fluorescence of merocyanine on MgO (film p), after applying MgO background correction. The small points indicate measured values, line is a smoothed as a guide to the eye.

whereas the line at 720 nm is a vibrational sideband of this transition [72]. The less prominent peaks in the same range are further vibrational sidebands of the same transition.

The fluorescence spectrum of magnesium oxide on irradiation with a 532 nm laser looks unchanged before and after the evaporation of NO_2BIPS molecules. This indicates that no fluorescence emission from these molecules is observable, which suggests the molecules being in the spiropyran state. The spiropyran state has no absorption at 532 nm (2.33 eV), so fluorescence can not be excited using this laser. Figure 3.20 shows the fluorescence after UV irradiation. The spectrum contains a broad peak centered around 625 nm, which is assigned to the merocyanine state. The scale on the Y axis of figures 3.19 and 3.20 is identical, so the background signal of the MgO substrate dominates the NO_2BIPS fluorescence in the left half of the peak (wavelength longer than 650 nm), while the right half (wavelength lower than 630 nm) of the peak is in a wavelength range with no substrate fluorescence. The high background level at longer wavelengths is responsible for the noisy signal, which supports the approach of using a detection mode with low background signal.

While the big background signal in the long wavelength area prevents taking full advantage of the fluorescence measurement, the short wavelength region shows the potential in fluorescence detection. The fluorescence intensity is likely to be increased further by using a longer excitation wavelength, as the absorption maxi-

mum is around 580 to 600 nm for NO_2BIPS on MgO, as seen in figure 3.13. While this might also increase the background intensity fluorescence, in the range of 600 to 650 nm, signal-to-noise ratio is still expected to improve.

4 Results: Kinetic Behaviour

First of all, the application of spiropyran as molecular switches requires investigations of the two states as shown in the previous chapter. To develop methods how to reliably switch molecules from one state into the other state, the spectral changes on illumination of both UV and VIS light as well as thermal relaxation have been investigated depending on temperature, environment, film thickness and illumination duration and intensity.

Both the photo-induced switching to the merocyanine state and also the photo-induced switching back to the spiropyran state could be observed in solution and for samples grown in vacuum.

4.1 Thermal Relaxation of Dissolved Spiropyran

The spiropyran solution samples presented in the previous chapter have been irradiated by UV (filtered light from a xenon arc lamp) and VIS light (a 25 mW green laser at 532 nm) respectively. After the irradiation, the merocyanine absorption band (represented by the absorption at 2.3 eV= 539 nm) has been continuously measured to monitor the relaxation back into the equilibrium state. For the solutions in acetone exponential relaxation was observed (figures 4.1), while the monoexponential model fits the NO_2BIPS-in-methanol solution only after some time (figure 4.2).

The non-exponential behavior of the solution in methanol indicates that this is not just a first-order process between two states. For the spectra in methanol, the shape can also not be explained by two different merocyanine conformations relax to spiropyran with different time constants. In that case, one would observe the combined absorption of both conformations directly after illumination while some time later the amount of the component with fast decay is negligible, and only the conformation with the slower decay is would be observed. So fitting to the end of the decay curve would results in a fit that only describes the slow component, and stays below the experimental curve that also includes the fast component. The observed data shows the contrary: The fit from the late end of the curve predicts higher absorption in the early time after illumination than observed, which indicates that directly after illumination there is still something happening which increases the merocyanine absorption. This could be a long-lived excited state that slowly decays into the merocyanine state and compensates thermal relaxation, but no excited states with life times in the order of 20 minutes are known. More likely is thus a second dynamic equilibrium between aggregated and monomeric merocyanine with

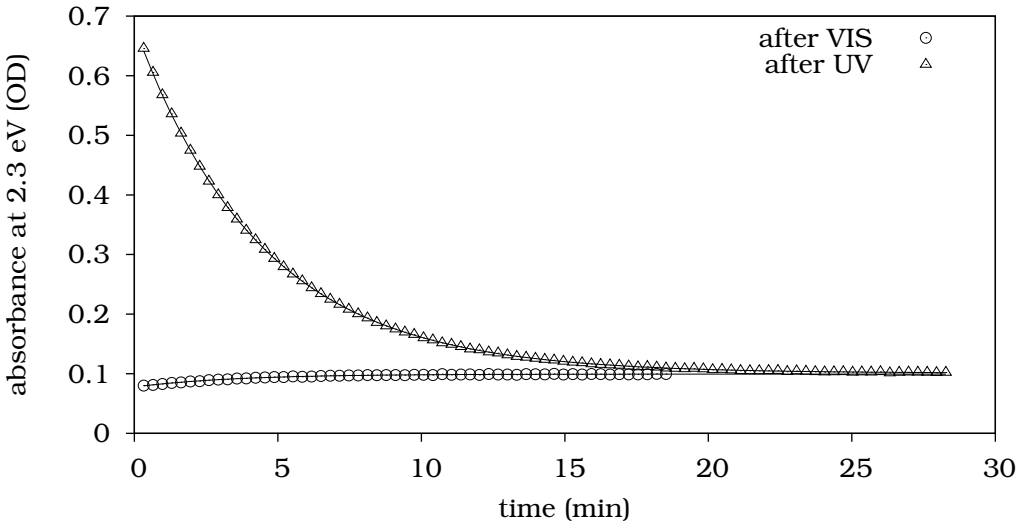

Figure 4.1: Absorbance of the merocyanine fraction (measured at 2.3 eV (539 nm) as representative wavelength) of the NO_2BIPS dissolved in acetone after irradiation with VIS or UV light. The solid lines show a single exponential decay to equilibrium.

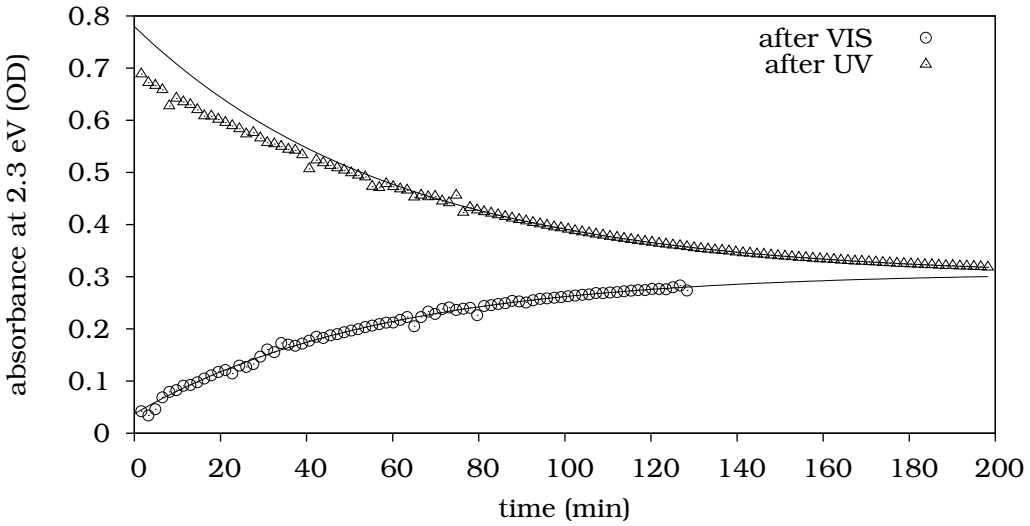

Figure 4.2: Absorbance of the merocyanine fraction (measured at 2.3 eV (539 nm) as representative wavelength) of the NO_2BIPS dissolved in methanol after irradiation with VIS or UV light. The solid lines show a single exponential decay to equilibrium. In the UV case the model doesn't match the data in the first hour, see the text for discussion.

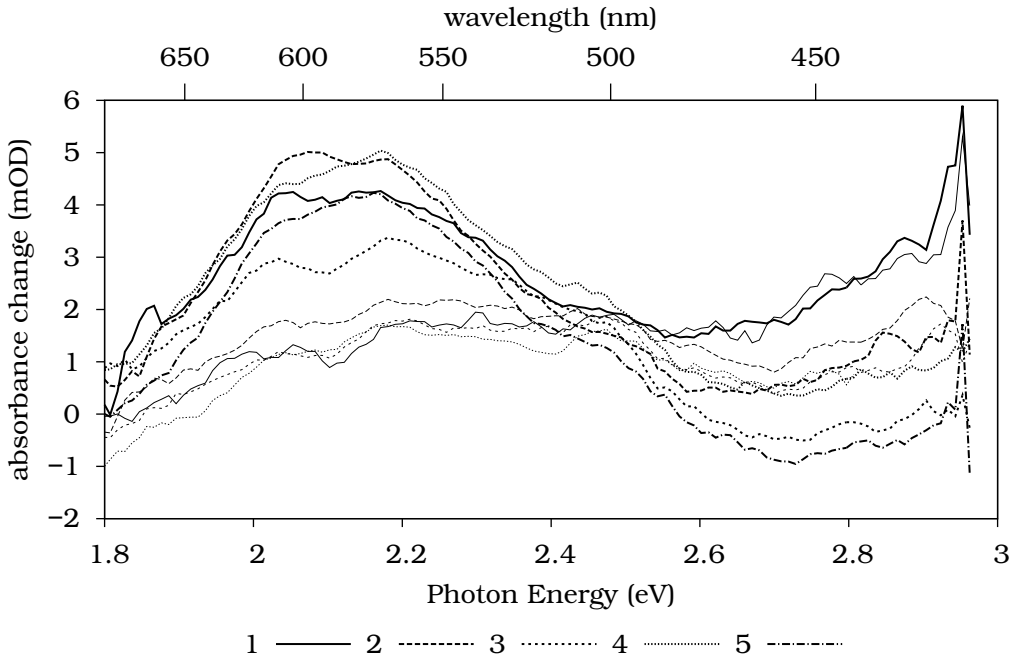

Figure 4.3: Spectra of repeatedly switching film *c* (40 nm/quartz). The thick lines are after UV irradiation, the thin lines after the next VIS irradiation. The numbers 1 to 5 indicate successive switching cycles. The spectra have been smoothed by a five-point moving average filter.

the aggregated merocyanine having a lower absorbance at 2.3 eV than the monomeric one.

In a dynamic equilibrium, relaxation towards the equilibrium has the same time constant for approaching the equilibrium state from both sides, so only one time constant is expected for relaxation both after UV and after VIS irradiation, and this is also observed experimentally. Relaxation is considerably slower in methanol ($\tau = (3500 \pm 100)$ s) than in acetone ($\tau \approx (230 \pm 20)$ s), indicating a lower energy difference or higher barrier in methanol caused by the higher polarity of the solvent. According to [73], the main influence is the energy difference.

4.2 Samples on Quartz

Figure 4.3 shows the reversible photochromism in the UV-VIS spectra of a 40 nm NO_2BIPS film on quartz. It shows the absorption spectrum after background correction by subtracting the spectrum of an unilluminated spot (a scale factor of 0.96 was applied to the absorbance of the unilluminated spot to compensate for small thickness differences). Film *c* has been alternately irradiated by UV and VIS light. The thick lines show the absorption spectra after UV irradiation, while the thin lines of the same dashing pattern show the absorption pattern after the corresponding

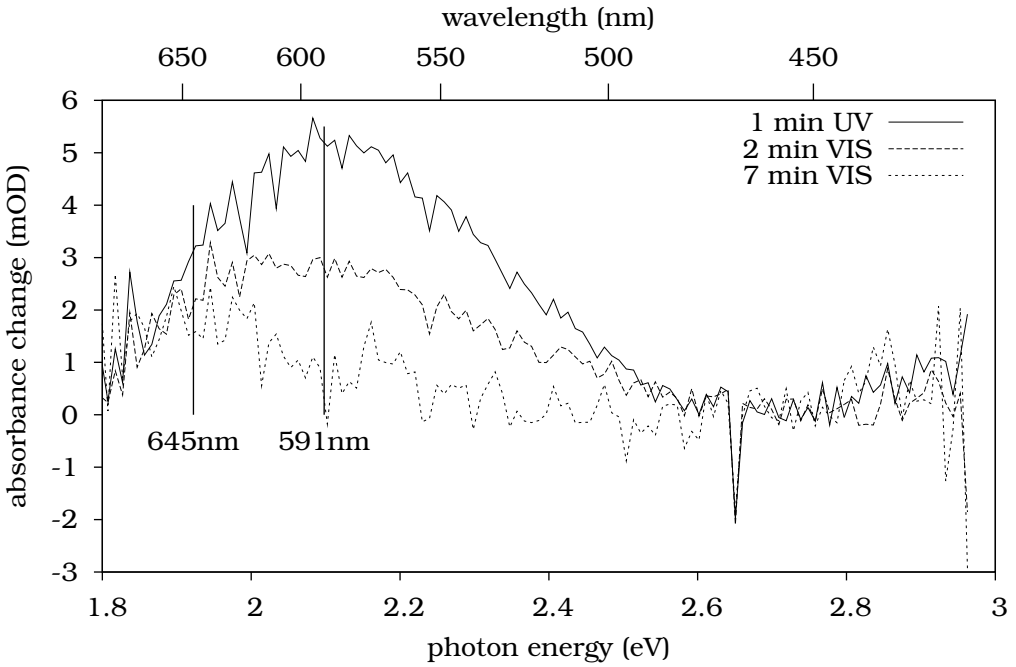

Figure 4.4: Absorbance change of film *e* (40nm NO_2BIPS on quartz) after the first three irradiation.

VIS irradiation. The acquisition time of the absorption spectra (around 20 to 30 minutes) is short compared to observed thermal relaxation with a half-life of around a day. The irradiation time was 5 minutes for UV and 10 minutes for VIS light, performed outside the spectrometer. The sample has been realigned in the spectrometer to an accuracy of 0.05 mm after irradiation. The spectrum after the third UV irradiation seems misaligned, and is thus not included in the discussion.

The spectra show a quite good overall reversibility and reproducibility of the switching in the range between 1.8 and 2.4 eV, which is the merocyanine absorption peak. They also show a change of the absorption in the range above 2.5 eV. The absorbance in the range above 2.5 eV is monotonically decreasing, which might be due to bleaching of spiropyran molecules, i.e. UV-induced destruction of the adsorbed spiropyran film.

Figure 4.4 shows the initial response of film *e* to light irradiation. This film has been irradiated inside the spectrometer to get rid off alignment errors on removal/reinsertion of the film, but for technical reasons, it made sharp focussing difficult, so a wide area on that sample has been exposed to the light irradiation. The consequence is that all experiments on that sample accumulate. The figure shows the absorbance change of the film as prepared, without previous illumination experiments performed on it. After one minute UV irradiation, a maximum is clearly visible around 591 nm. The dashed line shows the absorbance change between the initial state before light irradiation and the absorbance after one minute UV followed

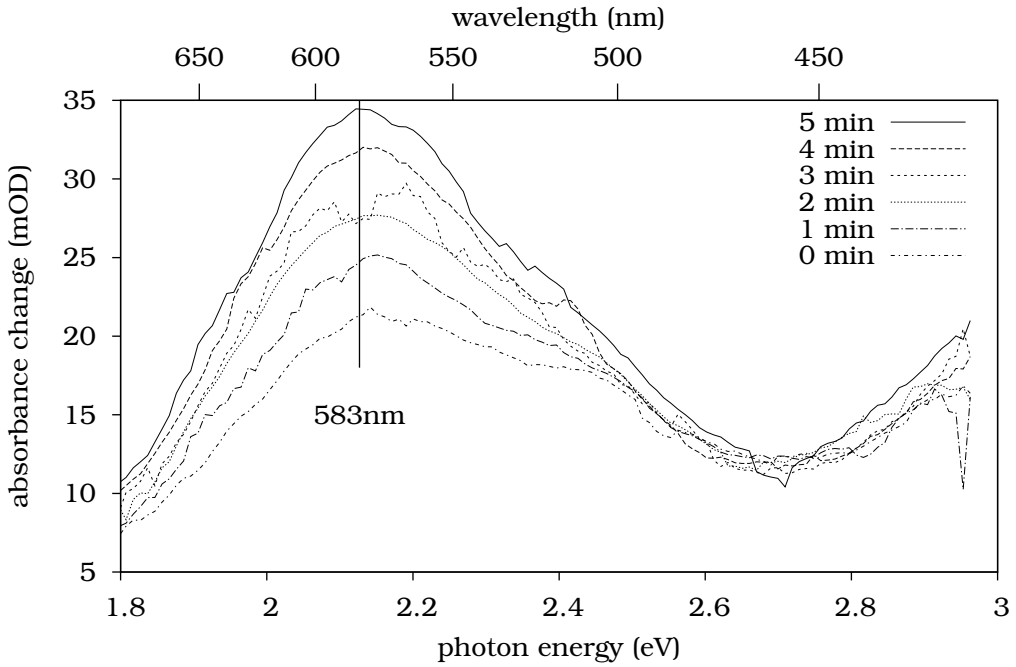

Figure 4.5: Absorbance change of film *e* (40nm NO_2BIPS on quartz) on a one-minute-per-cycle illumination series.

by 2 min VIS irradiation. A shift of the absorbance towards lower energies is visible in that spectrum.

This shift is considered to be caused by a fraction of merocyanine with an absorption maximum at longer wavelength than 591 nm which is not responding to VIS light irradiation. This claim is supported by the spectrum obtained after irradiating VIS light for another five minutes to a total of seven minutes. The main merocyanine peak has vanished, but a residue is remaining at 645 nm.

Figure 4.5 shows the absorption spectra of film *e* during a series of one-minute UV irradiation processes. This series has been acquired after some previous illumination experiments on that film, which causes the not easily switchable background visible in that figure. This figure shows a rising peak near 583 nm. This does not match the 591 nm observed as maximum position in the first switching experiments on that sample (see figure 4.4), but keep in mind that these spectra are on the one hand on a big background having a peak near 580 nm, and on the other hand are obtained by 1 minute irradiation followed by a spectrum measurement taking around 20 minutes. This has the effect that the spectral change recorded by the spectrometer might be some state the optically excited state decays into. As we will see, with longer exposure times, the peak moves back towards 591 nm.

To investigate behavior on increasing merocyanine fraction, film *e* has been repeatedly exposed to UV light until the effect started to decrease. Figure 4.6 shows a typical series of spectra acquired between 2 minutes of UV irradiation inside the

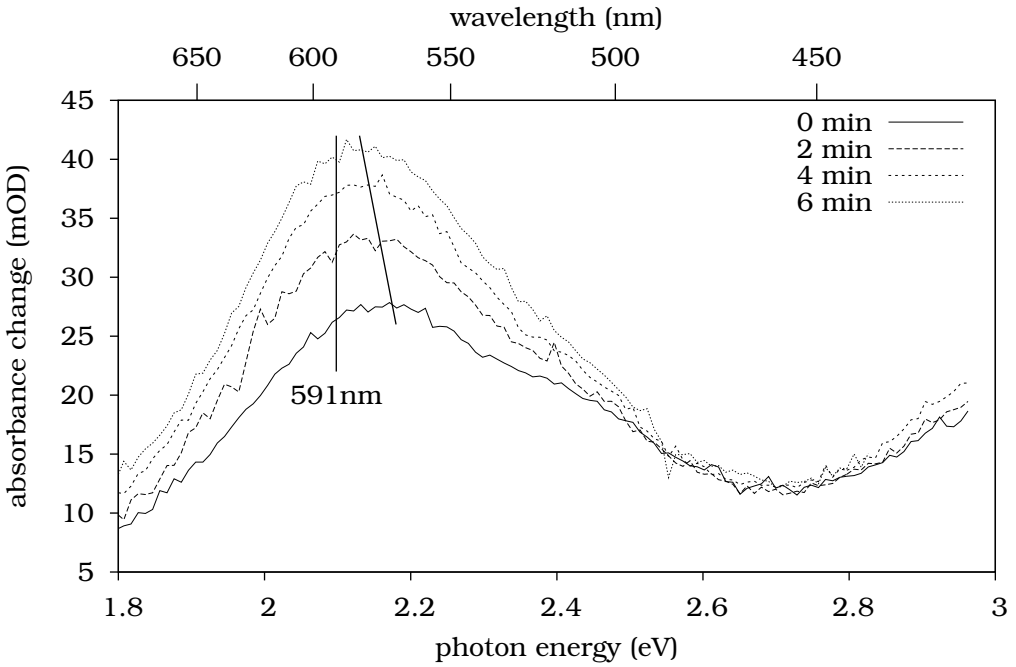

Figure 4.6: Influence of UV irradiation on the VIS absorption spectrum. spectra of film *e* (40nm/quartz) between repeated 2 min UV irradiation processes, accumulated time printed in the key. An unilluminated area of the sample was used as reference; the baseline of the series from previous switching experiments is the solid line. Spectra have been smoothed by a 5-point moving average filter.

spectrometer, so no alignment errors between the different spectra are to be considered. One sees one broad peak rising at around 2.13 eV, but the remaining parts of the VIS spectrum (like the dip at 2.72 eV) stay constant. The shoulder at 2.5 eV is considered to be from some photo-induced molecule state that does not take part in switching.

The maximum of the main peak shifts towards lower energies (longer wave length) on continued irradiation. The interpretation is that what appears as a big peak is in fact a multi-peak system with one of the peaks rising. As the ratio between the peaks shifts, the apparent maximum of the sum of all these peaks shifts, too. The inclined line is a guide to the eye crossing the maxima, while the line at 591 nm is at the maximum position of the rising peak. The claim of a multi-peak system is supported by looking at the differences between consecutive absorption spectra, that is looking at the changes induced by one 2 minute irradiation period, as has been done in figure 4.7. While these difference spectra are quite noisy, they show that the change has a maximum around 591 nm, which indicates one rising peak.

The 591 nm peak is in the region the merocyanine peak has been observed in other NO_2BIPS on MgO films, see spectra of film *j* and film *l* in figure 3.13 on page 43,

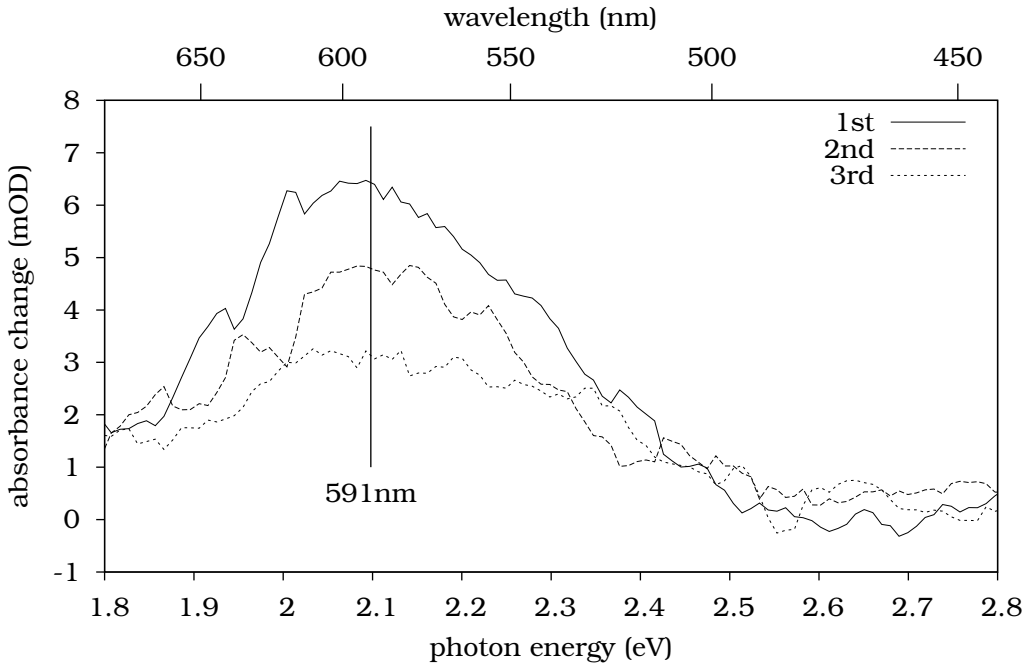

Figure 4.7: Absorbance change during each two-minute illumination period.

where maxima at 600 nm and 580 nm were identified. The shorter wavelength component might be an self-stabilizing H-aggregate that is not easily switchable by VIS irradiation and thus remained from the previous UV irradiation experiments.

After acquiring the series of two-minute-illuminations to the sample, it has been exposed 20 minutes to VIS light to switch the reversible switchable spiropyrans back from merocyanine into the spiropyran state. Figure 4.8(a) shows essentially the same process on the same sample, but this time with 4 minute illumination cycles, after having exposed the sample to VIS light for 20 minutes to remove the reversible switching spiropyran fraction. The base line of both of these pictures is caused by previous residues of switching experiments.

Figure 4.8(b) shows a coarse fit of a single exponential saturation models to the average absorption in the range of 2.0 to 2.4 eV for the four-minute series. The resultant time constant is around 7.4 min. One sees a decrease of absorption intensity in the end, which is attributed to degradation of the sample.

The increased final absorption can still be explained by components that are not effectively switchable and slowly increase during the saturation experiments. These components might be from sterically hindered molecules that are either inefficiently optically switched or switched by inter-molecular interactions to optically switched molecules.

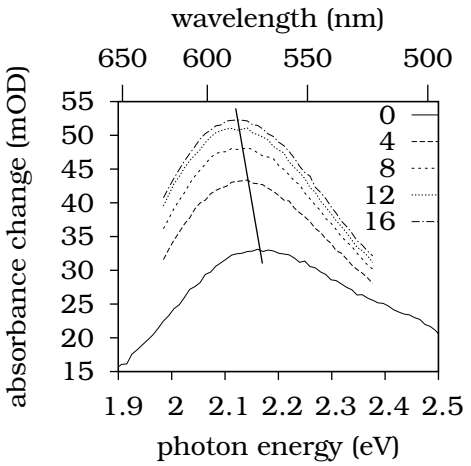

(a) spectra after repeated 4 min UV irradiation processes, difference to a different, unilluminated spot is shown. Total illumination time is given in minutes.

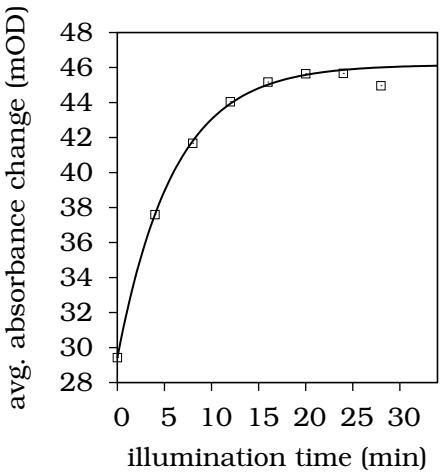

(b) average absorbance in the range between 2.0 and 2.4 eV for the 4-minute series of consequent UV irradiation (fig 4.8(a)). The straight line shows an exponential saturation model, the decrease at the end is caused by sample degradation.

Figure 4.8: Saturation of film *e* (40nm/quartz)

4.3 Samples on magnesium oxide

4.3.1 Switching Observed by Absorption

In order to characterize the switching process and its reversibility, further measurements were carried out as follows: The first spectrum of the as-prepared film was used as reference to which all following transmission spectra are referenced. A typical spectra obtained this way is depicted in Figure 4.10. The spectrum is part of the kinetic series shown in figure 4.9. This series illustrates the evolution of the spectrum during light irradiation. Ten illumination/measurement cycles of 7 seconds each using UV light where followed by 30 cycles using white light. This procedure has been repeated five times. The merocyanine absorption peak rises during the UV-light cycles and decays during the visible light cycles. The position of the maximum at 580 nm remains unchanged. As can be seen from the spectra extracted from the 3D kinetic plot, a permanent, non-reversible peak around 641 nm develops during switching. This peak is very similar to the residual peak at 645 nm of film *e*, which was shown in figure 4.4.

This kind of measurement has been performed on NO_2BIPS films of different thicknesses in the range of 5 to 40 nm to investigate the switchability of each of them. For the sake of clarity, Figure 4.11 shows the average optical density in the range of 576 to 583 nm as an indicator for the absorption intensity. The time-evolution of the optical density clearly reveals a reversible switching process for all

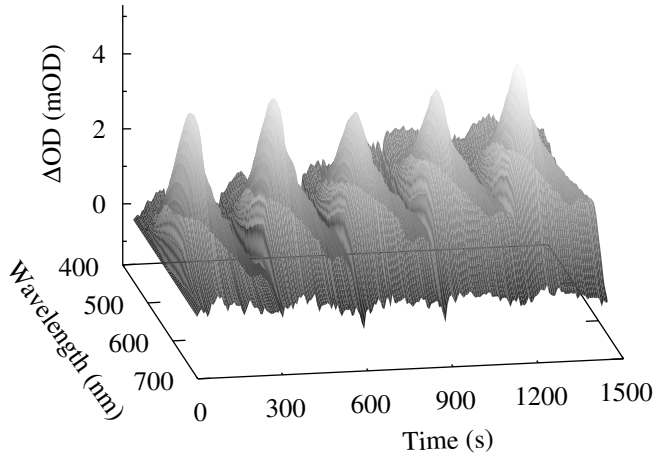

Figure 4.9: time-dependent spectra of a 40 nm NO_2BIPS during five switching cycles [74]

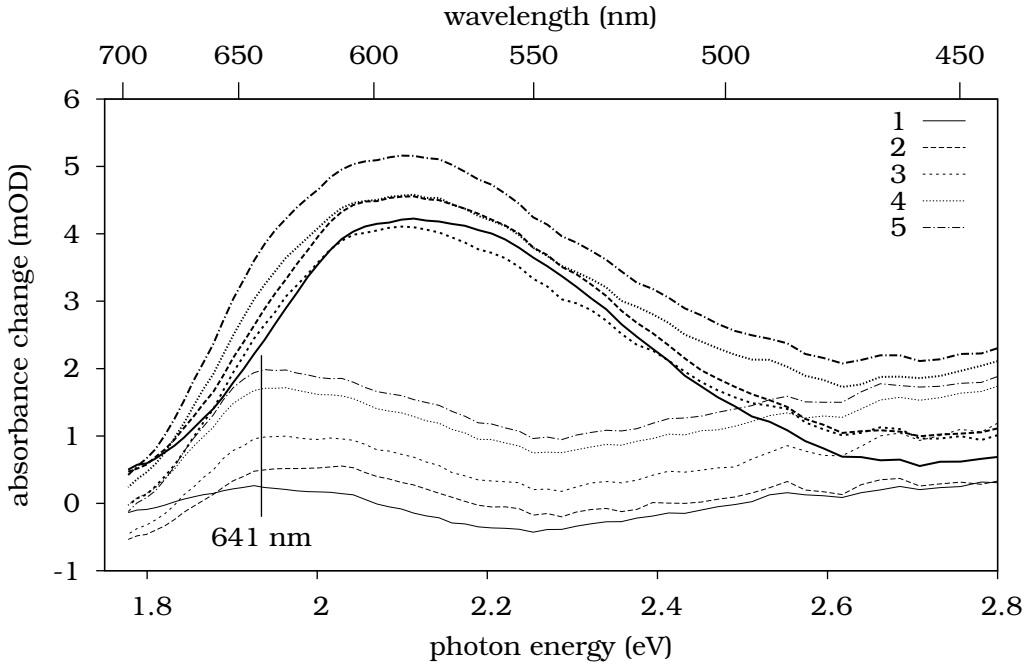

Figure 4.10: spectra at the end of the UV and VIS illumination processes from figure 4.9. Thick lines after UV illumination, and thin lines after VIS illumination [74]

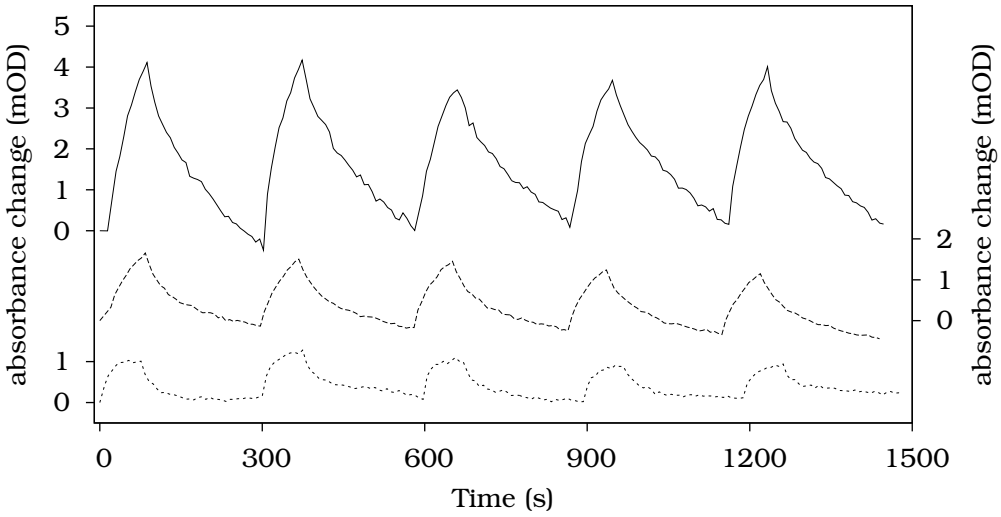

Figure 4.11: Time evolution of the averaged optical density around 580 nm on repeated UV/VIS irradiation to NO_2BIPS films with thicknesses of 5 nm (dotted), 10 nm (dashed) and 40 nm (solid). [74]

investigated films.

The absolute signal intensity is larger for thicker films suggesting that not only the topmost monolayer of molecules but the whole film contributes to the switching phenomenon. Since the UV light intensity varied up to 30% between measurements of different films due to optical realignment, a quantitative comparison of the non-saturated curves shown in Figure 4.11 will not yield reliable numbers. Nevertheless, a very rough estimate using the UV power density from the data sheet of the lamp and estimating the losses in the optics yields a UV power of about 0.4 W/cm^2 distributed over wavelengths between 200 and 400 nm.

Long-time UV light exposure of the samples was investigated to examine the saturation behavior of the switching process. For the 40 and 10 nm films the same cycle times were used as described previously whereas for the 5 nm film the cycle time was doubled in order to improve the signal-to-noise ratio. Directly after this measurement, the relaxation to the spiropyran form was monitored, detecting the decrease of the merocyanine absorption signal. For this, the UV light used to switch towards the merocyanine form was blocked but the white light used for absorption measurements remained. To determine the origin of the relaxation, the 40 nm sample was measured a second time using a 25 times lower white light intensity. The results are shown in Figure 4.12 (symbols). The optical density during excitation of the merocyanine state as well as during the relaxation to the spiropyran state exhibits a monotonic behavior. The experimental data were fitted using a bi-exponential model,

$$OD(t) = OD_\infty + A_1\,\mathrm{e}^{-t/\tau_1} + A_2\,\mathrm{e}^{-t/\tau_2}, \tag{4.1}$$

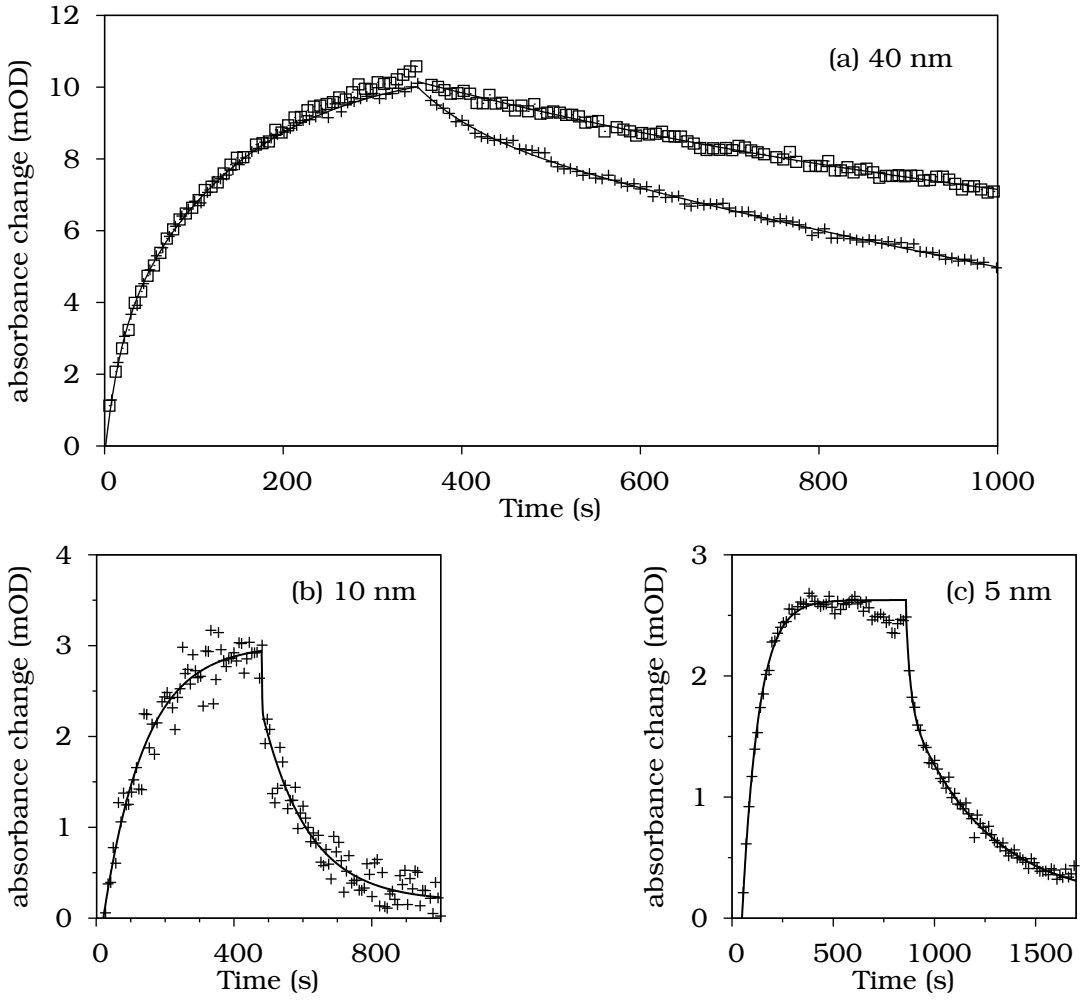

Figure 4.12: Combined saturation and relaxation behavior of NO_2BIPS films of different thickness. The left part of each figure shows the rise in absorbance on UV irradiation. The decay in the right part is induced by thermal relaxation and by the white light used for spectroscopy. This decay is illustrated for the 40nm film in (a) for two different light intensities (ratio 1:25). The symbols show the experimental data, while the solid lines are fits according to equation 4.1 [74]

		OD_∞	A_1	τ_1	A_2	τ_2
film	light	mOD	mOD	s	mOD	s
40 nm	UV	11	−8	144	−3	19
10 nm	UV	3.0	−3.0	124		
5 nm	UV	2.6	−2.6	81		
40 nm	white	−4	12	1800	1.2	70
40 nm	white (weak)	4	5	900		
10 nm	white	−0.2	2.1	128		
5 nm	white	0.1	1.6	380	0.7	21

Table 4.1: Fit results using a bi-exponential model according to Equation (4.1) [74].

yielding the saturation optical density OD_∞ and the relative weights A_1 and A_2 of two exponential components with time constants τ_1 and τ_2, respectively. The results of the nonlinear least-squares fit are listed in Table 4.1. In some cases, where a single exponential model sufficiently matched the experimental data, A_2 and τ_2 are not given.

The two data sets for the 40 nm thin film depicted in figure 4.12(a) were acquired in direct sequence on different sample positions but with strongly different white light intensities, as already mentioned. As can be clearly seen, the optical densities exhibit nearly identical behavior for the saturation. Hence, we conclude that changes induced by the UV light prevail the influence of white-light irradiation. Moreover, we assume that thermal relaxation is negligible. In this case, in contrast to the time constants τ_1 and τ_2, the saturation value OD_∞ must not depend on the UV light intensity according to first-order reaction kinetics. However, a thickness dependence of OD_∞ is visible in Table 4.1, in agreement with the observations made for the multi-cycle measurement. As expected for a bulk effect, OD_∞ decreases monotonically with film thickness. In first approximation, it should scale linearly with thickness, which is not the case here. The value of $3 \cdot 10^{-3}$ OD for the 10 nm film is only slightly larger than the value of $2.6 \cdot 10^{-3}$ OD found in the 5 nm film. This is either due to a change of the optical response on reducing the film thickness or indicates thickness inhomogeneities, as the quartz microbalance only yields averaged thickness values. Furthermore, we observe a decreasing time constant τ_1 with decreasing film thickness.

To calculate the quantum efficiency, we estimate the photon flux rate from an estimated illumination power of $0.4\,\mathrm{W/cm^2}$ and an average photon energy of 4 eV resulting in $6.2 \cdot 10^{17}\,1/(\mathrm{cm^2\,s})$. The optical density of 25 mOD at the peak at 390 nm indicates an absorption probability of 5.5%, so the number of absorbed photons is $3.5 \cdot 10^{16}\,1/(\mathrm{cm^2\,s})$. The nominal thickness of 40 nm obtained by the quartz micro balance yields a coverage with NO_2BIPS of $9.5 \cdot 10^{15}\,\mathrm{cm^{-2}}$. The time constant obtained for UV illumination is $\tau_1 = 144\,\mathrm{s}$ for real time seconds. As the chopper shuts the UV light for 90% of the time, the equivalent time constant for continuous

irradiation is $\tau' = 14.4\,\mathrm{s}$, so the switching rate for a molecule is $1/\tau' \approx 0.069\,1/\mathrm{s}$. The photoswitching thus succeeds at a rate of $6.6 \cdot 10^{14}\,1/\mathrm{cm}^2\,\mathrm{s}$, so a quantum efficiency of approximately 2% can be obtained. The calculation is based on an estimate of the absorbance and the light intensity, and includes spectral ranges where absorption is clearly lower than assumed. The value supports the assumption of a bulk effect since it is comparable to a quantum efficiency of 10% found by Atassi et al. [20].

Above 350 s the experimental data for different white light intensities differ significantly. Whereas the curve obtained with low intensity shows only a slight decrease (squares), the decay of the data recorded with 25 times larger intensity (crosses) is much more pronounced. The fits according to Equation (4.1) yield $\tau_1 = 900\,\mathrm{s}$ and $\tau_1 = 1800\,\mathrm{s}$, $\tau_2 = 70\,\mathrm{s}$, respectively. The values for τ_1 are of the same order of magnitude. Therefore, we attribute them to thermal relaxation. Since the data set acquired at larger light intensity contains a second relaxation time $\tau_2 = 70\,\mathrm{s}$, we ascribe it to optical ring-closing. Investigations of thermal relaxations of NO_2BIPS molecules in PMMA films by Atassi *et. al.* [20] yielded two different time constants, $\tau_a = 1400\,\mathrm{s}$ and $\tau_b = 10000\,\mathrm{s}$. While τ_a is comparable to our values for τ_1 supporting our interpretation of the process as thermal relaxation, our data set acquisition time was too short to identify a component in the range of τ_b.

4.3.2 Switching Observed by Fluorescence

As seen especially for thin films in the last section, the baseline drift of the absorption spectrometer makes analyzing the switching kinetics difficult. As discussed in the spectroscopic result chapter, fluorescence spectroscopy is less prone to experimental drifts, as the relative change is orders of magnitude bigger.

The fluorescence of film *o* has been observed between irradiating UV and green light to the sample, with the sample being exposed to UHV conditions. A typical fluorescence signal is shown in figure 4.13. The solid line shows the fluorescence intensity of the sample (spectrum before illumination has been subtracted as baseline); the dotted line shows the fluorescence of a pure MgO sample scaled to fit as background to the fluorescence spectrum of the sample. As the MgO fluorescence *decreased* during the first UV period, the scaling factor is negative. The difference of the estimated MgO background and the fluorescence signal is shown in figure 4.14. The Gaussian shaped model of the fluorescent peak is used in the analysis of the fluorescent data, as presented below.

After VIS irradiation to the sample, decomposition of the fluorescence signal into MgO background and the merocyanine fluorescence peak model established above is no longer possible. The fluorescence exhibited by the sample in response the VIS irradiation following the UV irradiation is displayed in figure 4.15 after MgO background subtraction. The dotted line shows a component of the spectrum that is present in addition to the merocyanine fluorescence peak and the MgO background (not shown, as already removed from the data). A possible source for this third component is phosphorescence of spiropyran around 510 nm [47, 75]. The truncated

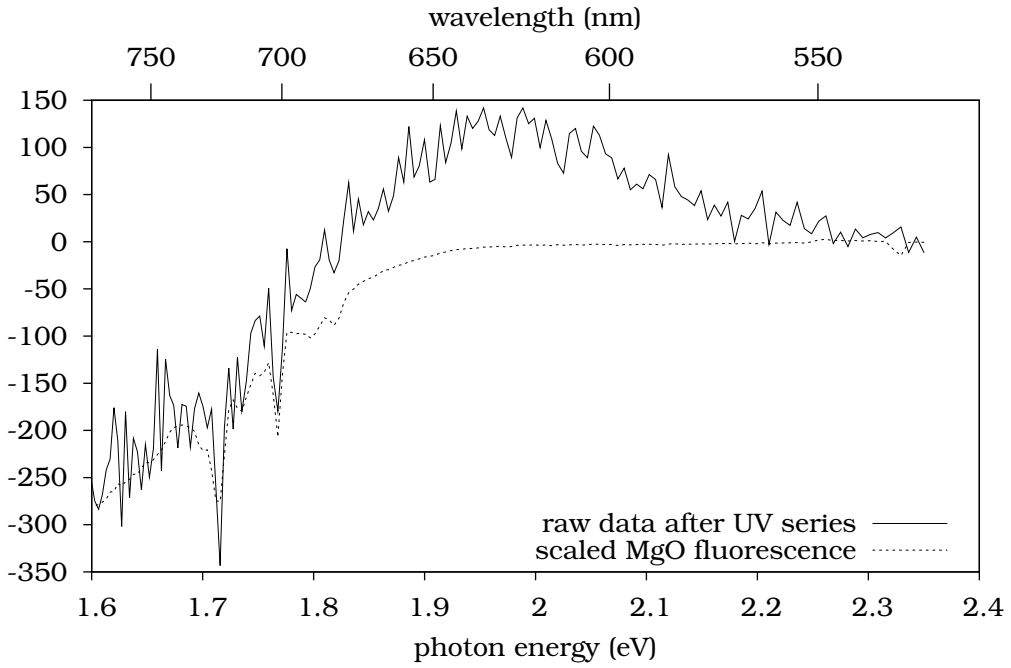

Figure 4.13: Fluorescence signal (baseline corrected) of film *o* after UV irradiation (solid), scaled MgO background used for correction (dashed).

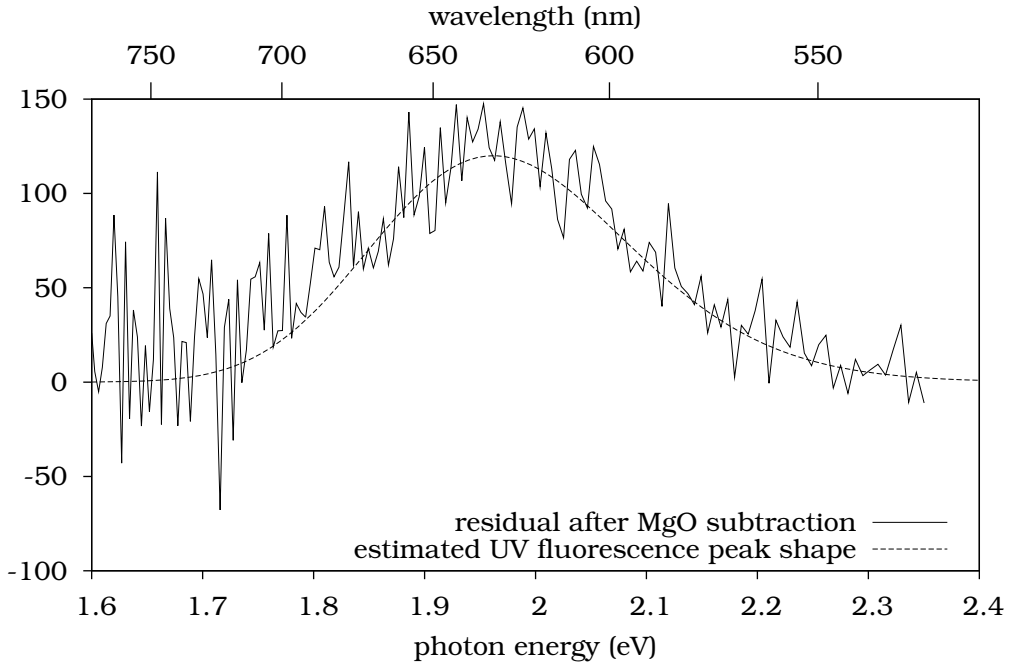

Figure 4.14: Residual after background correction of figure 4.13. It shows one peak which is interpreted as the merocyanine fluorescence, and the estimated shape of that peak as Gaussian.

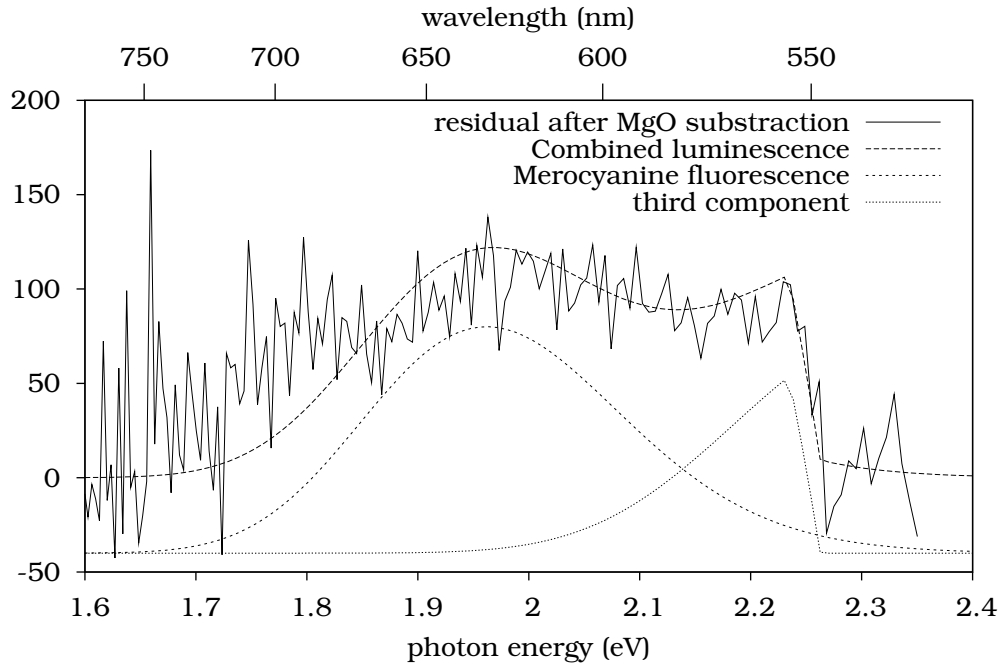

Figure 4.15: Residual after background correction of the luminescence signal after UV and VIS irradiation. The spectrum contains luminescence near the filter edge at 550 nm that was not present only after UV irradiation.

shape of the peak is due to the long-pass filter applied to remove the 532 nm excitation from the spectrum, so emitted light at wavelengths below 550 nm does not reach the detector.

As discussed above, fluorescence spectroscopy is less prone to artifacts. To interpret the spectra, they were decomposed into the superposition of the three components introduced above: The MgO background (as measured on that sample before illumination), the merocyanine fluorescence and a third component. The two peaks from the film were modelled as Gaussian-shaped. The change of the two fluorescent peak intensities is shown in figure 4.16(a), while the change in background signal intensity (which probably is not related to the switching process but to experimental difficulties) is shown in figure 4.16(b). One sees a clear response of both luminescence peaks to light illumination, although the behavior during the first cycle is quite surprising.

The peak assigned to the merocyanine conformation of the spiropyran rises quite quickly during the first UV illumination period to some certain level. Interestingly, it stays at this level during the following VIS irradiation. During the next cycles, a further increase of the peak intensity is observable, which returns back on VIS irradiation to the level observed at the end of the first cycle. The peak assigned to spiropyran phosphorescence on the other hand stays at zero during the first UV irradiation period and rises considerably during the first VIS period to some equilib-

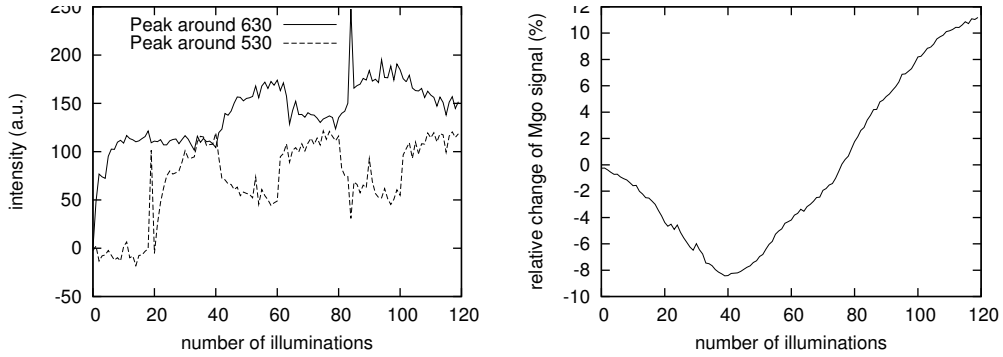

(a) fluorescence peak intensities (b) background fluorescence intensity

Figure 4.16: evolution of the spectral components in the *in-situ* fluorescence measurement

rium level. During the next cycles, the peak intensity drops during UV irradiation and recovers to the same equilibrium level during VIS irradiation.

The fluorescence behavior which turns out more involved than expected seems to indicate that the two-state model (just merocyanine and spiropyran ground state considered) is not enough to describe what is observed, even though the measurements are not performed with sub-second time resolution, so short-lived excited states can't explain the observed behavior. As the experiments are performed in vacuum, also adsorption of non-spiropyran material (like water) is unable to explain the observed behavior. So mainly two further possibilities of extra states remain: Long-lived excited states or aggregate formation.

In the sample investigated in vacuum, on UV irradiation, the peak at a wavelength below 550 nm does not appear, although the isomerization towards the merocyanine is indicated by the peak around 630 nm. The VIS irradiation on the other hand is able to excite that peak, so the path towards the molecular state that exhibits this peak involves a transition below the typical spiropyran absorption bands. This is a sign that the initial state is merocyanine. If this sub-550 nm peak would be the decay of an excited merocyanine state back to the ground state, the intensity of that peak should drop during the VIS period, as the amount of merocyanine drops in the VIS period. Contrary to this, the peak intensity rises during the VIS period, so this peak is clearly assignable to something that develops during VIS irradiation. For this something, there still are different possibilities: merocyanine or spiropyran complexes on the one hand, or metastable excited states on the other hand.

The possibility of metastable excited states seems unlikely, as the lifetime must be several minutes at least to have an excited state to show the saturating accumulation behavior in the experiment. As the experiment took place at room temperature, a life time in that area is implausible, leaving the possibilities of photoinduced aggregate formation, which then could be merocyanine or spiropyran aggregates. The creation of these aggregates can be induced by the photoexcitation or by sample

heating from the IR part of the spectrum of the Xenon gas-discharge lamp. The stability of the merocyanine peak during the first VIS period can be interpreted as sign that the merocyanine molecules created in the UV period are not affected by the VIS irradiation, and thus the VIS light is interacting with molecules in the spiropyran state. On the other hand, spiropyran molecules are not known to expose fluorescence when irradiated with 532 nm light, which would indicate that merocyanine molecules are emitting the extra fluorescent peak. Looking into the next period might resolve the puzzle, though. At the end of the first UV period, the merocyanine emission level kept at a constant saturated value. During the second UV irradiation period, the merocyanine emission rises to a higher level. This can again be interpreted in multiple ways, one of them being more spiropyran molecules taking part in photoswitching, the other being a change of the photostationary equilibrium during UV irradiation towards merocyanine due to stabilization of the merocyanine conformation.

In the second and third cycles, spectra return to the state observed at the end of the first cycle, so that state is a photostationary state under the VIS irradiation present in the experiment. An interpretation of the observed spectra is that during the first UV irradiation period, some molecules get switched into a fluorescent state permanently (e. g. like in the sub-monolayer films investigated in [36], where on conducting substrates the substrate-molecule interaction stabilizes the merocyanine form), on the subsequent VIS period, these molecules don't react to the VIS light. At the same time, some effect of the VIS light irradiation enables more spiropyran molecules to switch (e. g. by loosening molecules on the top of clusters), which can then reversibly be switched between the spiropyran and merocyanine state.

Another interpretation, involving aggregate formation in the first VIS cycle would go along the lines that in the first UV cycle, molecules get switched from the spiropyran to the merocyanine state. In the first VIS cycle, aggregates of the merocyanine molecules are formed that stabilize the merocyanine form, so in the second UV phase, the photostationary equilibrium is shifted farther towards the merocyanine state. At the same time, the decreasing peak at below 550 nm which would be interpreted as aggregate indicator decays, showing a slow aggregate cleaving induced by the UV light. The subsequent VIS irradiation restores aggregates and at the same time, it non-aggregable merocyanine molecules are switched back to the spiropyran state.

Both of these models have weak points, like in the first model, there needs to be an explanation, why spiropyran molecules suddenly show luminescence when excited by a 532 nm laser, or in the second model, why no switching of merocyanine back to spiropyran is observed in the first period, but only in the later periods.

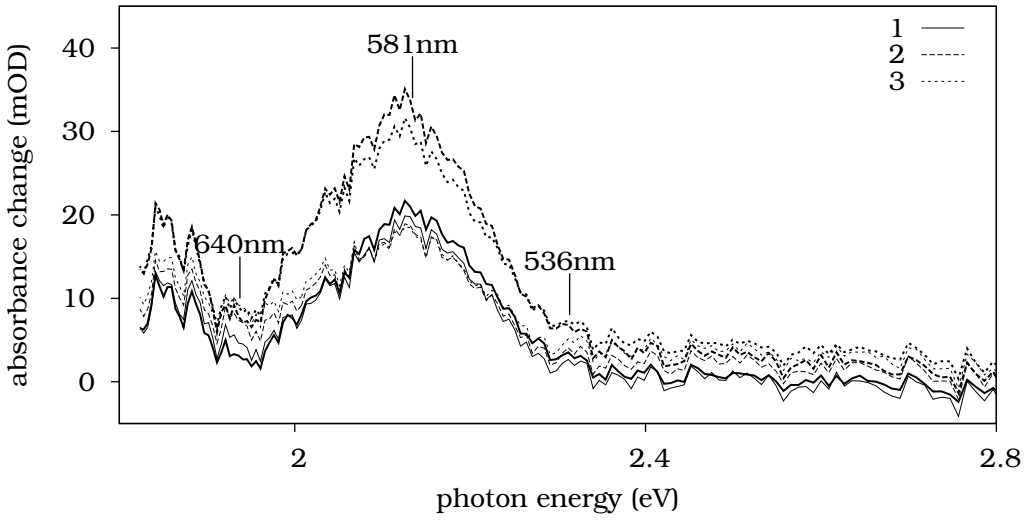

Figure 4.17: Absorption of the 10nm NO_2BIPS film *o* on Si(111), measured *in-situ*. Thick lines after UV irradiation, thin lines after VIS irradiation.

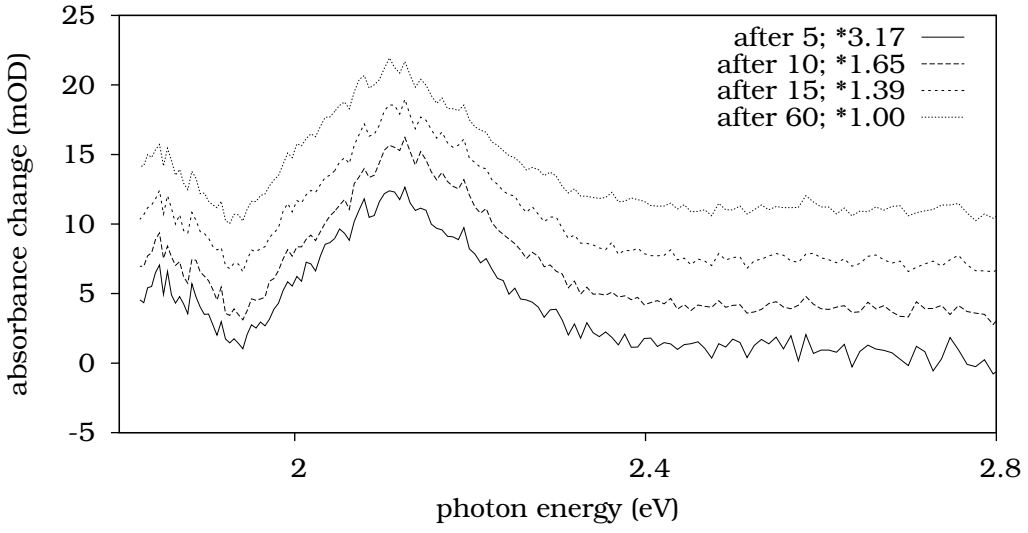

Figure 4.18: Absorbance change of film *o* during the third UV period. Lines have been scaled to the same hight, and shifted for separation

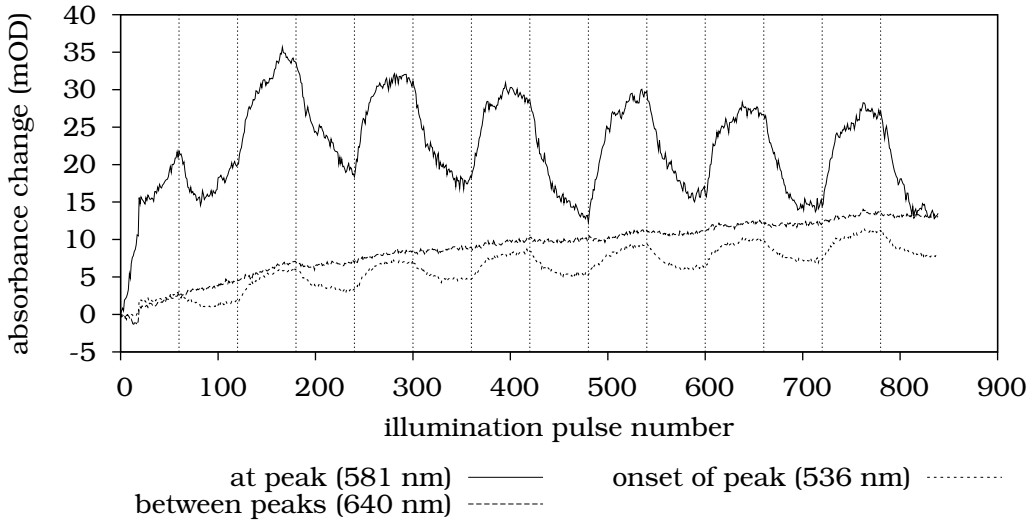

Figure 4.19: Absorbance change at different wavelengths of the 10nm NO_2BIPS film on silicon over time. The dotted vertical lines indicate the points in time the illumination light was switched from UV to VIS and vice-versa.

4.4 Samples on Silicon

Figure 4.17 shows a 10 nm film NO_2BIPS on silicon that has been examined *in-situ* in UHV by reflection spectroscopy. The displayed absorption assumes that scattering is not significant. Considering the explanation of many experimental problems observed earlier being explained by scattering effects, this assumption seems quite risky, but while aligning the optical setup, scattering was in fact not visible: A bright spot on the sample could only be seen when looking to the sample from the direction the incident beam was reflected to. The spectrum shows two peaks. One at 2.13 eV which is the well-known merocyanine absorption peak, but also a new peak at 1.84 eV that was not visible in ex-situ measurements. It is possible that the double-peak structure of this sample has the same origin as the double peak observed on magnesium oxide in UHV, see section 3.3.3.

The acquired series on gradual switching from and to the merocyanine state shows only one component, as illustrated in figure 4.18, showing the absorbance at different states of the saturation process scaled to the same amplitude. In contrast to the ex-situ examined magnesium oxide sample, the scaled spectra look very similar to each other, and after the second cycle quite reproducible.

A more in-depth analysis of the switching spectra reveals a very good reversibility of the switching process, as well as an indication that the starting point of the kinetic series was not completely in the spiropyran state. To obtain this information, the time dependent absorption at different wavelengths have been compared (see figure 4.19). One interesting point is at 640 nm between the two peaks. At this wavelength, no switching-induced effects seem to be present, so the spectrum

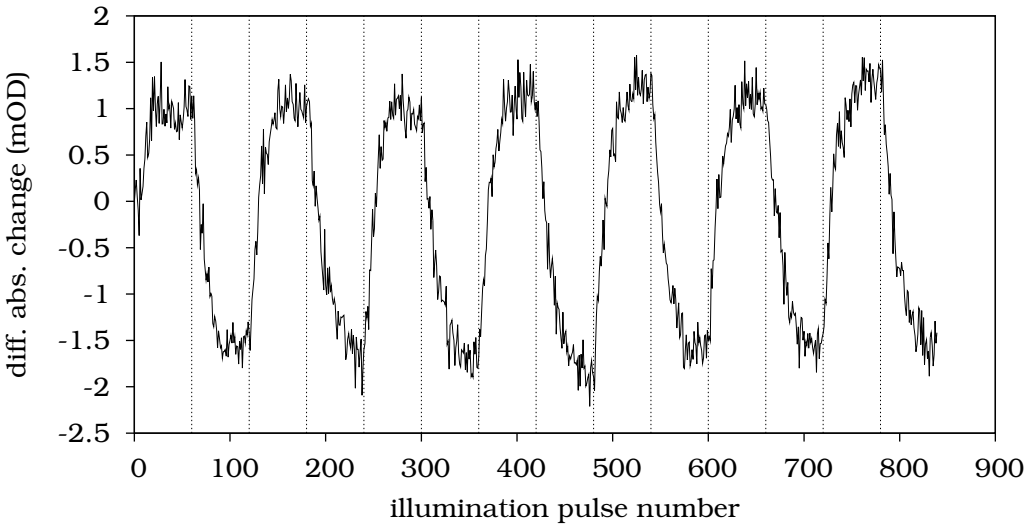

Figure 4.20: Absorbance of film *o* (10nm/Si(111) with UHV preparation) at 536 nm, with scaled background from 640 nm subtracted

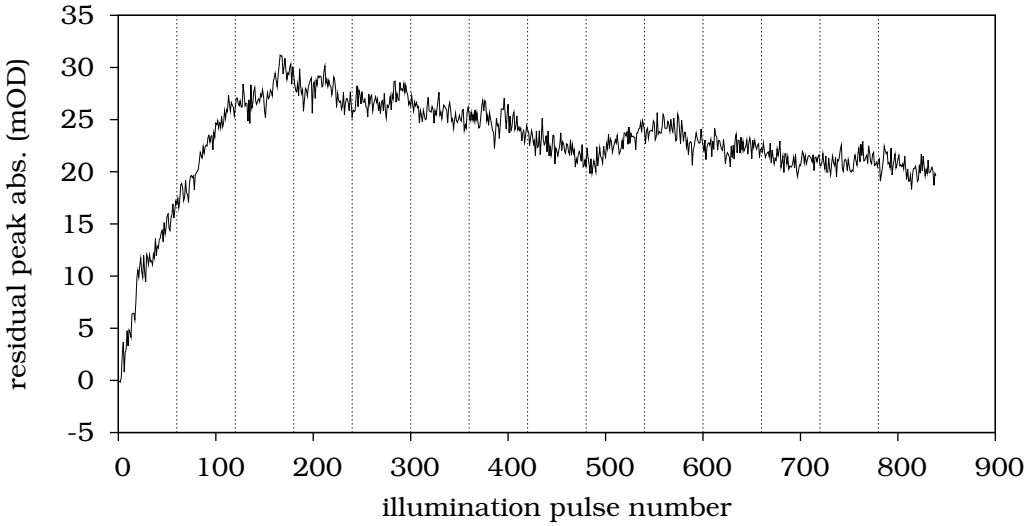

Figure 4.21: Non-switching component of the absorbance at 581 nm

at this wavelength can be considered to show a background of different origin. Interestingly, while not having very strong absorption, the background of the spectrum at 536 nm quite closely resembles the background spectrum, except for having switching-induced effects in it, too. The switching-induced component of the spectrum at 536 nm is shown in figure 4.20. It has been obtained by subtracting the background observed at 640 nm (after scaling) from the absorbance measured at 536 nm. It shows a non-degrading switching pattern with a contrast of 3 mOD.

To show that there really is just one component, the switching pattern has also been subtracted from the absorbances observed at 581 nm, after being multiplied by 4.3 to compensate for the higher absorption efficiency at that wavelength, to show that the component caused by reversible switching looks the same at the top of the peak than on the onset. The residual spectrum after subtracting the switching-induced component is shown in figure 4.21. No apparent structure with the period of the illumination process is visible in that spectrum.

5 Conclusion

In this thesis, the possibility of creating spiropyran films by vacuum deposition of non-functionalized molecules is demonstrated. Vacuum deposition provides a cheap and versatile method of creating spiropyran films, as the molecules neither need to be functionalized to enable film preparation (as would be in Langmuir-Blodgett techniques) nor have they to be matched to the substrate type (as is used in self-assembled monolayers to obtain chemical binding). This provides researchers freedom to add or remove side groups of the spiropyran molecule to tune the behavior of the molecule without being limited by film preparation requirements. Also the same molecule can be applied to different types of substrates without the need to prepare different linking groups.

Photochromism in films prepared this way has been observed and for films between 5 and 40 nanometer thickness identified as bulk effect. While some non-reversible effects were observed in the first switching cycle on most samples, quite good reversibility of the switching process is obtained in later cycles. The reversible transition between spiropyran and merocyanine has been observed on all kinds of substrates, quartz glass, crystalline magnesium oxide, silicon with native oxide layer and flashed silicon; confirming the substrate independence.

The switching has been observed using absorption spectroscopy and fluorescence. The advantage of the absorption spectroscopy measurement is the simple setup, which can easily be used to monitor absorbance changes especially if the light inducing the switching is irradiated with the sample staying inside the spectrometer setup. The measurement of absolute absorbance of the spiropyran is also possible on partly coated substrates, but it is greatly influenced by film morphology via scattering effects. If the morphology of the film is affected by the switching process, even absorbance change measurements are distorted by morphologic effects. Fluorescence spectroscopy on the other hand needs a more sensitive setup, as fluorescence is emitted isotropic, and only a part of the fluorescent light gets to the detector. Usually, the advantage of fluorescence detection is the zero background, as photons from the source that did not interact with the material are easily separated from the fluorescence spectrum. However, Magnesium oxide substrates turned out to be unsuited to make full use of the advantage of fluorescence measurement, as MgO impurities exhibit fluorescence too, which makes the method no longer have zero background.

Using both absorption spectroscopy and fluorescence spectroscopy, the merocyanine and the spiropyran state of the molecule could be distinguished clearly, so it is possible to read the state of the molecules without the probe touching it. While single-molecule-addressability is not possible by far-field optics in a closed film of

spiropyrans, optic readout of the molecule state can prove useful for multi-layered data storage media (using techniques as described by Berkovic et al [5]).

The molecule used in this thesis works as optically controlled electrical dipole and optically controlled dye. By adding functional groups, further optically controlled effects can be introduced into the system, by making use of the mechanical rearrangement inside the molecule or by adding side groups that change other properties as a response to the electron distribution change.

A Supplementary material

A.1 Abstract

The classic photochromic molecule 1',3'-Dihydro-1',3',3'-trimethyl-6-nitro-Spiro[2H-1-benzopyran-2,2'-[2H]indole] (NO_2BIPS) can be switched between its yellow spiropyran and its purple merocyanine state. This thesis describes the preparation of NO_2BIPS films by vapor deposition in vacuum of these molecules on quartz, magnesium oxide and silicon substrate and investigation of these films by optical spectroscopy. All of the evaporated films with a thickness between 5 and 80 nanometers are found to be initially in the spiropyran state, whereas in considerably thicker films, a fraction of molecules in the merocyanine state could be detected. In most films a part of the molecules could be switched to the merocyanine state by irradiating into the near-UV absorption bands, and switched back to the spiropyran state by irradiating into the green absorption band of merocyanine. This switching was repeatable over many cycles. As the intensity of the merocyanine signal is turned out proportional to the film thickness, the observed switching is considered a bulk effect. Furthermore, the kinetics of the switching process have been investigated on a timescale of seconds. After the first cycle which often shows involved behavior, the time constant of the switching process under the illumination conditions used during the thesis is in the range of tens to hundreds of seconds, depending on the exact conditions, depending on the illumination power available in the respective experimental setup. The results, especially the behavior during the first cycle, contain strong hints that the process on the surface is more complex than just switching between two states, for example aggregate formation or annealing of the film by the power of the light used for switching might be observed, too.

A.2 Kurzfassung (German Version of the Abstract)

Die Verbindung 1',3'-Dihydro-1',3',3'-trimethyl-6-nitro-spiro[2H-1-benzopyran-2,2'-[2H]indole] (NO_2BIPS) ist ein klassisches photochromes Molekül, dass zwischen dem gelben Spiropyran- und dem violetten Merocyanin-Zustand geschaltet werden kann. In dieser Arbeit wird die Herstellung von NO_2BIPS-Schichten auf Quarzglas-, Magnesiumoxid- und Siliziumsubstraten durch Aufdampfen im Vakuum beschrieben, sowie die Untersuchung der so hergestellten Schichten mit optischer Spektroskopie. Alle Schichten zwischen 5 und 80 Nanometer Dicke wurden im Spiropyranzustand vorgefunden, wogegen in deutlich dickeren Filmen auch ein geringer Merocyaninanteil gemessen wurde. In den meisten der in dieser Arbeit gezeigten Schichten konnte ein Teil der Moleküle durch die Einstrahlung in die Absorptionsbanden im nahen UV in den Merocyaninzustand und durch die Einstrahlung in Absorptionsbande des Merocyanins im gelben bis grünen Bereich zurück in den Spiropyranzustand geschaltet werden. Bei den meisten Proben war das über viele Zyklen möglich. Da die Intensität des Merocyaninsignals sich etwa proportional zur Schichtdicke verhält, wird das beobachtete Schalten als Volumeneffekt interpretiert. Darüberhinaus wurde auch das zeitliche Verhalten im Schaltvorgang auf einer Zeitskala von Sekunden betrachtet. Nach dem ersten Zyklus, der häufig kompliziertes Verhalten zeigte, lag die Zeitkonstanten des Schaltvorganges unter den in dieser Arbeit verwendeten Belichtungsbedingungen im Bereich von einigen zehn bis hundert Sekunden, je nach in der jeweiligen Anordnung erreichbaren Belichtungsintensität. Die komplexen Ergebnisse insbesondere im ersten Schaltzyklus deuten darauf hin, dass mehr als nur das Schalten zwischen zwei Zuständen beobachtet wurde, sondern zum Beispiel zusätzlich noch die Bildung von Aggregaten oder durch die Belichtungsleistung thermische induzierter Veränderungen in der Schichtstruktur.

A.3 List of Publications Derived from the Work on this Thesis

A.3.1 Papers

- M. Karcher, C. Rüdt, C. Elsäßer, and P. Fumagalli. Switching of nonfunctionalized spiropyran thin films on single crystalline MgO(100). *J. Appl. Phys.*, 102(8):084904, October 2007.
- C. Elsässer, A. Vüllings, M. Karcher, and P. Fumagalli. Photochromism of spiropyran-cyclodextrin inclusion complexes on Au(111). *J. Phys. Chem. C*, 113(44):19193–19198, November 2009.

A.3.2 Conference Contributions

- M. Karcher, C. Rüdt, C. Elsäßer, M. Schübbe and P. Fumagalli. Photochromism in Thin Films of a Spiropyran Derivative. *Talk on DPG Spring meeting*, March 2007.
- M. Schübbe, M. Karcher, C. Rüdt, C. Elsäßer and P. Fumagalli. Optical Investigation of Thin Photochromic Spiropyran films. *Poster on DPG Spring meeting*, March 2007.

A.4 Curriculum Vitae

The curriculum vitae is not included in the online edition for protection of private data.

B Acknowledgement

This work would not have been possible without funding and discussion. Especially, I want to thank

Prof. Dr. Paul Fumagalli The head of the working group this thesis was prepared in. I like to thank him for sharing his broad knowledge and experimental experience. He used to be a great help especially when unexpected problems arose. I also thank him for constructive criticism on both experimental setup and data interpretation.

Dr. Christoph Rüdt My supervisor during the first 3 years. He designed the vacuum chamber extension together with Martin Schübbe. He also had a good overview about the progress in the project. Also we made use of his extensive experience with ultra-high vacuum setups.

Dr. Celine Elsäßer The other post-doc in our working group. She introduced me into the CCD-camera/monochromator setup, and helped with her knowledge about chemistry and fluorescence spectroscopy.

Martin Schübbe The diploma student who expanded the UHV system with the organic molecule evaporator chamber and had to struggle with the typical UHV problems.

The people of AG Fumagalli Who ensured a nice working atmosphere, generally were ready to help, if additional hands were needed for some tasks, were nice to talk to and generally good friends. Especially I want to thank Björn Lewitz and Thomas Sieben, also Axel Luchterhand and Tobias Homberg.

Deutsche Forschungsgemeinschaft (German Research Foundation), for funding the work as part of the the Sonderforschungsbereich (Collaborative Research Centre) 658 with the title "Elementarprozesse in molekularen Schaltern auf Oberflächen" ("Elementary processes in Molecular Switches at Surfaces").

C Bibliography

[1] Y. Kishimoto and J. Abe. A fast photochromic molecule that colors only under UV light. *J. Am. Chem. Soc.*, 131(12):4227–4229, April 2009.

[2] J.W. Kang, J.J. Kim, and E. Kim. All-optical Mach–Zehnder modulator using a photochromic dye-doped polymer. *Appl. Phys. Lett.*, 80:1710, 2002.

[3] Ragip A. Pala, Ken T. Shimizu, Nicholas A. Melosh, and Mark L. Brongersma. A nonvolatile plasmonic switch employing photochromic molecules. *Nano Lett.*, 8(5):1506–1510, 2008. PMID: 18412401.

[4] A. S. Dvornikov, J. Malkin, and P. M. Rentzepis. Spectroscopy and kinetics of photochromic materials for 3D optical memory devices. *The Journal of Physical Chemistry*, 98(27):6746–6752, 1994.

[5] G. Berkovic, V. Krongauz, and V. Weiss. Spiropyrans and spirooxazines for memories and switches. *Chem. Rev.*, 100:1741, 2000.

[6] Bradley J. Siwick, Olga Kalinina, Eugenia Kumacheva, R. J. Dwayne Miller, and Jaan Noolandi. Polymeric nanostructured material for high-density three-dimensional optical memory storage. *Journal of Applied Physics*, 90(10):5328–5334, 2001.

[7] E. Fischer and Y. Hirshberg. Formation of coloured form of spirans by low–temperature irradiation. *J. Chem. Soc.*, 1:4518 (p. 4522), 1952. p. 4522.

[8] Y. Hirshberg. Reversible formation and eradication of colors by irradiation at low temperatures. a photochemical memory model. *J. Am. Chem. Soc.*, 78:2304, 1956.

[9] M. Bletz, U. Pfeifer-Fukumura, U. Kolb, and W. Baumann. Ground– and first–excited–singlet–state electric dipole moments of some photochromic spirobenzopyrans in their spiropyran and merocyanine form. *J. Phys. Chem. A*, 106:2232, 2002.

[10] Jin Z. Zhang, Benjamin J. Schwartz, Jason C. King, and Charles B. Harris. Ultrafast studies of photochromic spiropyrans in solution. *J. Am. Chem. Soc.*, 114(27):10921, 1992.

[11] Y. Kimura, Y. Takebayashi, and N. Hirota. Study on the chemical reaction of spiropyran in medium- and high-density fluids. *J. Phys. Chem.*, 100:11009, 1996.

[12] A.K. Chibisov and H. Görner. Photoprocesses in spiropyran–derived merocyanines. *J. Phys. Chem. A*, 101:4305, 1997.

[13] R. Rosario, D. Gust, M. Hayes, J. Springer, and A.A. Garcia. Solvatochromic study of the microenvironment of surface-bound spiropyrans. *Langmuir*, 19:8801, 2003.

[14] P. Uznanski. UV-assisted formation of nanoaggregates from photochromic spiropyrans in nonpolar solvents. *Langmuir*, 19:1919, 2003.

[15] Koichi Okamoto, Terrell D. Neal, Zhaoyu Zhang, David T. Wei, and Axel Scherer. Molecular dynamics study of photochromic molecules probed by the mask pattern transferred transient grating technique. *Chem. Phys. Lett.*, 414(1-3):155, 2005.

[16] M. Guillaume and B. Champagne. Investigation of the UV/visible absorption spectra of merocyanine dyes using time-dependent density functional theory. *J. Phys. Chem. A*, 110:13007, 2006.

[17] J. Andreasson, S. D. Straight, G. Kodis, C. Park, M. Hambourger, M. Gervaldo, B. Albinsson, T. A. Moore, A. L. Moore, and D. Gust. All–photonic molecular half–adder. *J. Am. Chem. Soc.*, 128:16259, 2006.

[18] J. Andreasson, S. D. Straight, S. Bandyopadhyay, R. H. Mitchell, T. A. Moore, A. L. Moore, and D. Gust. Molecular 2 : 1 digital multiplexer. *Angew. Chem. - Intern. Edt.*, 46(6):958–961, 2007.

[19] Takashi Yoshida and Akira Morinaka. Irreversible photochromism of spiropyran films at low temperatures. *J. Photochem. Photobiol. A: Chem.*, 78(2):179, March 1994.

[20] Y. Atassi, J.A. Delaire, and K. Nakatani. Coupling between photochromism and second-harmonic-generation in spiropyran- and spirooxazine-doped polymer films. *J. Phys. Chem.*, 99:16320, 1995.

[21] G. Chidichimo, P. Formoso, S. Manfredi, G. Favaro, U. Mazzucato, and A. Romani. Prototypes of bifunctional photochromic and electro-optical systems. *J. Appl. Phys.*, 90:4906, 2001.

[22] A. Athanassiou, M. Kalyva, K. Lakiotaki, S. Georgiou, and C. Fotakis. All-optical reversible actuation of photochromic-polymer microsystems. *Adv. Mater.*, 17(8):988, April 2005.

[23] A. Athanassiou, K. Lakiotaki, V. Tornari, S. Georgiou, and C. Fotakis. Photocontrolled mechanical phenomena in photochromic doped polymeric systems. *Appl. Phys. A*, 76(1):97, January 2003.

[24] A. Athanassiou, K. Lakiotaki, M. Kalyva, S. Georgiou, and C. Fotakis. Photoswitches operating upon ns pulsed laser irradiation. *Appl. Surf. Sci.*, 248:56, 2005. 4th International Conference on Photo-Excited Processes and Applications.

[25] T. Suzuki, N. Oda, T. Tanaka, and H. Shinozaki. Reversible photo-switching interaction between spiropyrans and polymer pyridine residues in a solid polymer membrane. *J. Mat. Chem.*, 16(19):1803–1807, 2006.

[26] A. Athanassiou, D. Sahinidou, V. Arima, S. Georgiou, R. Cingolani, and C. Fotakis. Influence of laser wavelength and pulse duration on the degradation of polymeric films embedding photochromic molecules. *J. Photochem. Photobiol. A: Chem.*, 183(1-2):182–189, September 2006.

[27] A. Athanassiou, M. Varda, E. Mele, M. I. Lygeraki, D. Pisignano, M. Farsari, C. Fotakis, R. Cingolani, and S. H. Anastasiadis. Combination of microstructuring and laser-light irradiation for the reversible wettability of photosensitised polymer surfaces. *Appl. Phys. A*, 83(3):351–356, June 2006.

[28] A. Doron, E. Katz, G. Tao, and I. Willner. Photochemically-, chemically- and pH-controlled electrochemistry at functionalized spiropyran monolayer electrodes. *Langmuir*, 13:1783, 1997.

[29] J. He, F. Chen, P. A. Liddell, J. Andreasson, S. D. Straight, D. Gust, T. A. Moore, A. L. Moore, J. Li, O. F. Sankey, and S. M. Lindsay. Switching of a photochromic molecule on gold electrodes: single-molecule measurements. *Nanotechnology*, 16(6):695–702, 2005.

[30] S. Kado, K. Yamada, T. Murakami, and K. Kimura. Photoswitching of single association force between a pair of photoionizable spirobenzopyrans. *J. Am. Chem. Soc.*, 127:3026, 2005.

[31] M. H. Yang and M. C. Biewer. Monitoring surface reactions optically in a self-assembled monolayer with a photochromic core. *Tetrahedron Lett.*, 46(2):349–351, 2005.

[32] R. Rosario, D. Gust, M. Hayes, F. Jahnke, J. Springer, and A.A. Garcia. Photon-modulated wettability changes on spiropyran-coated surfaces. *Langmuir*, 18:8062, 2002.

[33] M. Suzuki, T. Asahi, and H. Masuhara. Photochromic reactions of crystalline spiropyrans and spirooxazines induced by intense femtosecond laser excitation. *Phys. Chem. Chem. Phys.*, 4(2):185, 2002.

[34] T. Huang, Z. Hu, A. Zhao, H. Wang, B. Wang, J. Yang, and J.G. Hou. Quasi chiral phase separation in a two–dimensional orientationally disordered system: 6–nitrospiropyran on Au(111). *J. Am. Chem. Soc.*, 129:3857, 2007.

[35] Marten Piantek, Gunnar Schulze, Matthias Koch, Katharina J. Franke, Felix Leyssner, Alex Krüger, Cristina Navío, Jorge Miguel, Matthias Bernien, Martin Wolf, Wolfgang Kuch, Petra Tegeder, and José Ignacio Pascual. Reversing the thermal stability of a molecular switch on a gold surface: Ring-opening reaction of nitrospiropyran. *J. Am. Chem. Soc.*, 131(35):12729–12735, September 2009.

[36] Gunnar Schulze. *Elementary Processes in Single Molecule Devices: Electronic Transport and Molecular Isomerization*. Dissertation, Freie Universität Berlin, 2009.

[37] Harald Ibach. *Physics of Surfaces and Interfaces*. Springer, 2006.

[38] Max Born and Emil Wolf. *Principles of Optics: Electromagnetic Theory of Propagation, Interference and Diffraction of Light*. Cambridge University Press, 6 edition, 1997.

[39] William W. Parson. *Modern Optical Spectroscopy*. Springer, 2007.

[40] W. Clegg, N.C. Norman, T. Flood, L. Sallans, W.S. Kwak, P.L. Kwiatkowski, and J.G. Lasch. Structures of three photochromic compounds and three non–photochromic derivatives; the effect of methyl substituents. *Acta Cryst.*, 47:817, 1991.

[41] A. Löwenbein and W. Katz. Über substituierte spiro-dibenzopyrane. *Ber. deut. Chem. Ges.*, 59(7):1377–1383, 1926.

[42] W. Dilthey, C. Berres, E. Hölterhoff, and H. Wübken. Beitrag zur kenntnis der spiro-di-benzopyrane (heteropolare kohlenstoffverbindungen. iv). *J. Phys. Chem.*, 114(1):179–198, 1926.

[43] Robert Dickinson and Isidor Morris Heilbron. Ii.-styrylpyrylium salts. part viii. 3-styryl derivatives of [small beta]-naphthapyrylium chloride. *J. Chem. Soc.*, 2:14–20, 1927.

[44] Jesse H. Day. Thermochromism. *Chem. Rev.*, 63(1):65–80, 1963.

[45] Robert C. Bertelson. Photochromic processes involving heterocyclic cleavage. In Glenn H. Brown, editor, *Photochromism*, number 3 in Techniques of chemistry, chapter 3, pages 45–431. Wil, 1971.

[46] Helmut Görner, Levon S. Atabekyan, and Alexander K. Chibisov. Photoprocesses in spiropyran-derived merocyanines: singlet versus triplet pathway. *Chem. Phys. Lett.*, 260(1-2):59–64, 1996.

[47] H. Fidder, M. Rini, and E.T.J. Nibbering. The role of large conformational changes in efficient ultrafast internal conversion: Deviations from the energy gap law. *J. Am. Chem. Soc.*, 126:3789, 2004.

[48] Elliot Berman, Richard E. Fox, and Francis D. Thomson. Photochromic spiropyrans. i. the effect of substituents on the rate of ring closure. *J. Am. Chem. Soc.*, 81(21):5605–5608, 1959.

[49] Norris W. Tyer and Ralph Sherman. Becker. Photochromic spiropyrans. I. absorption spectra and evaluation of the π-electron orthogonality of the constituent halves. *J. Am. Chem. Soc.*, 92(5):1289–1294, March 1970.

[50] Daniel S. Kemp and Frank Vellaccio. *Organic chemistry.* Worth Publishers Inc., 1980.

[51] Helmut Görner. Photochromism of nitrospiropyrans: effects of structure, solvent and temperature. *Phys. Chem. Chem. Phys.*, 3(3):416–423, 2001.

[52] Katharine B. Blodgett. Films built by depositing successive monomolecular layers on a solid surface. *J. Am. Chem. Soc.*, 57(6):1007–1022, 1935.

[53] Marcel Morin, Roger M. Leblanc, and Ilona Gruda. Spectral and photochromic properties of two long-chain spiropyranindoline monolayers at the air–solid interface. 58(19):2038–2043, October 1980.

[54] R. H. Tredgold. The physics of Langmuir-Blodgett films. *Rep. Progr. Phys.*, 50(12):1609, 1987.

[55] A. Miyata, Y. Unuma, and Y. Higashigaki. Optical properties and molecular orientation of aggregates in langmuir-blodgett films of a long-chain spiropyran. *Bull. Chem. Soc. Jap.*, 66(4):993–998, 1993.

[56] Dimitri A. Parthenopoulos and Peter M. Rentzepis. Three-dimensional optical storage memory. *Science*, 245(4920):843–845, 1989.

[57] Martin Schübbe. Optische untersuchung dünner schichten photochromer moleküle sowie aufbau einer uhv. Diplomarbeit, Freie Universität Berlin, 2008.

[58] G. Binnig, H. Rohrer, Ch. Gerber, and E. Weibel. 7×7 reconstruction on si(111) resolved in real space. *Phys. Rev. Lett.*, 50(2):120–123, Jan 1983.

[59] Karl D. Brommer, M. Needels, B. Larson, and J. D. Joannopoulos. Ab initio theory of the Si(111)-(7×7) surface reconstruction: A challenge for massively parallel computation. *Phys. Rev. Lett.*, 68(9):1355–1358, Mar 1992.

[60] Kai Schwinge. *Wachstum von Manganschichten auf reinen und Bismut-rekonstruierten Si(111)-Oberflächen.* Doktorarbeit, Freie Universtität Berlin, 2005.

[61] Harland G. Tompkins. *A user's guide to ellipsometry.* Academic Press, 1993.

[62] Günter Sauerbrey. Verwendung von Schwingquarzen zur Wägung dünner Schichten und zur Mikrowägung. *Zeitschr. für Physik A*, 155(2):206–222, April 1959.

[63] David Lide. *CRC Handbook of Chemistry and Physics.* Twayne Publishers, Boston, 84th edition, 2004.

[64] Francesco P. Ballistreri, Cosimo G. Fortuna, Giuseppe Musumarra, Didier Pavone, and Salvatore Scirè. Principal properties (pps) as solvent descriptors for multivariate optimization in organic synthesis: specific pps for ethers. *ARKIVOC*, pages 54–64, 2002.

[65] L.R. Snyder. Classification of the solvent properties of common liquids. *Journal of Chromatography A*, 92(2):223–230, 1974.

[66] Takashi Yoshida, Akira Morinaka, and Nobuhiro Funakoshi. UV light-assisted vacuum deposition of spiropyran compounds. *Thin Solid Films*, 162:343 – 352, 1988.

[67] Philip Laven. Mieplot v4.2.03, March 2010. downloaded 12th of March 2010 from `http://www.philiplaven.com/MiePlot4203.zip`.

[68] Yoshimi Sueishi, Masanobu Ohcho, and Norio Nishimura. Kinetic studies of solvent and pressure effects on thermochromic behavior of 6-nitrospiropyran. *Bull. Chem. Soc. Jap.*, 58(9):2608–2613, 1985.

[69] V.I. Minkin. Photo-, thermo-, solvato-, and electrochromic spiroheterocyclic compounds. *Chem. Rev.*, 104:2751, 2004.

[70] L. Persano, E. Mele, A. Athanassiou, R. Cingolani, and D. Pisignano. Amplified spontaneous emission and waveguiding properties of the colored merocyanine form of (1 ',3 '-dihydro-1 ',3 ',3 '-trimethyl-6-nitrospiro[2H-1-benzopyran-2,2'-(2H)-indole] molecules. *Chem. Mater.*, 18(17):4171–4175, August 2006.

[71] A. P. Vink, M. A. de Bruin, and A. Meijerink. Line broadening studies for Cr^{3+} pairs and single ions in different oxide lattices. *J. Phys.: Condens. Matter*, 12(40):8607–8615, 2000.

[72] C.-C. Chao. Charge-transfer luminescence of Cr^{3+} in magnesium oxide. *J. Phys. Chem. Solids*, 32(11):2517 – 2528, 1971.

[73] John B. Flannery. Photo- and thermochromic transients from substituted 1',3',3'-trimethylindolinobenzospiropyrans. *J. Am. Chem. Soc.*, 90(21):5660–5671, 1968.

[74] M. Karcher, C. Rüdt, C. Elsäßer, and P. Fumagalli. Switching of nonfunctionalized spiropyran thin films on single crystalline MgO(100). *J. Appl. Phys.*, 102(8):084904, October 2007.

[75] David A. Reeves and Frank Wilkinson. Photochromism of spiropyrans. Part 1. – mechanism of photocolouration. *J. Chem. Soc., Farafay Trans. 2*, 69:1381–1390, 1973.